Aus dem Lehrstuhl für Neurologie
Prof. Dr. med. Ralf Linker
der Fakultät für Medizin
der Universität Regensburg

Characterization of the novel TSPO ligand GRT16085N in a human glioblastoma cell line

Inaugural – Dissertation
zur Erlangung des Doktorgrades
der Medizin

der
Fakultät für Medizin
der Universität Regensburg

vorgelegt von
Celine Rohrmus

2023

Aus dem Lehrstuhl für Neurologie
Prof. Dr. med. Ralf Linker
der Fakultät für Medizin
der Universität Regensburg

Characterization of the novel TSPO ligand GRT16085N in a human glioblastoma cell line

Inaugural – Dissertation
zur Erlangung des Doktorgrades
der Medizin

der
Fakultät für Medizin
der Universität Regensburg

vorgelegt von
Celine Rohrmus

2023

Dekan:	Prof. Dr. Dirk Hellwig
1. Berichterstatter:	Prof. Dr. Peter Hau
2. Berichterstatter:	Prof. Dr. rer. nat. Christian Wetzel
Tag der mündlichen Prüfung:	11. April 2024

Table of contents

1 Introduction

1.1 Glioblastoma

Adult-type diffuse gliomas are the most common brain tumors in adults and are divided into grades 2-4 based on histological as well as molecular criteria by the WHO classification of 2021 [1]. The most aggressive malignancy with the lowest overall survival is glioblastoma (GB), which accounts for approximately 48% of all malignant brain and CNS tumors in the U.S. [2]. The average survival time is 14-20 months [3] [4] [5] [6] with a 5-year chance of survival around 6%, depending on sex and age at diagnosis [7] [8]. An improved prognosis or even successful treatment for this type of cancer is one of the greatest challenges in neuro-oncology.

One prognostic relevant biomarker, which was already integrated into the 2016 classification, is the mutation status of the isocitrate dehydrogenase 1/2 (IDH 1/2) [9]. The heterozygous gain of function mutation (IDH^{mut}) [10], as opposed to the IDH wild type (IDH^{wt}), is associated with a longer survival time [11] [12] [13]. This can be explained by the altered DNA and histone methylation, as a result of an increased production of the oncometabolite D-2-hydroxyglutarate, which is associated with hypermethylated CpG-islands. This methylation status is also referred to as *glioma-CpG island methylator phenotype* or G-$CIMP^{\pm}$ [14].

IDH^{mut} glioblastoma, now referred to as astrocytoma, IDH^{mut}, are usually secondary tumors, that progress from lower-grade gliomas [11]. The genetic expression profile is therefore similar to low-grade gliomas with aberrations of the TP53 [12] and ATRX gene [15] as well as a G-$CIMP^{+}$ phenotype [14]. Furthermore, hypermethylation of the TSPO promoter has also been observed in IDH^{mut} gliomas, resulting in lower expression of TSPO in comparison to IDH^{wt} glioblastoma. In contrast, the promoter appeared unmethylated in non-neoplastic brain tissue, indicating a *de novo* methylation in IDH^{mut} gliomas [16]. On top of that, the homozygous deletion of CDKN2A/B is viewed as a marker for IDH^{mut} astrocytomas [1]. A younger age of onset ($\leq$ 50 years) is also a reason for the comparatively better prognosis of IDH^{mut} astrocytoma [17] [18] as well as the more frequent MGMT promoter methylation [9]. Further investigations revealed that less TSPO expression in IDH^{mut} astrocytomas corresponds to a lower grade of malignancy, leading to a correlation between TSPO

levels and survival time in both, primary [19] [20] [6] as well as recurrent glioblastoma [21]. Although, the survival benefit of TSPO was not differentiated from the IDH mutation status.

In contrast, IDH^{wt} GB are mostly primary (*de novo*) tumors, that are characterized by a short clinical history and a rapid progression. With about 90% of the cases, they are forming the vast majority of glioblastomas [9]. They can occur in all age groups, with an age of onset of $\geq$ 55 years [3] [22]. The genetic aberrations vary accordingly with some characteristic molecular changes such as amplification of the EGFR [23] [24] and the combinational gain of chromosome 7 and loss of chromosome 10 (+7/-10) [23]. Also, mutations of the TERT promoter are frequently seen in glioblastomas [25] [23]. The occurrence of all three aberrations is defining for glioblastoma, IDH^{wt} [1], besides the classic definition, which constitutes of necrosis and neovascularization, that establish a second trait to diagnosis.

1.1.1 Glioblastoma subtypes

To better meet the complexity of the heterogeneity of the disease, extensive research at the combined genomic, epigenetic and proteomic level, led to the characterization of core pathways associated with glioblastoma pathogenesis. Molecular genetic studies of *The Cancer Genome Atlas* database revealed regular changes in three main signaling pathways within the tumors. These are the activation of the RTK/Ras/PI3K as well as the inactivation of the p53 and the RB signaling pathways [26]. Further analyses of the genomes and transcriptomes identified certain gene expression patterns, based on which glioblastomas were divided into originally four subtypes (proneural, classical, mesenchymal and neural) [27]. However, subsequent studies questioned the neural phenotype to be an original subtype due to the lack of characteristic mutations [28] [29].

The three remaining subtypes, namely the classical, proneural and mesenchymal type, are each characterized by certain mutations. As for the classical type, amplification of EGFR and homozygous deletions of CDKN2A as well as rare mutations of TP53 [27] are characteristic. On the other hand, proneural tumors present themselves with changes in the PDGFRA signaling pathway, in addition to the prognostically favourable IDH mutation [30] [27]. The proneural group also has a high correlation with $G\text{-}CIMP^{+}$ glioblastomas, which are also associated with a longer survival period [31]. The third

group, namely the mesenchymal type, is characterized by deletion of PTEN and mutations of NF1 [30]. This entity is considered the most aggressive with the worst prognosis. Likewise, they express most PD-L1 [32], a finding which is in line with the fact that the mesenchymal subtype is particularly immunogenic and could, in consequence, respond to immunotherapy [33]. Furthermore, highest TSPO expression levels were found in the mesenchymal subtype as well as mesenchymal- like states [20] [16], a more comprehensive approach for the classification of glioblastoma subtypes including plasticity and cellular states [34]. Therefore, TSPO could be of clinical interest, serving as predictive biomarker for immunotherapies. However, the subtypes do not precisely reflect the variable and mutable nature of glioblastomas. Single cell RNA sequencing revealed that glioblastoma subtype classifiers are expressed differently among individual cells within a tumor and also, that the cells exhibit a spectrum of stemness and differentiational states [35].
Altogether, the results show a pronounced heterogeneity within glioblastomas, which is characterized by a plethora of cells with partly different, partly overlapping characteristics.

1.1.2 Glioma stem cell (GSC)

Glioma stem cells (GSC) describe a cell population within gliomas, that are oftentimes referred to as brain tumor initiating cells (BTIC) and that are defined by self-renewal and multi-lineage differentiation [36].
For a long time, it was not known exactly whether all cells had the same influence on growth and differentiation of the tumor, until Singh et al. described the brain tumor stem cell in a glioblastoma cell line [37]. Currently, there are two widely accepted views of the stem cell theory. The first is that tumors mimic the hierarchical structure of normal tissue. This means that cells with stem cell function represent the origin of differentiated cells and enable dynamic adaptation of the tumor through their regenerative and differentiational ability (as reviewed in [38]). The second model assumes that every tumor cell is tumorigenic and that stem cells as well as non-stem cells can undergo phenotypic transitions. This was substantiated as it was shown that all GB subpopulations displayed stem cell markers and showed tumorigenic potential, supporting the high plasticity within glioblastoma [39].

GSCs also display extensive cellular heterogeneity, as expected, in regard of GB's heterogeneous histology [35]. The distinction of GSCs is based on membrane antigens, yet there is not a universal marker, which can define the entire GSC population. Instead, a panel of multiple biomarkers was identified [40]. Notably, neither presence nor absence of such biomarkers are defining for stem cells [41].

Another characteristic feature of GSCs is the ability to change from quiescent, slow cycling cells into proliferating cells, migrating to nutrient-rich areas for differentiation and proliferation [42]. Upon stimulation, GSCs can transition between their reversible states [43] [44], depending on the favourability of the surrounding for survival, including acidic stress [45] [46], nutrient supply [47] [48] or extrinsic stressors like radiation [49]. This transition also has an impact on the energy metabolism of the cells. Recent studies on metabolic features of GSCs revealed that especially quiescent and differentiated GSCs mainly depend on oxidative phosphorylation (OXPHOS) and lipid oxidation [50]. In contrast, proliferating GSCs show a more complex phenotype by switching between glycolysis and oxidative pathways [51] [38], while furthermore making use of glutamine [52], a primary energy source alongside glucose [48].

Next to differentiated GB cells, GSCs were categorized into mesenchymal and proneural subtypes [53] on the basis of gene signatures [54] [55] [56], with both subtypes displaying certain characteristics. In comparison to proneural, mesenchymal GSCs were associated with shortened *in vivo* survival after transplantation [57]. They also presented a more aggressive growth pattern through IL-6/JAK/STAT3 [58], which was previously shown to be upregulated on GSCs [59]. In addition, the mesenchymal phenotype showed increased expression of genes related to vascularization, motility and wound healing, while proneural gene signatures were related to homeostatic activity [55]. Furthermore, both phenotypes showed different distributions within the tumor. Whereas proneural cells were primarily found in persivascular niches, mesenchymal cells were linked to necrotic niches, able to survive stress conditions like hypoxia and nutrient deprivation [56]. This is reflected in the preferred energy sources. In contrast to proneural GSCs, mesenchymal cells showed low glutamine levels and high lipids [60], pointing to a higher adaptability of their metabolic phenotype.

To add additional complexity, individual tumors or tumor areas can switch between subtypes, depending on microenvironmental factors such as nutrient and oxygen restrictions [55] [61] [34], cell interactions [62] as well as specific microenvironmental niches [56]. It was further hypothesized that, when investigating the disease *ex vivo*,

cell culture conditions promote the adoption of a certain phenotype [63]. This is a significant factor, that should be considered when working with glioblastoma cells.

1.1.3 Tumor microenvironment

It is widely accepted that GSCs are preserved in microenvironments, which are known as niches and that maintain and affect the behaviour of GSCs. These niches were divided into five categories, namely perivascular, hypoxic/necrotic, peri-arteriolar, peri-immune and extracellular, that are comprised of specific types of cells, proteins and molecular mechanisms (as reviewed in [64]). Recent investigations concluded that the original five categories are not distinct from another, therefore proposing a more comprehensive concept of the so-called hypoxic peri-arteriolar GSC niche [64]. By simplifying the multitude of GSCs niches, this dynamic model enhances understanding of the interplay between niches and GSCs.
In the microenvironment of glioblastomas, hypoxic conditions occur due to rapid growth with consequently inadequate supply of nutrients and oxygen [65] and are considered to be a hallmark of cancer [66]. As a result of the low oxygen content, hypoxia-inducible factors (HIF) are upregulated. HIF-1/2 are involved in central signaling pathways, thus explaining the impact of hypoxia on self-renewal, proliferation, invasion and maintenance of stem function (as reviewed in [67]). Furthermore, it is associated with the activation of a glutamine metabolism in tumor cells [68] and causes acidification of the surrounding, which affects the proliferation-quiescence transition of GSCs [46]. Upon acidic pH shift, the cells converted into a quiescent state, while similarly mitochondria changed from a tubular to a donut shape. By creating a less acidic environment, this could be reversed, suggesting that shape as well as function of mitochondria is dependent on GSC phenotype [46]. Mitochondria play a crucial role in the maintenance of the oxidant-antioxidant system in cells. Accordingly, GSCs have developed scavenger systems to adapt to oxidative stress [69]. Mitochondrial dysfunction, e.g. due to mutations of genes encoding components of NADH- protein complexes, can cause an accumulation of superoxide radicals. Subsequently, prolonged activation of ROS-dependent oncogenic pathways is associated with tumorigenesis and metastasis (as reviewed in [70]) as well as cell cycle arrest in G0/G1 phase, thus resulting in maintenance of the quiescent state [71].

Additionally, hypoxic conditions induce an immunosuppressive environment by the release and recruitment of immunosuppressive cytokines and cells [72] [73] [74]. Glioblastomas are lymphocyte-depleted and highly infiltrated by tumor associated macrophages (TAM), whose formation and recruitment of M2- like states are connected to GSCs [75]. TAMs are either brain intrinsic microglia or macrophages recruited from the periphery [75] [76] [77] and are especially associated with the mesenchymal subtype. They have been shown to express the most TSPO within tissue surrounding the malignancy [78] [16]. Instead of creating a tumor-suppressive microenvironment, TAMs are immunogenic cells, that secrete cytokines upon stimulation by malignant cells. These include cytokines like IL-10 and TGFβ, to suppress immune responses, and pro-proliferative cytokines such as IL-6 and TNFα, thus establishing a hostile TME [79]. As TGFβ exhibits strong immunosuppressive ability, it inhibits invasion and function of immune cells [80]. The majority of tumor-infiltrating T cells in glioblastoma is composed of Tregs, the transition of which is favoured by IL-10 and TGFβ [81] [82] [83]. These cells in turn, successfully suppress T helper cells [84], e.g. through the secretion of TGFβ and IL-10, which leads to diminished levels of IL-2 and IFNγ in T cells [85], while CD4- and CD8- positive T cells are exhausted [86] [87]. Whereas it could be shown that proneural GSCs express TGFβ, they could not be influenced by the cytokine but instead, efficiently induced TGFβ-mediated immunosuppression. In contrast, mesenchymal GSCs showed higher infiltration of CD8- positive T cells [88]. The lower infiltration of immunocytes in proneural compared mesenchymal GSCs, may therefore relate to the efficacy of GSCs sensitivity to immunotherapy.

1.1.4 Therapeutic approaches

The current standard of care in the treatment of glioblastoma in Germany includes surgical resection to the amount feasible, followed by radiochemotherapy. In the U.S., additional treatment with tumor treating fields was approved by the FDA in 2015 [89] and in Germany, approval followed in 2020 [88].

The most commonly used chemotherapeutical agent is the alkylating agent temozolomide (TMZ) [3]. In this context, MGMT expression is crucial as it is a repair protein, that reduces the effect of TMZ. Hypermethylation of the promotor of the

enzyme leads to a decreased expression of the MGMT gene, which in turn, results in increased chemosensitivity. Hence, MGMT promoter methylation is associated with a better response to this therapy and is part of the neuropathological screening [90].
Nevertheless, resistance mechanisms towards especially classical therapeutic approaches are the reason for only modest effects in the therapy of glioblastoma [91]. Thus, comprehending the underlying mechanisms of resistance as well as the complex interplay of GSCs with its environment might lead to the discovery of new strategies.
An important part for the survival of all cells, is the provision of sufficient energy. Based on the assumption, that glucose is a major source of energy, simultaneous therapy with glucose deprivation and TMZ was attempted. However, the cells entered quiescence after glucose starvation, upon upregulation of autophagic activity, thus promoting resistance to chemotherapy [92]. Nevertheless, it has only recently been shown that metformin could negatively affect explicitly GSC viability, which was reflected in a reduced proliferative capacity, lower invasiveness and reduced ability for self-renewal [93]. Since ROS is also crucial for survival and regulation of apoptosis [94], it was further questioned whether ROS presents a possible target. Especially as it was shown that low levels of ROS protected the cells from radiation-induced apoptosis [95], while increased levels of ROS caused augmented TMZ sensitivity [88]. In a former study, a dose-dependent reduction in the viability of GSCs and a reduced ability to self-renew was demonstrated by treatment with curcumin. Mechanistically, this was due to enhanced ROS accumulation with subsequent inhibition of STAT3 [93]. Moreover, the inhibition of STAT3 effectively prevented the transition from a proneural to a mesenchymal phenotype (PMT) [96], which can be induced upon radiation [97] [49]. This transition occurred TNFα/ NF-κB-dependently [55] [49]. Additionally, it was previously evidenced that one of the first responses to radiation-induced DNA damage was NF-κB upregulation, leading to enhanced DNA damage repair [49] [84], which could link mesenchymal differentiation to radio-resistance [55].
In order to circumvent the multiple resistance mechanisms to radiochemotherapy, hopes were high that the addition of novel and targeted immunotherapies would improve prognosis. But until now, novel therapies have only resulted in moderate clinical benefits [98] [99] [100] [101]. This is clearly due to the immunosuppressive environment, as improved patient outcome was correlated with T-cell response to tumor-associated antigens [102] [103]. To successfully restore a sufficient and effective T cell response, a full understanding of the immunological events in the tumor

is of great importance. Based on these considerations, genome-wide siRNA screening was performed in the lab of our collaborator P. Beckhove and revealed that TSPO is among the possible immunological targets of T cells in the context of glioblastoma [104], making the protein a suitable therapeutic target.

1.2 TSPO

1.2.1 TSPO structure, characteristics, and distribution

The 18-kDa translocator protein (TSPO) was originally discovered in 1977 as a peripheral binding site for benzodiazepines outside the CNS [105]. It is composed of 169 amino acids [106]. Its structure is characterized by five transmembrane α-helices in the outer mitochondrial membrane (OMM), stretching into the intermembrane space with an extramitochondrial C-terminal and intramitochondrial N-terminal [107]. Within this structure separate binding sites for TSPO ligands are contained. As for cholesterol, an endogenous TSPO ligand, a cholesterol recognition amino acid consensus sequence (CRAC) was found in the C-terminus [108] [109]. Although several studies aimed to identify the exact binding site of TSPO, it was found that different amino acid sequences, distributed across the transmembrane domains, are responsible and the exact mechanisms of ligand binding remain elusive [110] [111]. TSPO shows high conformational plasticity as it can function in a monomeric state but it can also form dimers and higher oligomers [112] [113] [114] [111]. In general, TSPO is widely expressed throughout the body but it is specifically found in tissue associated with steroidogenesis, such as the adrenal cortex or adipocytes [112] [115]. Within the healthy brain, it is only expressed on very low levels but it is upregulated in several neuropathological conditions [116] [117] [118]. Next to glia cells [118] [119] [120], it was found that TSPO is also upregulated in neoplastic cells [121] [19] [122] [119].

1.2.2 TSPO function

Due to its location in the outer mitochondrial membrane, TSPO has been associated with a variety of cellular functions. The main tasks include the binding and transportation of cholesterol into mitochondria for steroid and neurosteroid synthesis as well as porphyrins for heme synthesis [115]. As one of the most prominent features,

it has been extensively studied using TSPO ligands. There, TSPO agonists were found to enhance neurosteroid synthesis throughout the body and in various cell lines *in vitro* and *in vivo* [123] [124] [125].

Among the diseases, in which TSPO is highly expressed, are gliomas [126]. Although most mechanisms of action are not fully defined yet, many studies point to a functional relevance of TSPO in glioblastoma.

There is evidence that TSPO is part of a complex consisting of the voltage-dependent anion channel, 32 kDa (VDAC) and the adenine nucleotide transporter, 30 kDa (ANT). Both components are part of the mitochondrial permeability transition pore (mPTP) [127]. Accordingly, among the tasks attributed to TSPO is the regulation of mitochondrial structure as well as function. This includes mitochondrial respiration and oxidative stress [128] [129]. As a consequence of mPTP opening, the proton gradient of the mitochondrial intermembrane space collapses and the mitochondrial proton gradient ($\Delta\Psi m$) dissipates. This is followed by subsequent release of apoptotic factors, initiating apoptosis [130]. In the last decades, different pathways have been investigated in glioblastoma cell lines, all of which have been associated with the modulation of apoptotic cell death, including oxidative stress and mitochondrial membrane potential [131]. The crosstalk between oxidative stress and TSPO may also act vice versa, as TSPO transcription is regulated by PKCε, which is a ROS sensitive pathway [132] [133]. In U-118MG cells, pharmacological targeting of TSPO, together with the NO donor sodium nitroprusside (SNP), attenuated cell death. Therefore associating TSPO to nitric oxide (NO)- induced cell death [134].

Not only cell death, but also proliferation processes are affected by TSPO. TSPO expression was related to enhanced proliferation in a C6 rat glioma cell line [121], which was later confirmed by TSPO overexpression in the same cells, ameliorating their proliferative capacities [135]. On the other hand, deficiency of the protein also led to increased proliferation in mouse as well as human glioma cells [136] [137]. The results of the latter studies were both linked to cell cycle progression. With TSPO depletion, more cells were found in the S phase than in the G0/1 phase [138] [137].

With regard to mitochondria-to-nucleus-signaling, generation of ROS and the collapse of the mitochondrial membrane potential ($\Delta\Psi m$) are important modulators acting through changes of ATP levels, NADPH oxidase activity and the release of Ca^{2+} [139] [140] [141]. Downregulation of TSPO has been shown to decrease oxidative stress [142] and ROS is also among the pro-inflammatory molecules that are released upon

activation of microglia. Other pro-inflammatory cytokines are IL-6, IL-8 and IL-1β, which altogether define the M1 as opposed to the anti-inflammatory M2 polarization of microglia [143] [144] [145]. Even though anti-inflammatory effects are attributed to TSPO, no clear assignment could be made, as TSPO was associated with the M1 [146] [147] [120] as well as the M2 type [146] [148] [149]. This was also found to be the case in glioblastoma cells. While an upregulation of IFNγ/TNFα as part of the M1 phenotype was observed in TSPO- rich tumors, an enhancement of M2 interleukin genes could also be detected [16].

Considering the plethora of functions that are modulated by TSPO, the assumption is obvious that TSPO acts through the regulation of gene expression [150].

This hypothesis was recently verified in a GB cell line. Notably, augmentation of TSPO in the nucleus was only seen in xenografts, whereas cultured U-87MG cells showed no significant upregulation of TSPO [151]. Pharmacological targeting of TSPO led to diminished expression of immunomodulatory-related genes, pointing to another role of TSPO.

Recent investigations revealed that TSPO expression in GSCs is triggered by T cells through secretion of TNFα and IFNγ and that, paradoxically, TSPO expression is a protective factor for GB against cytotoxic T cell attacks [152], which play an important role in the control of malignancies.

1.2.3 TSPO ligands

1.2.3.1 Synthetic TSPO ligands

To further characterize TSPO, there has been great interest in providing synthetic ligands, to investigate its functions and develop diagnostic and therapeutic applications.

One of the first prototypical ligands was the isiquinoline carboxamide derivative PK11195, to which an antagonistic mode of action was attributed [153]. Widely used as radiotracer in PET imaging, it allowed for visualization of TSPO expression and distribution. Since it was developed decades ago, there are some limitations to it, like a low signal to noise ratio due to non-specific binding and rather low uptake in the brain. This, in turn, resulted in several improved ligands on the market [154], including GRT16085N, XBD173 and Etifoxine.

1.2.3.2 GRT16085N (GRT16)

GRT16 is a novel, dual-mechanism Kv7 potassium channel/TSPO receptor activator, which was originally designed as an activator of Kv7 channels in the quest for alternatives to treat neuropathic pain [155]. To test the selectivity of the compound, extensive profiling of 140 targets was carried out, which showed a high selectivity for TSPO in addition to Kv7.2/3. Displacement of [3H]-PK11195, revealed a binding affinity for TSPO of 4.6 μM in human U-118MG glioblastoma cells [156].

TSPO has long been associated with a number of CNS pathologies [157] and TSPO agonists are known for their neuroprotective effects. Thus, GRT16 promoted survival rates of rats after crush lesion of the cervical spinal nerves and accelerated the rate of axonal regrowth [156]. Preliminary results validated the protective effects in retinal neurons [158]. Supposedly, these effects are achieved by promoting an anti-inflammatory response, together with an increase in neurosteroid synthesis [128], which could be confirmed for GRT16 as well. GRT16 administration resulted in significant increases of pregnenolone levels in C6 glioma cells. In comparison, pregnenolone levels were even higher in the brain than plasma levels [156], indicating an unimpeded crossing of the blood-brain barrier. Monitoring the distribution of GRT16 in the brain paralleled the concentration-time course of plasma after oral application. Additionally, oral bioavailability it rats was declared to reach 73% *in vivo* [156].

All these prerequisites make GRT16 a promising candidate for the treatment of CNS diseases.

1.2.3.3 XBD173

The phenylpurine XBD173, also referred to as Emapunil or AC-521, is a selective, high-affinity TSPO agonist, which induces neurosteroid synthesis in the periphery as well as the brain [159]. This could be validated in glioblastoma cells as well [125]. It has also been demonstrated that XBD173 efficiently inhibits microglial response, thereby dampening pro-inflammatory signaling and decreasing neuroinflammation [160] [161].

The ligand has been extensively studied as possible alternative to benzodiazepines in psychiatric diseases over the past years, where it revealed anxiolytic properties without benzodiazepine-like side effects in the treatment of general anxiety [162] [123] [163].

It also lacks withdrawal symptoms after cessation or tolerance with regard to anxiolysis [164]. Importantly, XBD173 was tested for tolerability and safety in clinical studies, where no severe drug-related adverse events were reported [123] [165].

1.2.3.4 Etifoxine

In addition to rather diagnostic ligands, some ligands show potential as therapeutics. Etifoxine, also known as Stresam®, has been approved in France as anxiolytic agent in the treatment of anxiety and adjustment disorder. It was shown to have a better profile compared to benzodiazepines regarding tolerability as well as efficaciousness. Also, fewer adverse effects were reported. Etifoxine caused neurological, such as drowsiness, as well as gastrointestinal symptoms, but to a lesser extend compared to benzodiazepines. Besides, a greater decrease of anxiety after drug discontinuation as well as less rebound was experienced [166] [167] [168] [169]. This applies to both, young [166] and elderly patients [170]. Etifoxine makes use of a direct and an indirect way to unfold its mode of action. The direct pathway is based on the positive allosteric modulation of $GABA_A$ receptors with binding of the inhibitory β-subunits. The indirect pathway probably acts through enhanced cholesterol transport and subsequent conversion to allopregnanolone, an known endogenous anxiolytic [171]. Multiple studies have shown that by binding to TSPO, Etifoxine exerts modulatory effects on the immune system in the sense of anti-inflammatory activity [172]. In addition, Etifoxine increased the synthesis of neurosteroids through TSPO- binding [173].

1.2.3.5 Endogenous TSPO ligands

TSPO is binding to many endogenous ligands. Among the ones identified during the last decades are cholesterol [108] as well as porphyrins (PP) [174] and the Diazepam Binding Inhibitor (DBI) [175]. The most thoroughly investigated ligand is cholesterol, which binds TSPO with nanomolar affinity [176]. Cholesterol is then transported from the outer to the inner mitochondrial membrane where it is metabolized to pregnenolone by cytochrome P450 [177]. This is considered the rate-limiting step in the synthesis of steroids [112] [113]. Therefore, TSPO has been implicated to play an essential role in steroidogenesis. However, this hypothesis has been challenged by different groups,

whose investigations with knockout mice have brought up inconsistent phenotypes [178] [179] [180] [181].

On another trait, it was found that porphyrins bind to TSPO with high affinity. Especially PPIX is important, as it forms heme when complexed with Fe^{2+} [174]. However, lately the influence of TSPO on heme synthesis has been challenged, as TSPO KO mice did not show a negative impact regarding heme biosynthesis [182]. Nevertheless, PPIX and TSPO may still present multiple interactions that modulate indispensable functions like attenuation of ROS [183].

A third group of ligands is the DBI as part of an acyl-CoA-binding domain. Together with TSPO, it is supposed to participate in steroidogenesis as regulators of cholesterol transport [184]. Possibly, the interaction between the two proteins might not be limited to steroidogenesis, but also include other metabolic processes such as inflammation [185].

2 Aim of this work

Gliomas make up the largest proportion of malignant brain and CNS tumors in the U.S. [186]. Among this entity, glioblastoma is the most aggressive malignancy with an average survival time of 15 months [5] [8]. The treatment of glioblastoma remains challenging until today, especially due to the plasticity of GSCs, allowing the cells to transition into a quiescent, low cycling state to evade therapies aiming at proliferating cells [187]. The long-known 18-kDa translocator protein (TSPO) was formerly discovered to be upregulated in GB [126] [19] and also associated with the prognostically unfavourable mesenchymal glioblastoma phenotype [16]. Since the protein is located at the outer mitochondrial membrane, it was linked to numerous key cellular functions, which were shown to be altered in glioblastomas [188].

The ineffectiveness of current immunotherapeutic approaches for GB suggests that not all mechanisms of immune resistance have been discovered [189]. Recent results uncovered TSPO as part of such a mechanism [104] [152], making this protein a potential therapeutic target in glioblastoma.

Recently, the German pharmaceutical company Grünenthal GmbH, designed the dual-mechanism TSPO agonist, GRT16085N (GRT16). To formulate a first characterization of the ligand, the effects of GRT16 were compared to established TSPO agonists, namely XBD173 and Etifoxine. Modulation of TSPO was examined in a human, mesenchymal glioma stem cell line (BTIC13) with respect to cytotoxicity, cytokine expression, mitochondrial respiration, generation of ROS and apoptosis.

The aim of our study was to evaluate the effects of GRT16 in order to develop translational pathways for the inhibition of pathophysiologically relevant mechanisms in patients with GB.

3 Zielsetzung der Arbeit

Gliome bilden den größten Anteil primärer Hirntumoren [186]. Das Glioblastom stellt dabei, mit einer mittleren Überlebensdauer von 15 Monaten, den aggressivsten malignen Tumor dar [5] und bleibt bis heute eine therapeutische Herausforderung. Dazu tragen einerseits die außerordentliche Heterogenität innerhalb des Tumors und andererseits die Plastizität insbesondere der Glioblastom-Stammzellen bei. Doch gerade diese Eigenschaften eröffnen der Medizin eine Vielzahl an therapeutischen Angriffspunkten.

Einer dieser Ansatzpunkte ist das bereits länger bekannte 18-kDa Translokationsprotein (TSPO), welches von Glioblastomen, insbesondere im Rahmen des prognostisch ungünstigen mesenchymalen Glioblastom-Phänotyps [16], vermehrt exprimiert wird [126] [19]. Aufgrund seiner Lokalisation an der äußeren Mitochondrienmembran, wurde das Protein mit zahlreichen zellulären Schlüsselfunktionen in Verbindung gebracht, die in der Pathogenese des Glioblastoms eine Rolle spielen [188].

Die Unwirksamkeit der derzeitigen immuntherapeutischen Ansätze deuten auf eine noch nicht vollständige Erfassung aller Immunresistenzmechanismen des Tumors hin [189]. Gleichwohl konnte TSPO erst kürzlich mittels Einzelzell-RNA- Sequenzierung als Teil eines solchen Mechanismus aufgedeckt werden [104] [152], wodurch sich dieses Protein als ein potenzielles therapeutischen Ziel beim Glioblastom qualifiziert.

Das deutsche Pharmaunternehmen Grünenthal GmbH entwickelte erst kürzlich einen TSPO-Agonisten mit dualem Wirkmechanismus. Dieser, GRT16085N (GRT16) genannte Ligand, wurde mit den zwei bereits etablierten TSPO- Agonisten, XBD173 und Etifoxin, verglichen. Mit dieser Arbeit erfolgte eine erste Charakterisierung von GRT16 hinsichtlich Zytotoxizität, Zytokinexpression, mitochondriale Zellatmung, ROS Synthese und Apoptose in einer humanen Hirntumor Stammzelllinie (BTIC13) vom mesenchymalen Typ.

Ziel dieser Studie ist es, durch ein besseres Verständnis des Wirkprofils des TSPO Liganden GRT16, dazu beizutragen, translationale Wege zur Hemmung pathophysiologisch relevanter Mechanismen bei Glioblastompatienten zu entwickeln.

4 Material and Methods

4.1 Material

4.1.1 Chemicals and reagents

Table 1: Chemicals and reagents

Substance	Company
Accutase	Sigma-Aldrich, Germany
30% Acrylamid/ Bis Solution	Bio-Rad, Germany
4-(2-Aminoethyl)-benzolsulfonylfluorid (AEBSF)	Sigma-Aldrich, Germany
Ammoniumpersulfate (APS)	Sigma-Aldrich, Germany
Antimycin A	LKT Laboratories Inc., USA
BCA-Assay Reagents A&B	Interchim, France
Bromphenol Blue	Sigma-Aldrich, Germany
$CoCl_2$	Sigma-Aldrich, Germany
4‘, 6-Diamidin-2-phenylidol (DAPI)	Sigma-Aldrich, Germany
Dimethylsulfoxid (DMSO)	Roth, Germany
Dithiothreitol (DTT)	Sigma-Aldrich, Germany
Epidermal growth factor (EGF)	Miltenyi-Biotec, Germany
FCCP	Cayman Chemical Company, USA
Fibroblast growth factor (FGF)	Miltenyi-Biotec, Germany
α-D-Glucose	Serva, Germany
Glycerol	Sigma-Aldrich, Germany
Glycerolphosphat	Sigma-Aldrich, Germany
Glycin	Roth, Germany
10x HALT Protease inhibitor	Thermo Fisher Scientific, USA
HCl	Merck, Germany

H_2SO_4	Carl Roth, Germany
Isobutanolol	Merck, Germany
Isopropanol	Merck, Germany
Laminine	Becon Dickinson, Germany
L-glutamine	Sigma-Aldrich, Germany
Menandion	Sigma-Aldrich, Germany
Methanol	Merck, Germany
2-Methylbutane	Sigma-Aldrich, Germany
Milk powder	Roth, Germany
NaCl	Roth, Germany
NaOH	Merck, Germany
Na_4P2O_7	Merck, Germany
Na_3VO_4	Merck, Germany
Oligomycin	Cayman Chemical Company, USA
PageRuler Plus Pre-stained Protein Ladder	Thermo Fisher Scientific, USA
Paraformaldehyde (PFA)	Sigma-Aldrich, Germany
Penicillin /Streptomycin (P/S)	Sigma-Aldrich, Germany
Phosphate buffered Saline (PBS)	Sigma-Aldrich, Germany
Ponceau S	Sigma-Aldrich, Germany
Pre-stained Protein Standard	Thermo Fisher Scientific, USA
Resazurin	R&D Systems, USA
RHB-A stem cell culture medium	Stem Cell Technologies, Germany
Rotenone	Cayman Chemical Company, USA
Sodium deoxycholate	Sigma-Aldrich, Germany
Sodium dodecyl sulfate (SDS)	Sigma-Aldrich, Germany

Tetramethylethylendiamine (TEMED)	Sigma-Aldrich, Germany
Tris (Trizma Base)	Sigma-Aldrich, Germany
Triton X-100	Sigma-Aldrich, Germany
Trypan blue	Sigma-Aldrich, Germany
Tween 20	Sigma-Aldrich, Germany
XF Base Medium minimal DMEM	Agilent Technologies, USA
XF Calibrant pH 7,4	Agilent Technologies, USA

4.1.2 Assay kits

Table 2: Assay kits

Kit	Company
Brilliant III Ultra-Fast SYBR® Green QPCR Master Mix	Agilent Technologies, USA
FITC Annexin V Apoptosis Detection Kit with 7-AAD	BioLegends®, USA
GoScript™ Reverse Transcription System	Promega, USA
H2DCFDA-Cellular ROS Assay Kit	Abcam, GB
IL-6 Human Uncoated ELISA Kit	Thermo Fisher Scientific, USA
IL-8 Human Uncoated ELISA Kit	Thermo Fisher Scientific, USA
NucleoSpin® RNA	Macherey & Nagel, Germany

4.1.3 TSPO ligands

Table 3: TSPO ligands, stock and final concentration

TSPO ligand	Stock concentration	Final concentration	Company
GRT16	5 mM	1-25 μM	Grünenthal GmbH, Germany
XBD173	5 mM	1 μM	Kindly provided by V. Milenkovic and C. Wetzel,

			Department of Psychiatry and Psychotherapy
Etifoxine	10 mM	1 μM	Sigma-Aldrich, Germany

4.1.4 Cytokines

Table 4: Cytokines, stock and final concentration

Cytokine	Stock concentration	Final concentration	Company
IFNγ	100 μg/mg	50 ng/ml	PeproTech, Germany
TNFα	100 μg/mg	50 ng/ml	PeproTech, Germany
TRAIL	100 μg/mg	50 ng/ml	PeproTech, Germany

4.1.5 Consumables

Table 5: Consumables

Product	Company
6-well culture plates	TPP, Switzerland
96-well cell culture plates	TPP, Switzerland
96-well black, flat bottom plates	SPL Life Sciences, Korea
96-well plate, PCR compatible	Eppendorf, USA
96-well black, transparent bottom plates	Brand, Germany
Combi tips advanced 1ml, 2,5 ml, 5 ml	Eppendorf, USA
Eppendorf Tubes (0.2 mL, 1.5 mL)	Sarstedt, Germany
Cryotubes 1,5 ml	Roth GmbH, Germany
Pipette tips 10 μl, 20 μl, 100 μl, 1000 μl	Sarstedt, Germany
Polyvinylidenfluoride (PVDF) membrane (0.2 μm)	GE Healthcare, USA
Seahorse XFp cell culture mini plate	Agilent Technologies, USA
Seahorse XFp extracellular flux cartridge	Agilent Technologies, USA
Tubes (15 mL, 50 mL)	Sarstedt, Germany

Whatman paper	GE Healthcare, USA
T75 cell culture flask	TPP, Switzerland

4.1.6 Equipment

Table 6: Equipment

Product	Specification	Company
BD FACSCanto™ II Flow Cytometer		BD, Biosciences, USA
Cell culture centrifuge	Megafuge 1.0R	Thero Fisher Scientific, USA
Cell culture incubator	HeraCell 150	Thero Fisher Scientific, USA
Centrifuge mini	Haereus Biofuge pico	Thermo Fisher Scientific, USA
Counting chamber	Neubauer Hemocytometer	Carl Roth, Germany
Cryo Freezing Container	5100-0001	Nalgene, USA
Fluorescence microscope	Zeiss Axio Observer Z1	Visitron Systems GmbH, Germany
Heating block	Thermomixer 5436	Eppendorf, Germany
InCucyte® ZOOM		Essen Bioscience, GB
LaminarFlow Safety cabinet	HeraSafe laminar flow	Thermo Fisher Scientific, USA
Light optical microscope	Fluovert Typ 090-135.001	Leitz, Germany
Light microscope camera	ProgRes C3B	Jenoptik, Germany
Microplate Reader	VarioSkan Flash Multimode Reader	Thermo Fisher Scientific, USA
NanoPhotometer P300 Implen		Kisker, Germany
PCR machine	qTOWER^3 Thermocycler	Analytik Jena GmbH, Germany

pH meter	CG 842	Schott, Germany
SDS-Page equipment	PerfectBlue Double Gel System Twin S	Peglab, Germany
Seahorse Extracellular Flux Analyzer	XFp	Agilent Technologies, USA
Semi-Dry-Blotter	Pegasus	Phase GmbH, Germany
Waterbath	1083	GFL, Germany
Western Blot spectrophotometer	ImageQuant LAS4000	GE Healthcare, USA

4.1.7 Software

Table 7: Software

Software	Purpose	Company
GraphPad Prism	Statistics	Graph Pad Software, USA
ImageJ	Image editing and analysis	NIH, USA
Microsoft Excel	Data analysis	Microsoft Corporation, USA
Seahorse Wave Desktop Software	Data analysis	Agilent Technologies, USA
VisiView	Image taking	Visitron Systems GmbH, Germany

4.2 Cell culture

When working with cells, care was always taken to ensure sterility and only sterile medium, buffer and materials were used. All work steps were carried out in a sterile workbench (Herasafe, Thermo Fisher Scientific, USA).

4.2.1 Cell lines

The cell lines used in this work are established brain tumor initiating cells (BTICs), showing a mesenchymal phenotype. For the extraction of these cells, resected glioblastoma samples from patients of the University Hospital Regensburg were prepared as described [190]. All cells were cultured in the nutrient medium RHB-A at 37°C and 5% carbon dioxide (CO_2) under stem cell-like conditions.
The sampling of tumor specimens and enrichment of BTICs was approved by the Ethics Committee of the University of Regensburg (No° 18–207-101). Informed consent was obtained from all patients.

Table 8: Cell lines

Cell line (DMSZ Nr.)	Cell type	Histology	Culture medium
BTIC13	Human glioblastoma stem cells	mesenchymal	RHB-A+5% PS+20 ng/ml EGF+FGF

Several times a week, growth and morphology of the cells was evaluated with the aid of a microscope. Cells were split up when confluency of 80 to 90 % was reached, scaling up the passage. For this purpose, the culture medium was first transferred into a 15 ml tube and the adherent cells were detached with the help of Accutase. After a two-minute exposure time, the enzymatic reaction was stopped with the previously removed culture medium, whereupon the entire content was pipetted into the tube. The cell suspension was centrifuged at 1200 rpm for 4 min. Following this, the supernatant was discarded, and the pellet was resuspended in fresh culture medium. During the last step, the cell suspension was transferred into two cell culture bottles containing a final volume of 10 ml. When using a bottle repeatedly, it was first rinsed with PBS to

free it from cell residues. The cell lines were used for experiments up to the 22nd passage.

4.2.2 Freezing of cells

For the preservation of low passages, the cells were frozen and stored at -80°C. In this case, a pellet was prepared as described in 4.2.1. After the supernatant was discarded, the cells were suspended in a culture medium containing 10% of DMSO to prevent the formation of ice crystals, that could damage the cells. Subsequently, 1 ml of the cell suspension was transferred into each cryotube and stored in isopropanolol- filled freezing containers for 48h at -80°C. Due to the alcohol, the cells were frozen at a constant cooling rate of -1°C/min.

4.2.3 Thawing of cells

For a successful thawing of the cells, the work steps were carried out quickly. The cryotubes were defrosted in a 37°C water bath for 1 min. Next, the cells were transferred into a 15 ml tube and centrifuged (1200 rpm, 4min). After the supernatant was discarded, the cells were placed in a cell culture bottle. 24h to 48h later, half of the medium was renewed. When adequate confluency was reached, the cells were split up.

4.2.4 Determination of cell number

To determine the cell number, 10 µl of trypan blue was added to 40 µl of a previously produced cell suspension. Trypan blue is an anionic diazo dye, that selectively stains dead cells. Therefore, it can be used to assess cell viability, although it does not allow to draw any conclusions about functionality. Subsequently, 10 µl of the solution was pipetted onto a Neubauer counting chamber and the cells were counted using a light microscope. The cell number per millilitre was determined using the following formula:

$$\text{Cell count/ ml} = \frac{\text{Number of cells}}{\text{Number of counting chambers}}\ x\ 1{,}25x\ 10.000$$

4.2.5 Seeding and harvesting of cells

The cell culture formats used in this work as well as the cell number and the corresponding amount of culture medium are listed in table 9.

Table 9: Cell culture, methods and formats

Method	Cell culture format	Cell number/ well	Culture medium [µl]
ELISA	96-well plate	1-2 x 10^5	100
FACS Analyse	6-well plate	2 x 10^5	2000
IncuCyte® ZOOM	96-well plate	5 x 10^3	100
Resazurin assay	96-well plate	2,5 x 10^3	100
RNA isolation	6-well plate	1,5 x 10^5	2000
ROS-Microassay	96-well plate	25 x 10^3	100
qPCR	6-well plate	3 x 10^5	2000
Seahorse analysis	8-well plate	25 x 10^3	2000
Western Blot	6-well plate	4 x 10^5	2000

To seed the cells, a cell suspension containing the desired density was prepared. Afterwards, the cells were transferred onto a plate using a multi pipette. For harvesting, the culture medium was removed, and the cells were enzymatically detached. The pellets produced by centrifugation (1200 rpm, 4 min) were taken up in PBS and transferred to 1.5 ml Eppendorf tubes. This was followed by another centrifugation step (2500 rpm, 6min). The pellets could now either be used for experiments or stored in methyl butane at -80°C for further use.

4.3 Cell biological methods

4.3.1 Proliferation assay

For determining cell viability, the resazurin assay was chosen. This method is based on the spectrophotometric measurement of the metabolic activity of living cells. In this

case, the non-fluorescent dye resazurin is converted into the fluorescent dye resorufin and the absorbance is measured at 544 nm.
48h prior to treatment, cells were seeded with a density of $2,5x10^3$ cells per well into a 96-well plate. Then, the ligands were applied in concentrations ranging from 0-500 μM. The measurement was carried out at the time points of 48h and 96h.

4.3.2 Enzyme-linked Immunosorbent Assay (ELISA)

For the ELISA, the IL-6/IL-8 Human Uncoated ELISA Kit from Thermofisher was used. For this purpose, cells were seeded in a density of $2x10^6$/ well and allowed to grow for 48h. Thereupon, the treatment with 1 μM GRT16, XBD173 and Etifoxine was carried out alone and in combination with cytokines, following a two-hour pretreatment with the ligands. Before the cells were harvested, 1 ml of supernatant from each well was removed and stored at -80°C until its usage. The cells were harvested as described in 4.2.5 and cell numbers of living and dead cells were determined for normalization of the results. The procedure was carried out as described in the manufacturers protocol, starting with coating of the plate with the primary antibody (IL6 / IL8) the day before the experiment. The next day, after several washing and incubation steps, the standard series and the samples were applied in previously determined dilution. This was followed by the addition of the secondary antibody. Staining was performed by means of another HRP-bound antibody, which was activated by tetramethylbenzidine (TMB) and stopped after 15 min. Afterwards, photometric measurement at 450 nm was carried out.

4.3.3 Seahorse Extracellular Flux Analyzer XFp

The Seahorse Extracellular Flux Analyzer XFp offers a non-invasive method for the simultaneous measurement of the oxygen consumption rate (OCR) and the degree of acidification (ECAR) of adherently growing cells. For this purpose, cell medium is measured using analyte-specific fluorophores and their fluorescence signal.
The change in the analyte O_2 allows for conclusions to be drawn about oxidative phosphorylation, while simultaneously the pH change in the supernatant is measured for glycolytic activity. In addition, parameters of oxidative phosphorylation are also determined more precisely by adding various substances. Oligomycin, an ATP

synthase inhibitor, allows investigations of ATP production. Furthermore, FCCP is injected, which leads to the uncoupling of the ATP synthase by losing the proton gradient and causing maximum respiration. Finally, the addition of the combination of rotenone and antimycin A (AA), an inhibitor of two complexes of the respiratory chain, is added, which blocks mitochondrial respiration and makes it possible to calculate the respiratory capacity.

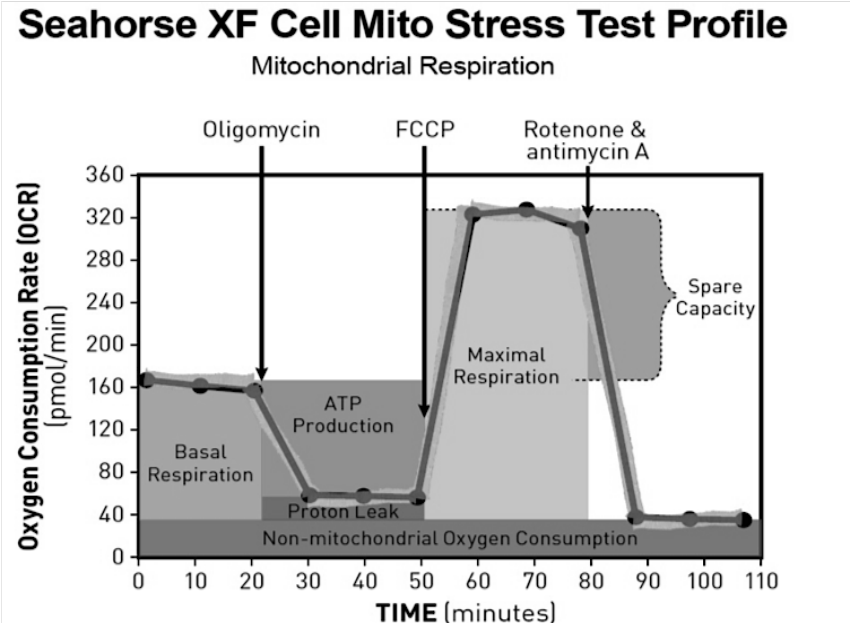

For the experiment, special 8 well cell culture plates were coated with 150 µl laminin (fc: 1µg/ml) before seeding the cells and incubated for at least 2h at 37°C. Subsequently, BTIC13 were seeded in a density of $2.5x10^3$ cells in 200 µl RHB-A and incubated for 48h also at 37°C and 5% CO_2. 400 µl PBS was added to the outer wells. In parallel, the wells of the sensor plate were filled with Seahorse XF Calibrant Solution, 200 µl on the inside and 400 µl on the outside and incubated for 24h at 37°C, CO_2-free. The next day, the measurement was carried out in 200 µl of unbuffered assay medium. The plate was then incubated again for 30 min in a CO_2-free surrounding. During this time, the device was able to calibrate itself using the sensor plate.

Table 10: Seahorse assay medium

Medium	Composition
Assay Medium	12,125 ml XF Base medium minimal DMEM

	125 µl Sodium pyruvate solution (stock 100 mM)
	125 µl L-Glutamine (stock 200 mM)
	250 µl α-D-Glucose (stock 1 M)
	Adjust pH 7,4 with 0,1 M NaOH

4.3.4 H2DCFDA Assay

To assess the formation of reactive oxygen species, the cells were seeded in a density of $2.5x10^4$/well. After 48h, the fluorescent dye 2', 7'-dichlorodihydrofluorescein diacetate (H2DCFDA) was added in a concentration of 20 nM and incubated for 45 min at 37°C. The principle is based on intracellular deacetylation by esterases of H2DCFDA to non-fluorescent 2', 7'-dichlorodihydrofluorescein (H2DCF). In the presence of ROS, H2DCF is then oxidized to 2', 7'-dichlorofluorescein (DCF), which in turn can be detected fluorometrically. After staining, the cells were pretreated with 1 µM GRT16 or XBD173 for 2h, after which the remaining substances were added. This included TNFα and $CoCl_2$, well known inducers of reactive oxygen species. Next to that, TBHP and Menadion were added as positive controls. The measurement with the VarioScan was carried out at the time points 0h, 3h, 6h, 24h, and 48h.

4.3.5 Real-time live-cell imaging system

IncuCyte® ZOOM live-cell imaging and analysis system was used to measure cell viability. Cells were seeded in a 96-well transparent flat bottom plate ($5x10^3$ cells/ well). The cells were cultured for two days to ensure adherence. Following a two-hour pretreatment with 1 µM of GRT16, XBD137 and Etifoxine, 50 ng/ml of TRAIL was added to the medium. Next, caspase 3/7 dye was added at a dilution of 1:1000. Afterwards, the plate was directly transferred into the IncuCyte® ZOOM device, where the cells were incubated at 37°C, 5% CO_2 for 48h. When the membrane integrity of a cell is lost, the dye can enter the dying cell. In doing so, it binds to double-stranded DNA, resulting in the emission of green light. This signal was used as reference for apoptotic cells and captured by the IncuCyte® ZOOM analyser in defined intervals. Based on pictures, the total green object area (µm²/well) could be calculated by the IncuCyte® software to evaluate apoptosis.

4.4 Molecular biological methods

4.4.1 RNA isolation

For the isolation of total RNA, the NucleoSpin RNA Plus Kit was used. The isolation and purification of RNA was carried out according to the manufacturer's protocol.
After the previously obtained cell pellets were lysed, genomic DNA was removed. The RNA was then bound and purified in further washing steps. By adding 30 µl of nuclease-free water, total RNA was eluted by centrifugation. To yield a higher concentrated eluate, the previous step was repeated by loading the same 30 µl onto the membrane and centrifuging it once more (11000g; 1 min). The RNA could then be stored at -80°C until further use.

4.4.2 Determination of RNA content

The determination of the RNA content was carried out photometrically at 260 nm. For this, the nanophotometer P3000 Implen was used.

4.4.3 cDNA synthesis

For the transcription of the RNA into complementary, double-stranded cDNA, the commercial kit GoScript™ Reverse Transcriptase Kit was used. In a first step, a reaction mixture was prepared, comprised of the calculated amount of RNA, diluted with nuclease-free water to a volume of 8 µl. Depending on the RNA concentration, this was either 0.5 or 1 µg. Subsequently, the denaturation was carried out at 75°C for 10 min. To prevent the secondary structures from being reassembled, the next step was carried out on ice. A master mix, consisting of buffers, an RNAse inhibitor and various primers as well as nucleotides was pipetted to the reaction mixture. During incubation in the thermal block, the reverse transcriptase led to the synthesis of complementary cDNA. Samples were diluted 1:10 when used for qPCR. cDNA was stored at -20°C.
The components used in the process are summarized in table 11.

Table 11: Reaction mixture cDNA synthesis

Component	Volume	Incubation
Total RNA	1000 ng or 500 ng	70°C, 10 min
5 x buffer	4 µl	
MgCl	4 µl	
PCR nucleotide mix	1 µl	
RNAsin	0,5 µl	25°C, 5 min
Random primers	0,5 µl	42°C, 60 min
Oligo dT primers	0,5 µl	75°C, 10 min
Reverse transcriptase	0,5 µl	4°C, ∞
Nuclease-free water	1 µl	
Total Volume	20 µl	

4.4.4 Semiquantitative real-time PCR (qPCR)

Semiquantitative real-time PCR is a method, that allows to measure the amplification of a target gene in real time via DNA-intercalating, fluorescence-labelled probes. Therefore, fluorescence-labelled, intercalating probes are needed. The retrospective determination of the initial relative amount of the target gene's mRNA can be done by comparison to a reference/housekeeping gene.

The process comprises three steps: denaturation, primer hybridization (annealing) and elongation. First, double strands are separated from each other by heating. During the next step, the temperature is adjusted for the primers to attach and the DNA polymerase to fill in the new nucleotides. The detection of the product is carried out by measurement of fluorescence. For this, the dye Sybr Green is used, which is intercalated in the strands and propagated in each cycle. The experiment requires a reaction mixture, consisting of specific primers for the target as well as the housekeeping gene, together with the fluorescent Sybr Green dye and nuclease-free water. 16 µl of this PCR mix is pipetted into each well and supplemented with 1:10 diluted cDNA samples, reaching a total volume of 20 µl. The samples were applied in

triplicates. The plate was placed in the qTOWER3 and the program listed in the table was started.

Table 12: Program Thermocycler qPCR

Temperature	Time	Cycles
95°C	3 min	1
95°C	15 sec	45
58°C	25 sec	

Table 13: Primer qPCR

Gene	Sequence	Annealing temperature
Interleukin 6	fwd 5‘-CTC AGC CCT GAG AAA GGA GA-3‘ rev 5‘-AGG TTG TTT TCT GCC AGT GC-3‘	58 °C
Interleukin 8	fwd 5‘-TGC GCC AAC ACA GAA ATT AT-3‘ rev 5‘-TGA ATT CTC AGC CCT CTT CAA-3‘	58 °C
TSPO	fwd 5‘-TCT TTG GTG CCC GAC AAA t-3‘ rev 5‘-GGT ACC AGG CCA CGG	58 °C
18 S	fwd 5‘-AGT CCC TGC CCT TTG AC ACA-3‘ rev 5‘-GAT CCG AGG GCC TCA CTA AAC-3‘	58 °C

4.5 Protein biochemical methods

4.5.1 Determination of protein concentration

First, as described above, cells were seeded in a density of $2{,}5x10^3$ in 6-well plates. The following day, after microscopicic verification of confluence and vitality, cells were treated with the appropriate test substances. A two-hour pretreatment with 1 μM of each of the ligands was carried out. This was followed by treatment with 50 ng/ml of TRAIL. After the desired incubation period (3h or 6h), the cells were harvested, pelletized and snap-frozen away at –80°C.

To ensure loading of the SDS-PAGE gel with an equal amount of protein, the protein concentration has to be quantified. This was carried out by BCA assay. The method is based on the reduction of Cu^{2+} to Cu^{1+}, which then forms a violet colour complex with bicinchoninic acid (BCA). This allows a colorimetric detection with an extinction of 562 nm.

In a first step, the proteins had to be isolated from the obtained pellet. Depending on the size of the pellet, between 70 and 100 µl RIPA buffer was added to the cells. After complete cell lysis by vortexing, samples were incubated for 10 min on ice. Subsequently, centrifugation at 14.000 rpm for 10 min at 4°C was carried out to separate insoluble cell components. The obtained lysate was transferred quickly to a new Eppendorf tube. The described work steps were all carried out on ice to prevent degradation of the proteins. Next, lysates were diluted with PBS in a ratio of 1:10. 25 µl each were applied in duplicates to a 96-well plate. The same procedure was done with the protein standard, which was used as reference to determine protein concentration. After adding 200 µl of reagent solution (ratio of A to B is 1:50), an incubation period of 30 min at 37°C followed. The VarioScan was then used to measure the absorption at 562 nm and to determine the protein concentration using the calibration curve.

4.5.2 SDS polyacrylamide gel electrophoresis

The principle of SDS-PAGE is based on the separation of proteins according to their mass within an electric field. To make this possible, anionic sodium dodecyl sulfate (SDS) is required, which attaches itself to denatured proteins, leading to a negative charge. This charge is significantly stronger than the self-charge of the proteins, that results in it's being negligible. As soon as the proteins pass through the polyacrylamide matrix towards the anode, they are separated by molecule size by their now identical charge, whereby larger proteins are retained earlier and don't migrate as far.

Gel electrophoresis was performed using a gel system with 5% collecting gel and 12% separating gel. After polymerization, the gel could be loaded with the samples. For this purpose, 40 µg of protein was diluted with PBS in a total volume of 20 µl. Subsequently, 5 µl 5x Laemmli buffer was added to each sample, denaturing the proteins, resulting in a final volume of 25 µl. This was followed by an incubation phase of 10 min at 75°C. The samples could then be transferred to the gel. As a reference for the molecular

size, a protein standard was also applied, using the PageRuler Plus Prestained Protein Ladder. Within the first 20 min at 80V, the samples were concentrated at the bottom of the collecting gel, then the separation took place at 120 V during the next 60 to 90 min, until complete separation of the coloured protein ladder was observed.

4.5.3 Western Blot

To visualize proteins of interest through specific antibody binding, the proteins from the gel were transferred to a PVDF membrane using the wet-blot method. For this purpose, a sandwich was formed: sponge – three Whatman papers – gel – PVDF membrane – three Whatman papers – sponge. All components were previously soaked in transfer buffer and checked for air bubbles before the next layer was added. The assembly was placed in a blot chamber filled with transfer buffer and connected to a power source, whereby, during a runtime of 2.5 hours, the proteins were electrophoretically plotted onto the membrane at 150 mA.
Subsequently, the transfer was evaluated using Ponceau S staining. After removal of the dye by rinsing with ddH_2O, non-specific binding sites were blocked with 5% milk while shaking. Next, primary antibodies were added, diluted 1:1000 in 2.5% milk in T-BST. Incubation took place over night at 4°C while shaking. To remove unbound antibodies, three washes with TBS-T followed, after which the secondary antibody was applied. Incubation in this case was one hour at room temperature in constant motion. Here, too, a three-time wash followed. The visualization was done by chemiluminescence in the ImageQuant. This process was based on the reaction of HRP bound to the secondary antibodies with the peroxide-containing developer solution Immobilon. When using the same membranes for other antibodies, the processes explained above were repeated after further washing.

Table 14: Primary and secondary antibodies

Antigen	Source	Dilution	Company
Caspase 9	rabbit	1:1000	Cell signaling, USA
cleaved Caspase 3	rabbit	1:1000	Cell signaling, USA

GAPDH	mouse	1:2000	Bio Technologies, USA
PARP	rabbit	1:1000	Cell signaling, USA
TSPO	rabbit	1:5000	Abcam, USA
α-mouse-IgG-HRP	donkey	1:5000	Santa Cruz, USA
α-rabbit-IgG-HRP	donkey	1:5000	Santa Cruz, USA

Table 15: Solutions used in Western Blot analysis

Solution	Composition	Application
Radioimmunoprecipitation assay stock (RIPA)	50 mM Tris-HCl 150 mM NaCl 0,5% Triton X-100 0,5% Sodium deoxycholate 10 mM Na4P2O7 1 mM Na3VO4 10 mM Glycerol phosphate	Protein lysis
RIPA buffer	1 ml RIPA stock solution 10 µl AEBSF 1 µl DTT 10 µl 10x HALT Protease inhibitor Cocktail	Protein lysis
SDS loading buffer (Laemmli)	12% SDS 60% Glycerol 600 mM DT 60 mM Tris (pH 6.8) 0.06% Bromphenol Blue	SDS PAGE
10x SDS running buffer	10G7L SDS 30.3 g/L Tris base 144.1 g/L Glycin Adjust to 1L with ddH_2O	SDS PAGE

1x SDS running buffer	100 mL 10x SDS running buffer in 990 mL ddH_2O	SDS PAGE
5 % Blocking solution	5% dried milk powder in 1x TBS-T	Western Blot
2,5 % Blocking solution	2,5% dried milk powder in 1x TBS-T	Western Blot
10x Tris buffered saline (TBS)	60.5 g/L Tris base 87.6 g/L NaCl Adjust to 1 L with ddH_2O Adjust pH to 7.5 with HCl	Western Blot
1x TBS	100 mL 10x TBS 900 mL ddH_2O 1 mL Tween 20	Western Blot
10x Transfer buffer	3.3 g/L Tris base 144.1 g/L Glycin Adjust to 1L with ddH_2O	Western Blot
1x Transfer buffer	100 mL 10x Transfer buffer 20 mL Methanol 700 mL ddH_2O	Western Blot

4.6 Data presentation and statistics

Statistical analysis was carried out using GraphPad Prism 8 software. Data are presented as mean ± SD (standard deviation) or mean ± SEM (standard error of the mean). Results are presented as baseline values. The levels of significance were set at *$p < 0.05$; **$p < 0.01$; ***$p < 0.001$; ****$p < 0.0001$.

5 Results

5.1 Impact of GRT16 on proliferation

In order to determine the concentrations for the following experiments, dose-dependent effects on cell proliferation after TSPO ligand treatment were evaluated first. Therefore, BTIC13 wildtype (wt) cells were treated with different concentrations of GRT16, as well as of the established TSPO ligands XBD173 and Etifoxine, ranging from 0.1 to 500 μM. Since DMSO served as solvent for all ligands, it was applied in parallel to elicit any toxic effects. Results were normalized to an untreated control. After 48h and 96h, proliferation was measured using the resazurin reduction assay. As shown in Figure 1 the assay evidenced a concentration dependence for the effect. Subsequent determination of the IC50 values revealed an inhibitory effect of GRT16 at 105 μM (Figure 1A). As for XBD173 the half-maximal response in survival inhibition was 44 μM (Figure 1B) and for Etifoxine 27 μM (Figure 1C). A final concentration of either 1, 10 or 25 μM was chosen for further experiments.

In summary, neither GRT16 nor XBD173 or Etifoxine affected cell growth to a significant extent when applied at low concentrations, namely in the nanomolar range. However, in the micromolar range, compounds were able to reduce cell viability of BTIC13 in a dose-dependent manner, suggesting specificity of their effect.

A

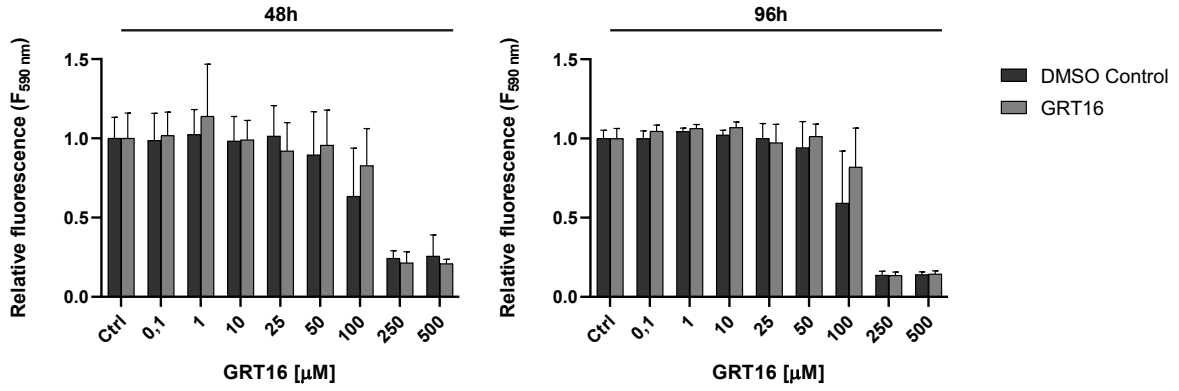

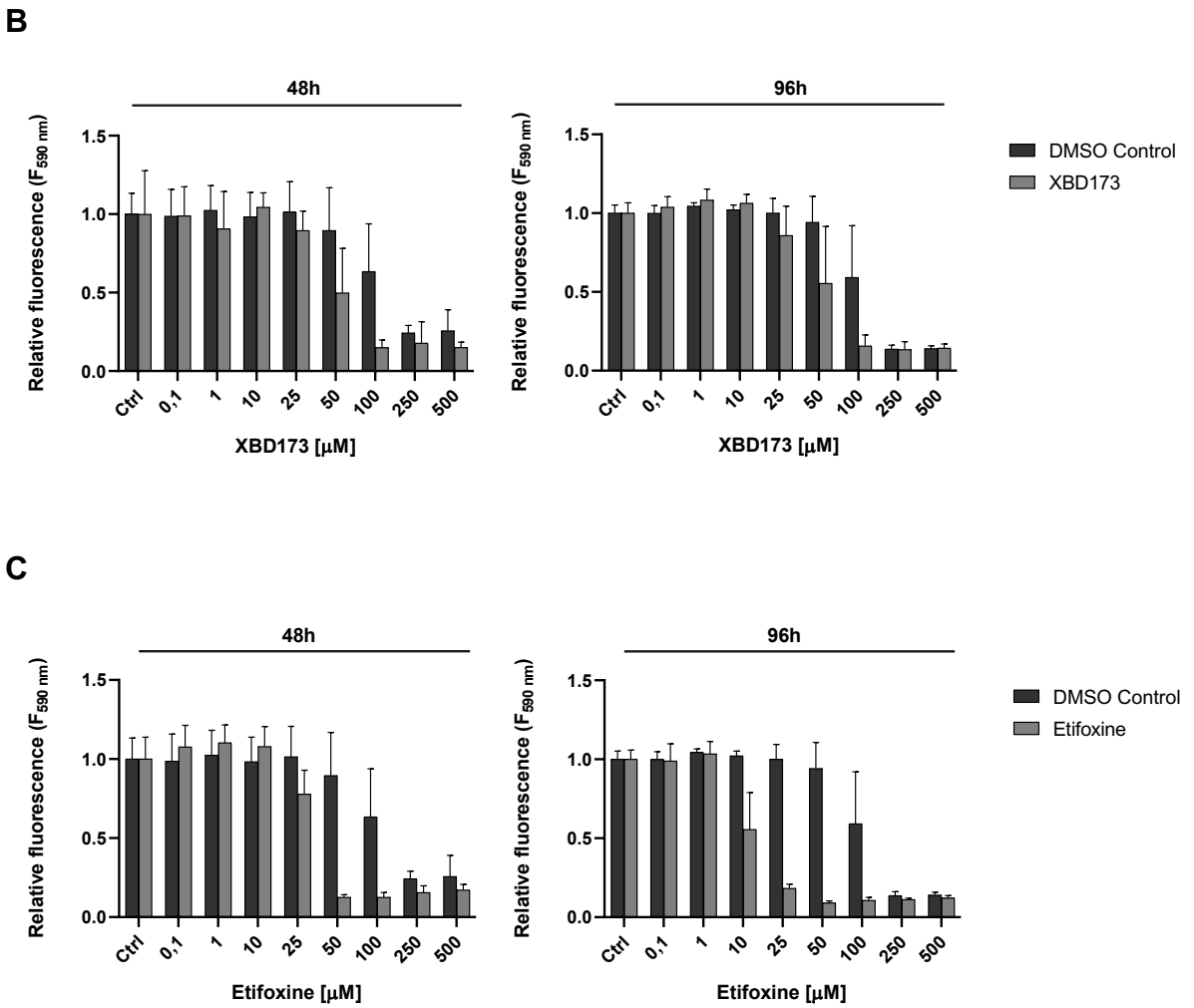

Figure 1: Cell proliferation of BTIC13 wt after TSPO ligand treatment.

BTIC13 wt were treated with 0.1 to 500 μM of **A:** GRT16, **B:** XBD173 and **C:** Etifoxine. Data are shown as ± SD (n=3).

5.2 Impact of GRT16 on cytokine expression

For the investigation of immune modulatory cytokine expression, the mRNA levels of IL-6 and IL-8 were determined. For this purpose, we examined the effects of TNFα and IFNγ treated cells after 6h and 48h, following a two-hour pretreatment with GRT16, XBD173 or Etifoxine.

Overall, treatment with the TSPO ligands did not impact the induction of IL-6 and IL-8 expression at either timepoint. IL-6 was significantly increased by TNFα, although pretreatment with either ligand could not modulate this response, neither after 6h nor after 48h. After 48h, the effect was already regressive. Contrary, the application of IFNγ led to just a small increase in IL-6 expression after 6h, which then consolidated over a time course of 48h (Figure 2A, B). Again, co-administration of IFNγ and ligands had no significant effect on IL-6 expression compared to single IFNγ treatment (Figure 2A, B). Nevertheless, a tendency of ligand-specific effects could be suspected, especially after 48h. TSPO ligands seemed to promote IL-6 expression with XBD173 having the strongest impact (Figure 2B). IL-8 secretion was induced upon activation with TNFα, reaching a maximum at the early timepoint (Figure 2C, D). After 48h, Etifoxine and GRT16 prolonged IL-8 elevation compared to single treatment with TNFα without reaching significance (Figure 2D). In contrast, IFNγ was not able to stimulate IL-8 expression.

To correlate possible effects of TSPO ligands on protein expression, mRNA levels of TSPO were measured. TSPO expression was upregulated upon cytokine stimulation after 48h. In addition, ligand-specific effects on TSPO expression after combinational treatment with IFNγ could be found, albeit without reaching significance. Nevertheless, XBD173 led to a small increase of TSPO expression that correlated with the enhanced expression of IL-8 (Figure 2F).

To elucidate if altered mRNA levels translated to protein levels, IL-6 and IL-8 were quantified in supernatants of treated cells using ELISA. Only upon TNFα treatment, a strong increase of both cytokines was observed, which is in line with our findings on the transcriptional level (Figure 2G). However, after 48h, an increase of IL-6 protein expression was detected which could not be detected at the mRNA level. In addition, IL-8 showed an increase at the protein level after treatment with TNFα, while less mRNA was transcribed after 48h.

In summary, these data showed that treatment with TNFα resulted in elevated transcription of both immune modulatory cytokines, IL-6 and IL-8, whereas IFNγ only induced IL-6. GRT16, as well as the two other TSPO ligands, could not significantly influence cytokine or TSPO expression, although further investigations are needed to substantiate the small effects seen in these first experiments.

Taken together, our results support the hypothesis that TSPO takes part in the regulation of the inflammatory response.

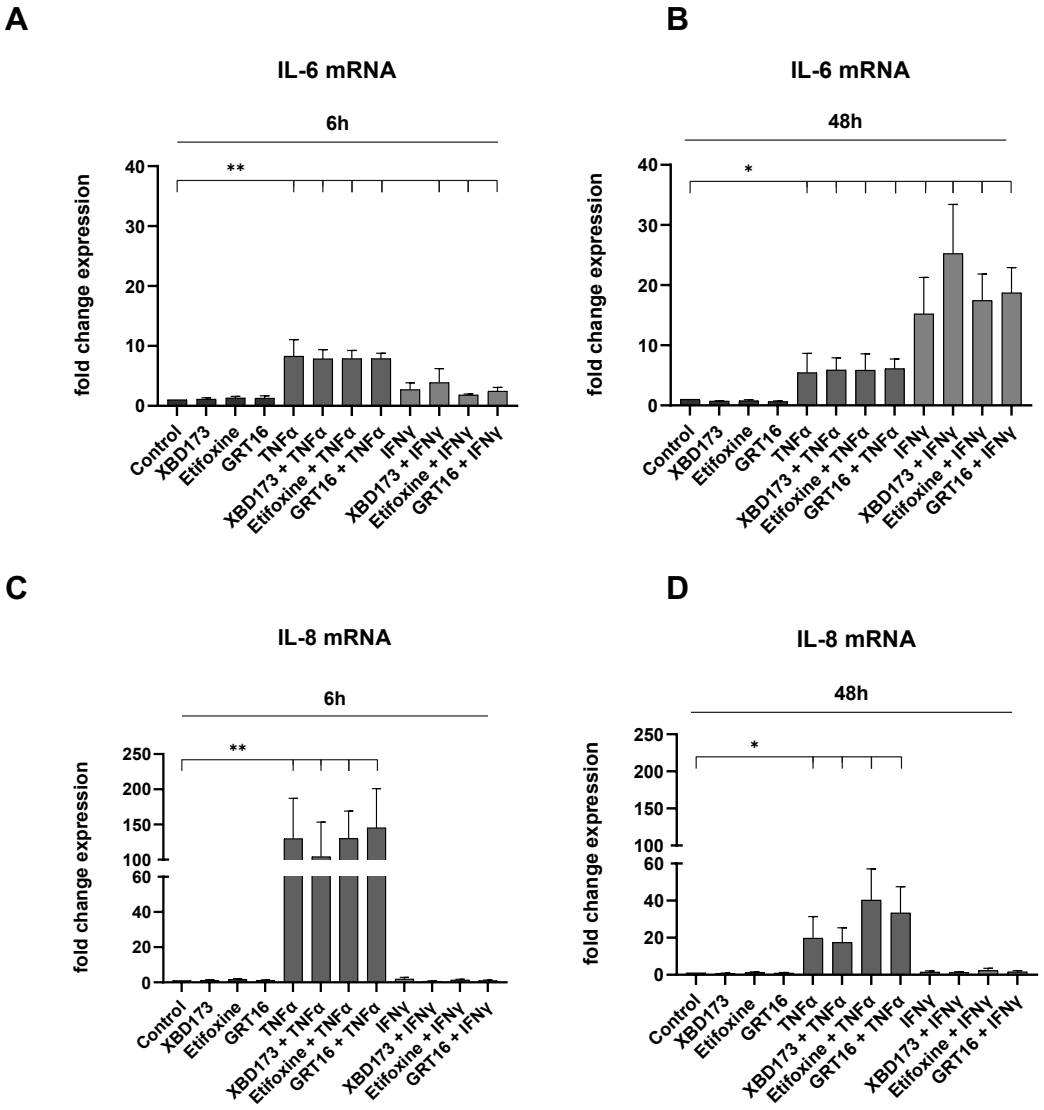

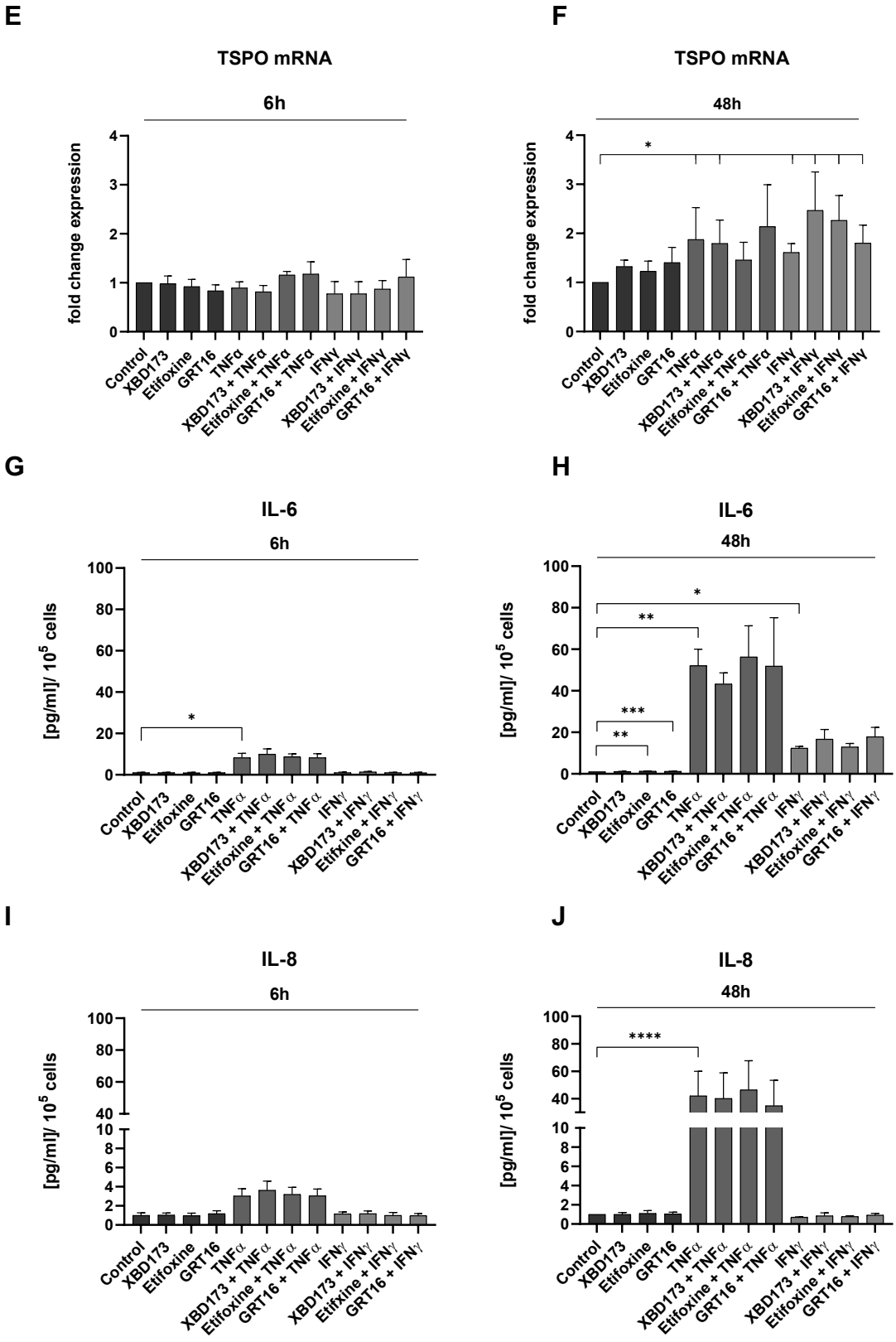

Figure 2: Impact of TSPO ligands on IL-6, IL-8 and TSPO expression after cytokine treatment.

BTIC13 wt cells were pretreated for 2h with 1 μM of XBD173, Etifoxine or GRT16, followed by 50 ng/ml of TNFα or IFNγ for another 6h. Results were set in reference to a 1:1000 dilution of DMSO as control. **A, B:** IL-6 mRNA expression; **C, D:** IL-8 mRNA expression; **E, F:** TSPO mRNA expression after 6h (n=7) and 48h (n=4). Data are shown as ± SEM. ELISA analysis of **G, H:** IL-6 and **I, J:**IL-8 expression after 6h (n=3) and 48h (n=5). Data are shown as ± SD. Student's t-test resulted in significant differences as indicated (p-values: * < 0.05; ** < 0.01; *** < 0.001; ****<0,0001).

5.3 Impact of GRT16 on mitochondrial respiration and glycolytic function

To evaluate the impact of the novel TSPO ligand GRT16 on mitochondrial metabolism, the Seahorse Analyzer was used, measuring the OCR and simultaneously different parameters of oxidative phosphorylation. That includes the dimensions of cellular respiration as represented by basal and maximal respiration, from which spare respiratory capacity was calculated as well as respiration used to drive mitochondrial ATP synthesis. Besides, the proton leak independent of the ATP synthase was determined as well as non-mitochondrial respiration after inhibition of the ETC. Treatment with GRT16 was compared to an untreated control.

After treatment with 1 μM of GRT16, no effects of the ligand could be observed except for a statistically non-significantly decreased proton leak (Figure 3 A, D). After increasing the concentration of GRT16 to 10 μM, minimal reductions of non-mitochondrial, basal and maximal respiration could be seen. The reserve capacity and the calculated ATP production were also decreased. Again, the proton leak showed slightly lower levels compared to the control (Figure 3 B, D). At 25 μM, these changes became partly significant. Basal and maximal respiration were significantly impaired when treated with GRT16. Spare respiratory capacity was significantly decreased. The calculated ATP turnover was also lower in comparison to the control. Proton leak was considerably reduced as well (Figure 3 C, D). Simultaneously to the oxygen consumption rate (OCR), the acidification of the medium (ECAR) of BTIC13 cells due to glycolysis was measured which showed a reverse baseline profile of the ECAR. The application of GRT16 at higher concentrations (25 μM) resulted in a decrease in both OCR and ECAR values.

In conclusion, GRT16 affected mitochondrial energy metabolism in a dose-dependent manner. This results in a reduction of all parameters that were investigated except for non-mitochondrial respiration, which remained comparatively unaffected.

In summary, our data point to a role of TSPO in mitochondrial respiration.

A

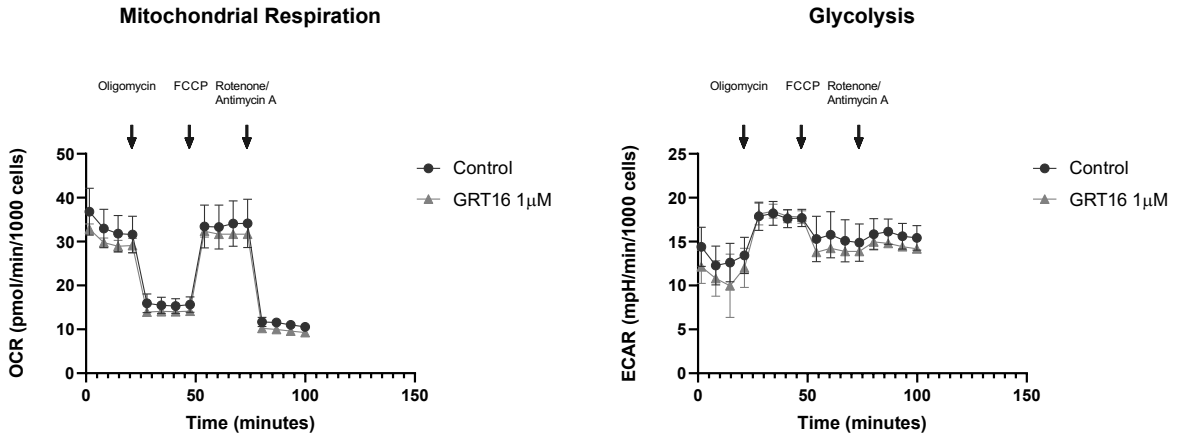
Mitochondrial Respiration
Oligomycin
FCCP
Rotenone/ Antimycin A
OCR (pmol/min/1000 cells)
Time (minutes)
Control
GRT16 1μM
Glycolysis
ECAR (mpH/min/1000 cells)
Time (minutes)
Control
GRT16 1μM

B

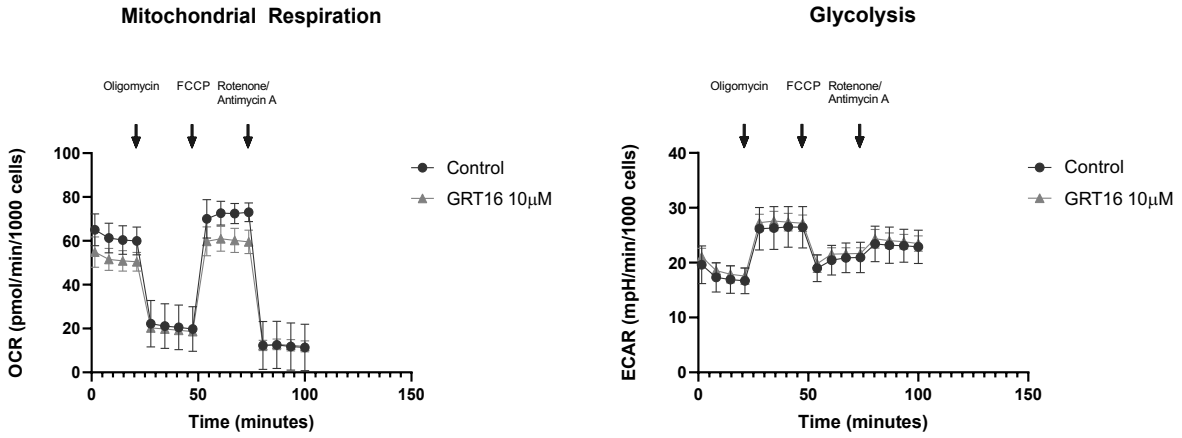
Mitochondrial Respiration
Oligomycin
FCCP
Rotenone/ Antimycin A
OCR (pmol/min/1000 cells)
Time (minutes)
Control
GRT16 10μM
Glycolysis
ECAR (mpH/min/1000 cells)
Time (minutes)
Control
GRT16 10μM

C

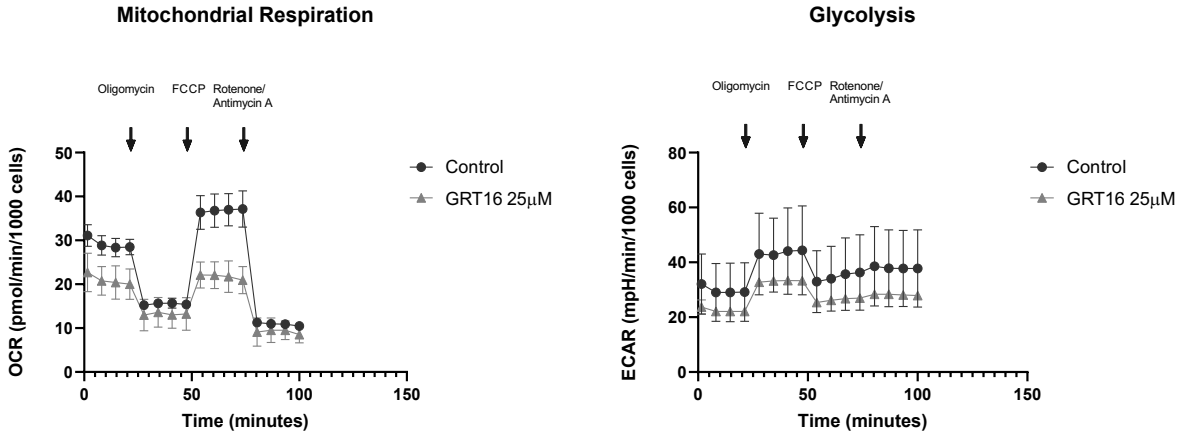
Mitochondrial Respiration
Oligomycin
FCCP
Rotenone/ Antimycin A
OCR (pmol/min/1000 cells)
Time (minutes)
Control
GRT16 25μM
Glycolysis
ECAR (mpH/min/1000 cells)
Time (minutes)
Control
GRT16 25μM

D

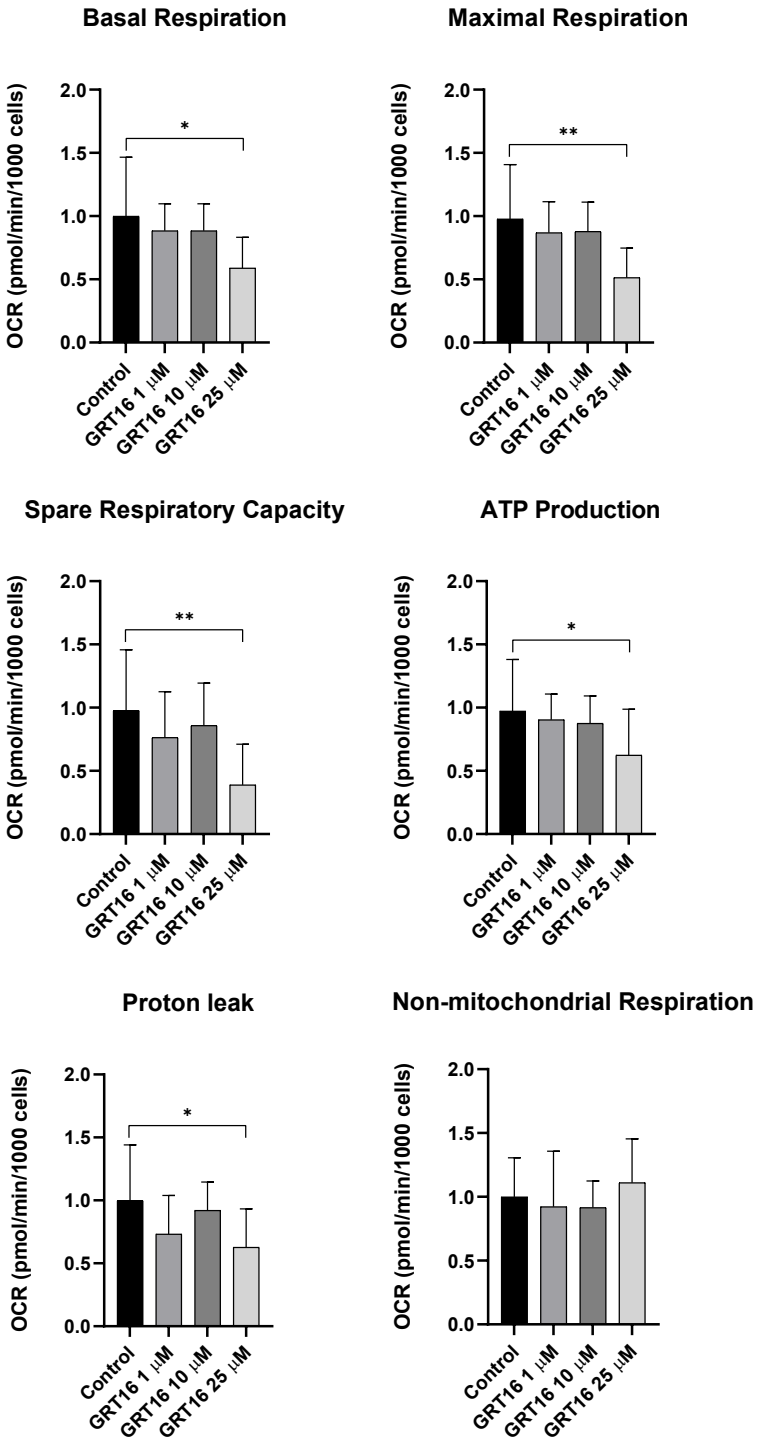

Figure 3: Seahorse Cell Mito Stress Test of BTIC13 wt.

BTIC13 cells were treated with 1, 10 and 25 μM of GRT16 for 2h. DMSO diluted 1:1000 in RHB-A complete medium was used as untreated control. Sequential injections of inhibitors of the electron transport chain (ETC) were applied. Oligomycin (1 μM) was used for inhibition of the ATP synthase, FCCP (2 μM) as an uncoupling agent and Rotenone/Antimycin A (0,5 μM) as an inhibitor of complex I and III of the ETC. Simultaneously the oxygen consumption rate (OCR) and the extracellular acidification rate (ECAR) were constantly measured over time. Seahorse raw data were normalized to 1000 cells. Displayed graphs are exemplary for three replicates (n=3). **A:** OCR and ECAR GRT 1 μM. **B:** OCR and ECAR GRT 10 μM. **C:** OCR and ECAR GRT16 25 μM. **D:** Parameters of mitochondrial respiration (n=3). Data are shown as mean ± SD. Two-Tailed Student's t-test resulted in significant differences as indicated (p-values: * < 0.05; ** < 0.01).

5.4 Impact of GRT16 on the production of reactive oxygen species

To investigate the possible effect of GRT16 and XBD173 on the synthesis of ROS, the H2DCFDA assay was used. For this known ROS inducers, namely $CoCl_2$ and TNFα, were added to the cells after a two-hour pretreatment with the ligands.

Overall, treatment with GRT16 as well as XBD173 did not impact ROS production, regardless of concentration or time-point (Figure 4 A- F). Small changes seen at the later timepoints (24h and 48h, Supplementary figure S6 A- C) did not consolidate when higher concentrations were used, which suggests that the effects are not concentration-dependent and probably off-target effects.

In addition, we confirmed that $CoCl_2$ strongly induces the synthesis of ROS, however, none of the ligands significantly influenced this effect (Figure 4 A, C, E). In contrast to $CoCl_2$, TNFα did not lead to an increased production of ROS (Figure 4 B, D, F). Even after 24h and 48h, TNFα didn't increase the amount of reactive oxygen species (Supplementary figure S6 A-C).

In summary, treatment with the TSPO ligands GRT16 and XBD173 did not lead to changes in the amount of ROS in any of the conditions investigated, questioning the role of TSPO on ROS synthesis.

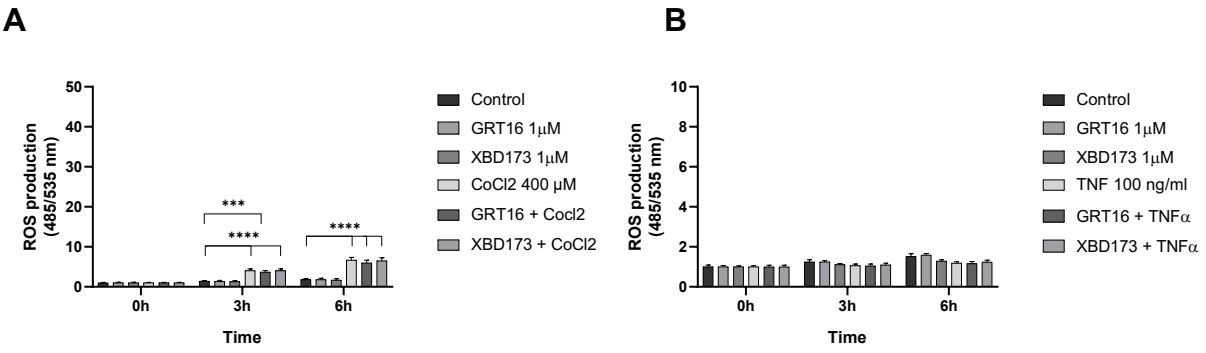

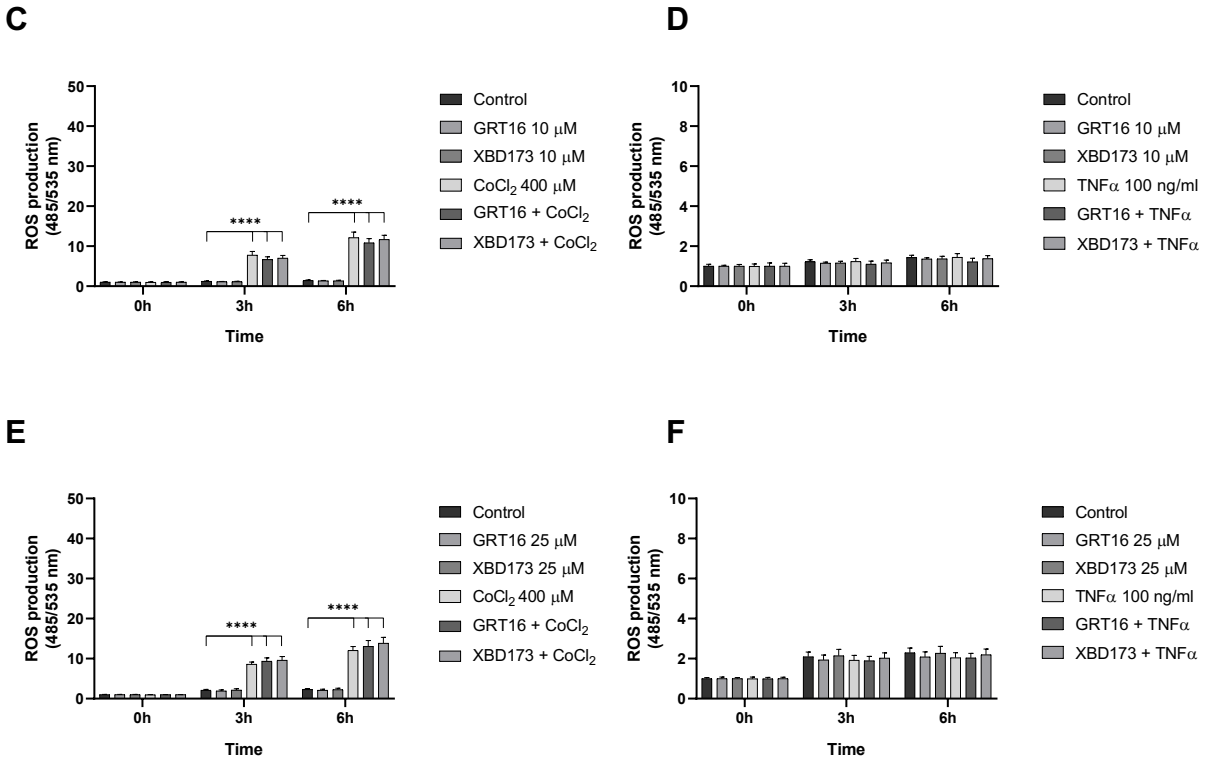

Figure 4: Impact of TSPO ligands on ROS formation in BTIC13 wt.

BTIC13 cells were pretreated with XBD173 and GRT for 2h, followed by 400 μM of $CoCl_2$ or 100 ng/ml TNFα. **A:** 1 μM of XBD173 and GRT16 (n=4), **B:** 10 μM of XBD173 and GRT16 (n=3), **C:** 25 μM of XBD173 and GRT16 (n=3). Data are shown as ± SEM. Two- way ANOVA with Tukey's multiple comparison resulted in significant differences as indicated (p-values: * < 0.05; ** < 0.01; *** < 0.001; ****<0,0001).

5.5 Impact of GRT16 on apoptosis

To investigate the effect of GRT16 on apoptosis, the established “death ligand” tumor necrosis factor related apoptosis inducing ligand (TRAIL) was applied alone or in combination with TSPO ligands GRT16, XBD173 or Etifoxine.

The effects were first monitored via Western Blot. Therefore, the cells were pretreated for 2h with 1 μM of GRT16, XBD173 or Etifoxine. Following this, TRAIL was added and after 3h and 6h, activation of apoptosis was evaluated. Cleavage of caspase 9 was used to monitor the activation of the intrinsic apoptotic pathway. The common end pathway of both signaling pathways (extrinsic and intrinsic) is the activation of effector caspases 3 and 7, leading to the fragmentation of death substrates like PARP. Caspase 3 and PARP were therefore used to monitor execution of apoptosis.

After 3h, activation of caspase 9 by TRAIL treatment could be observed. However, no significant impact of TSPO ligands was seen. Downstream signaling, as seen by caspase 3 and PARP cleavage, was activated by TRAIL as well. Here, pretreatment with TSPO ligands led to a significant increase in the amount of caspase 3 and PARP cleavage products (Figure 5 A, C). After 6h these effects were no longer visible (Figure 5B).

To validate the results with a complementary method, cell viability was visualized and analysed by means of live cell imaging using IncuCyte® ZOOM systems, over a time course of 48h. Here, the activity of caspase 3 and 7 was monitored. Again, cells were pretreated with 1 μM of ligands. For the induction of cell death, TRAIL was added in the same concentration as before (50 ng/ml). Cells pretreated with the ligands showed higher TRAIL-induced apoptotic rates compared to single TRAIL treatment, although the results did not reach statistical significance (Figure 5D).

The data show that treatment with TSPO ligands alone had no pro-apoptotic effect on BTIC13 cells. However, it could be assumed that they do promote the effects of pro-apoptotic substances.

In conclusion, we can confirm that TSPO influences apoptotic cell death in glioblastoma cells.

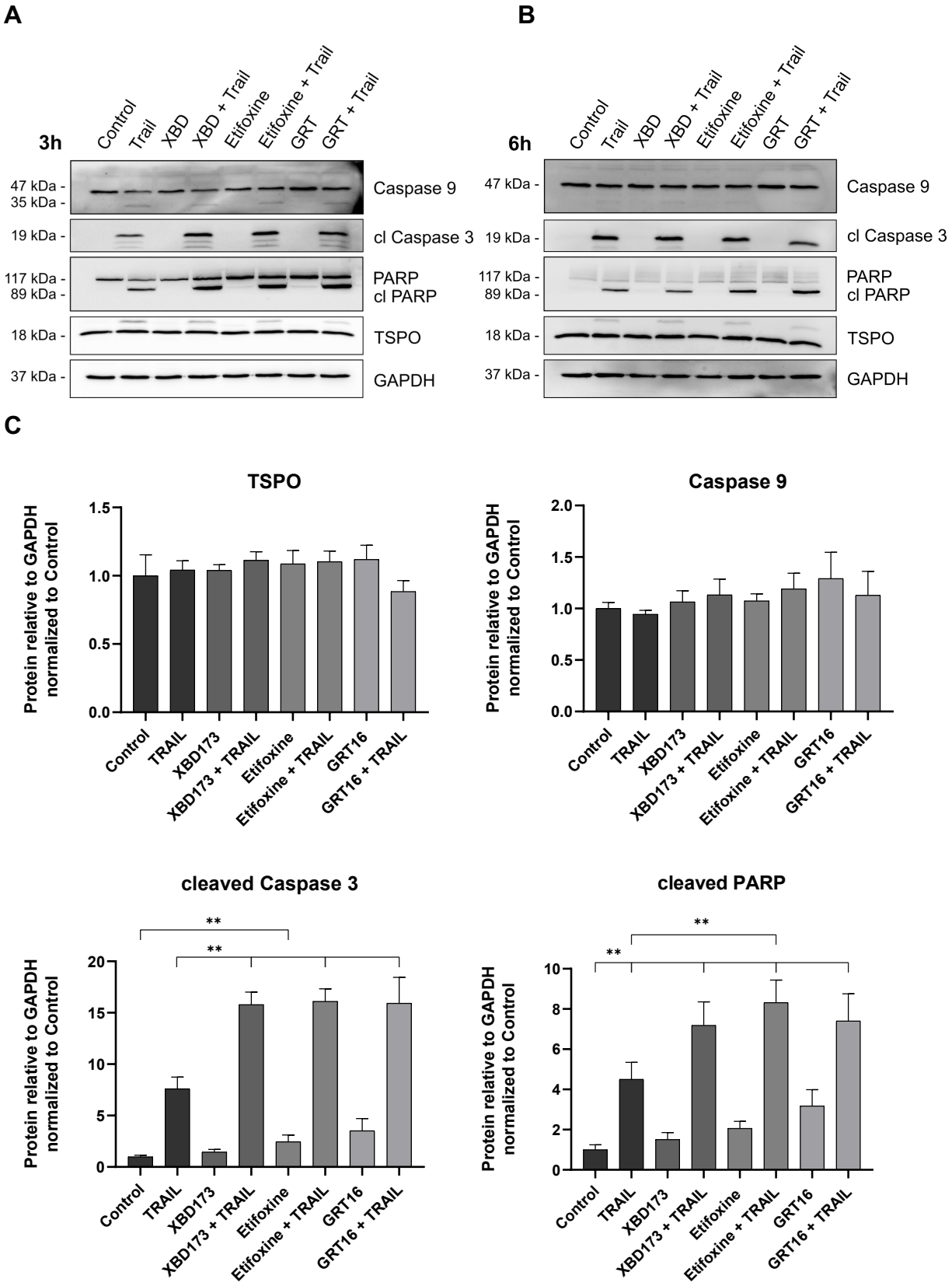
A
3h
Control
Trail
XBD
XBD + Trail
Etifoxine
Etifoxine + Trail
GRT
GRT + Trail
47 kDa -
35 kDa -
Caspase 9
19 kDa -
cl Caspase 3
117 kDa -
89 kDa -
PARP
cl PARP
18 kDa -
TSPO
37 kDa -
GAPDH
B
6h
C
TSPO
Caspase 9
cleaved Caspase 3
cleaved PARP
Protein relative to GAPDH normalized to Control
Control
TRAIL
XBD173
XBD173 + TRAIL
Etifoxine
Etifoxine + TRAIL
GRT16
GRT16 + TRAIL
**

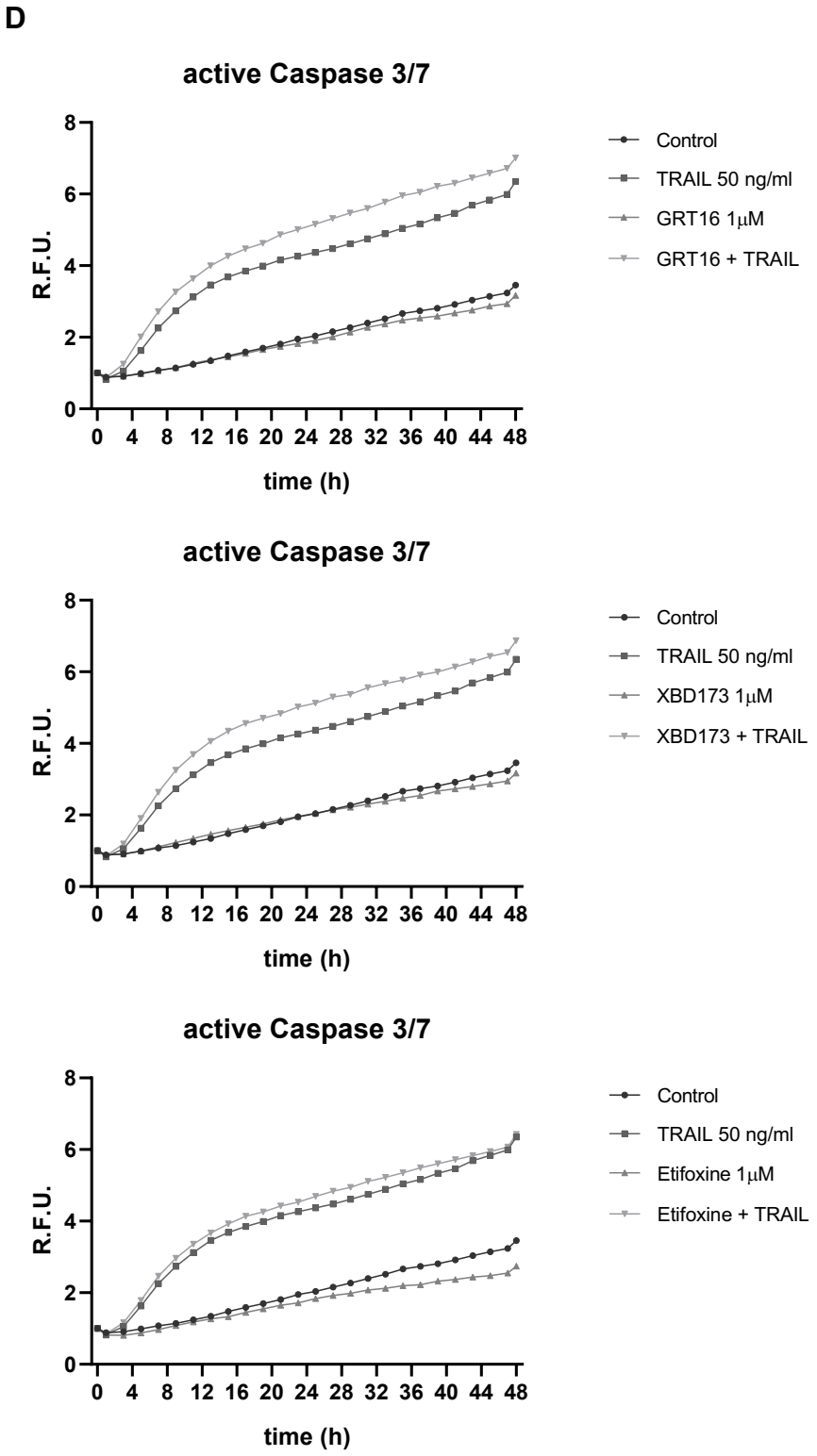

Figure 5: Impact of TSPO ligands on TRAIL-induced apoptosis in BTIC13 wt.

BTIC13 wt cells were pretreated with 1 μM of GRT16, XBD173 or Etifoxine for 2h, followed by 50 ng/ml of TRAIL. DMSO diluted 1:1000 in RHB-A complete medium was used as untreated control. **A:** Quantification of protein expression levels of TSPO, caspase 9, cleaved caspase 3 and cleaved PARP after 3h and **B:** 6h. **C:** Protein quantification after 3h. Data are shown as mean ± SEM (n=6). In each graph values are displayed in relation to the reference protein GAPDH and normalized to untreated control. Two-tailed Student's t-test resulted in significant differences as indicated (p-values: * <0.05; ** <0.01; *** <0.001). **D:** Real-time cytotoxicity was measured for 48h with IncuCyte® ZOOM systems. Displayed graphs are exemplary for three replicates (n=3). Unpaired two-tailed t-test resulted in no significant differences.

6 Discussion

Malignancies are the second leading cause of death in the Western world, surpassed only by cardiovascular diseases [191]. In recent years, great progress has been made in the field of screening and therapy [192], which could well reduce the prevalence and mortality of some cancers [193] [194] [191]. However, this does not apply to all entities in the same manner. Especially regarding glioblastoma, prognosis and median overall survival remain limited, even though the latest additions to treatment options have brought improvements [88] [195]. As TSPO is expressed in a variety of cell populations within the tumor [16], pharmacological approaches to modulate TSPO activity could therefore be a promising immunotherapeutic strategy in glioblastoma cells.

6.1 Impact of TSPO ligands on proliferation

Inhibition of proliferation represents a promising approach to cancer control. In healthy tissue, proliferation is a tightly regulated process. However, in degenerated cells, these control mechanisms are overridden to allow cancer cells to proliferate unchecked [66]. Therefore, proliferation gained entry into the “hallmarks of cancer”, a concept that summarizes the six central properties of neoplastic cells in carcinogenesis [66]. Hence, we analysed the effects of TSPO ligands on cell proliferation of BTIC13 wt cells.
Our investigations revealed that neither GRT16, nor XBD173, nor Etifoxine have an impact on cell proliferation at nanomolar concentrations. As for GRT16, we were able to determine an IC50 value of 105.1 μM. The IC50 values for XBD173 and Etifoxine were significantly lower compared to GRT16 (43.6 μM vs. 105.1 μM and 26.5 μM vs. 105.1 μM). In contrast, the binding affinities in human U-118MG glioblastoma cells were 4.6 μM for GRT16 and 10 μM for Etifoxine [156], and thus significantly lower than the IC50 values for both compounds. This was also seen for XBD173, as the IC50 value was well above the 2.73 nM that was found to be the binding affinity of XBD173 in Hs683 human glioma cells [162]. When investigating the C6 rat glioma cell line, Wolf et al. reported an even higher binding affinity of XBD173, namely 0.14 nM [196]. Albeit different species, a possible explanation for the different binding affinities could be the distinction between high-, mixed-, and low-affinity binders, which could be of great relevance regarding clinical application [197]. Especially considering the mismatch

between binding affinity and ligand efficacy, further characterization of individuals would be important to optimize pharmacodynamics and to avoid under- or overdosing. The study conducted by Wolf et al. revealed an inverse relationship between binding affinity and potency, comparing XBD173 to Etifoxine. In both cell lines investigated, C6 rat glioma and BV-2 microglial cells, XBD173 had lower K_i values (C6: 0.14 nM vs. 0.75 nM, BV-2: 0.16 nM vs. 22.8 nM) but Etifoxine showed higher efficacy regarding neurosteroid synthesis [196]. It was suggested earlier that binding affinity does not necessarily correlate positively with the potency and efficacy of TSPO ligands but rather depends on residence time at the binding site [198] [199].

Noteworthy, binding affinity is also species-, tissue-, and cell-dependent. Whereas for the above-mentioned C6 cell line it was in the nanomolar range, Verleye et al. investigated rat forebrain. Their results showed a K_i value of 18.3 μM for Etifoxine [200], which is largely comparable to latest results in human brain, showing a K_i value of 7.8μM [201]. The same was demonstrated for GRT16, as the *Ki* for rodent heart was 0.07 μM, evidencing a higher affinity than in U-118MG cells (4.6μM) [202]. Since we have not conducted any research on binding affinity, no statement can be made about the possible discrepancy between efficacy and binding affinity in BTIC13. However, if we assume that the binding affinities between U-118MG and BTIC13 are comparable, the only moderate affinity to U-118MG cells could provide a reason for the high IC50 in BTIC13.

The pharmacological safety profile of GRT16 was evaluated by determining plasma concentrations in rats after GRT16 application. Doses between 10 and 100 mg/kg p.o. led to plasma concentrations between 1.5 ± 0.2 μM and 2.6 ± 0.3 μM (mean ± S.D.), respectively [156]. The group around Verleye et al. used a mouse model to investigate the concentrations that could be achieved *in vivo*. For this purpose, they injected 25-50 mg/kg Etifoxine intraperitoneally and subsequently determined the concentrations in the plasma and the brain. There, concentrations in the micromolar range (3- 17μM) were found [200]. The amounts (25-50mg/kg) were widely used in subsequent studies. Hence, it can be assumed that concentrations in the micromolar range are well tolerated without serious complications [203] [204]. Nevertheless, when GRT16 was tested as anticonvulsant *in vivo* with dosages of 10, 30 and 100 mg/kg, a dose-dependent reduction of body temperature was reported. Further, at 100 mg/kg, ataxia and hypclomotion were described [202]. Even when taking into account a

bioavailability of 73%, the IC50 value of GRT16 was significantly higher than the plasma concentrations of 2.6 μM, where side effects were already reported [156]. Therefore, a physiological concentration can no longer be assumed, and adverse effects must be expected.

Regarding the general role of TSPO in cell growth, the debate is controversial. TSPO overexpression has previously led to increased proliferation in the C6 rat glioma cell line [135]. This is in line with transfected Jurkat cells, overexpressing TSPO, where a higher rate of proliferation and motility was detected, probably as a result of increased mitochondrial ATP production [205]. It is worth mentioning that initial TSPO expression levels in the C6 rat glioma cell line were higher than in the transfected Jurkat cells. Different behaviours due to initial differences in TSPO expression levels could therefore not be excluded and a comparison of the results should be done with caution. Nevertheless, also Bader et al. were able to detect a positive correlation between TSPO expression and cell growth. There, lentiviral knockdown resulted in a decreased proliferation rate in mouse BV-2 microglia cells [124]. This was recently confirmed by another group using the same cell line [206]. In contrast, Fu Y. et al. recently found an increase in proliferation after CRISPR/Cas9 TSPO gene knockout in a glioma mouse model, that could be explained by cell cycle progression. When comparing wild-type cells with TSPO KO, more cells were found in the S phase and fewer in the G0/G1 phase [137]. These findings were in line with investigations done by Bode et al. using U118MG glioblastoma cells [136].

Due to the different results regarding the role of TSPO in different cell lines, it is difficult to make a general statement about the ligands. In BTIC13 wt, all three ligands inhibit proliferation when applied in the micromolar range (GRT16: 105.1 μM, XBD173: 43.6 μM Etifoxine: 26.5 μM), which is consistent with the majority of findings in glioblastoma cell lines. However, in future studies, the experiment should be repeated with knockout cells to exclude possible off-target effects and to distinguish specific effects of ligand treatment.

6.2 Impact of TSPO ligands on cytokine expression

A substantial body of literature is based on the assumption that TSPO gene expression is upregulated in neuroinflammation, which is why TSPO is widely used as a PET imaging marker in this context [154], although the role of the protein in immunological

responses has not fully been elucidated. It is also known that by creating an immunosuppressive environment, malignant cells prevent interaction with cytotoxic T cells and thus prevent targeting the tumor (as reviewed in [207] [208]).

We therefore investigated the involvement of TSPO in immunological modulation, using BTIC13, which were previously described to express mitochondrial TSPO (DFG Proposal: Beckhove & Hau, 2019). Preliminary results suggested that TSPO influences the release of immunomodulatory cytokines. Using TSPO knockdown BTICs, our group was able to demonstrate that the response of IL-6 was inversely related to the degree of TSPO deficiency, establishing an interplay between TSPO and IL-6 (DFG FOR2858, Project A3, Beckhove & Hau, 2019 and 2023). Our evaluation focused on the release of IL-6 and IL-8, which have been linked to progression of GB by promoting tumor growth, invasion, and neovascularisation [209] [210] [211] [212]. As it was shown that the release of TNFα as well as IFNγ influence the microenvironment of GB [213] [214] [152], we investigated the potential of TSPO ligands to regulate the inflammatory response of GB cells upon TNFα and IFNγ-induced activation.

In response to stimulation with TNFα and IFNγ, mRNA expression of IL-6 was increased in BTIC13 cells, which was also translated into altered protein expression. While TNFα was responsible for an increase after 6h, IFNγ-induced IL-6 releases reached a maximum at the later timepoint of 48h. Pretreatment with TSPO ligands did not have any significant influence in this regard. A possible correlation could be suspected as XBD173 pretreated cells secreted slightly higher levels of IL-6 with simultaneously increased TSPO levels. IL-8 expression could solely be induced upon TNFα activation. A significant increase of IL-8 mRNA expression was observed within the first hours, which was still noticeable after 48h but to a lesser extent.

TSPO ligand treatment was able to modulate this response, but not statistically significant compared to single TNFα stimulation. This suggests that TNFα exerts its effects on pro-inflammatory cytokines faster after exposure and is primarily responsible for early inflammatory responses, while the maximum effect of IFNγ is reached at a later timepoint.

Both, TNFα and IFNγ led to an increased TSPO mRNA expression as was shown previously in several BTIC cell lines. Further analysis revealed a positive correlation between TSPO and TNFα/ IFNγ genes, hypothesizing that both signaling pathways play a role in increasing TSPO expression upon contact with cytotoxic T cells [152].

The results are contrary to studies in primary human myeloid cell lines, where pro-inflammatory stimulation led to decreased TSPO gene expression in monocyte-derived macrophages [215]. In line with these findings are the results obtained by Narayan et al., who showed that human monocyte-derived macrophages, activated to the pro-inflammatory M1 phenotype, had decreased levels of TSPO mRNA and protein levels, whereas, within the M2 phenotype, levels of TSPO were not altered upon activation [146]. However, rodent myeloid cells showed an increase in TSPO gene expression upon IFNγ/ LPS activation [215], which was also observed in human microglia [148]. These controversies point to cell line- and also species-dependent effects.

Taken together, we can confirm that TSPO upregulation is induced by TNFα and IFNγ and that pro-inflammatory stimulation also leads to cytokine secretion, as was shown previously. In T98G and U87-MG, two GB cell lines, an increase of pro-inflammatory cytokine levels was observed upon TNFα stimulation, which is in agreement with our findings. However, activation by IFNγ only increased IL-8 mRNA expression in T98G cells [216], as opposed to only IL-6 in our experiments, hinting again at the heterogeneity within GB cells.

Nevertheless, the cytokine release could not be influenced by GRT16, XBD173 or Etifoxine. This is in contrast to *in vitro* and *in vivo* studies, showing a dose-dependent inhibition of IL-6 in retinal microglial cells after treatment with XBD173, thus inducing a less inflammatory state [160] [217]. Similarly, XBD173 downregulated pro-inflammatory mRNA expression of multiple cytokines in retinal epithelium cells, with IL-8 being the only one to increase [218]. Etifoxine also reduced pro-inflammatory signaling as shown by reductions of IL-6, TNFα and IL-1 β in an ischemia/reperfusion model [219], without affecting the anti-inflammatory response [220]. In addition, Etifoxine impaired lymphocyte infiltration in a mouse model of multiple sclerosis, [221]. Of note, to the best of our knowledge, no studies with the above discussed TSPO ligands have been conducted using glioblastoma cells and as mentioned before, the high cell and species dependency does not allow any comparability of the results.

Based on our experiments, no clear statement can be made whether TSPO ligands have an influence on the release of immunomodulating interleukins. It can be stated that all three ligands have no effect on TSPO expression at an early timepoint. However, it is still possible that they would exert inhibitory effects at elevated TSPO levels. Since TSPO levels only increased significantly after 48h, therapy with ligands

would only show an effect after this increase. On the other hand, IL-6 and IL-8 both increased prior to TSPO, questioning the influence of TSPO and consequently also the effectiveness of TSPO ligands on these interleukins. Further evaluation, using higher dosages and multiple timepoints, is required to exclude the possibility that the small effects, seen after 48h, are based on variability within the experiment.

6.3 Impact of TSPO ligands on mitochondrial respiration

Even though the exact mechanism of action is not fully established yet, there is evidence linking TSPO to cellular energy production.

GSCs are metabolically flexible cells that can survive in extreme conditions marked by an abundance of hypoxic areas, necrosis and stressors such as radiation [49]. One of the main problems in the fight against glioblastomas continues to be the complete eradication of all cells, especially GSC. Therefore, a profound understanding of metabolic activity would be a possible therapeutic approach to address especially these cells.

To analyse real-time bioenergetic changes upon TSPO modulation, we used the Seahorse technology to compare control cells vs. cells that were treated with a TSPO ligand prior to the experiment. We demonstrated that GRT16 significantly impaired mitochondrial respiratory capacity and energy metabolism at a dosage of 25 μM, leading to a reduction of basal and maximal respiration as well as spare respiratory capacity and ATP synthesis-related oxygen consumption. Additionally, proton leak was significantly impaired, whereas non-mitochondrial respiration was not influenced.

This is in line with a study using TSPO depleted mouse GL261 glioma cells. TSPO knockout was shown to lead to a reduced ATP synthesis and impaired basal and maximal respiration [137]. A possible explanation for a decreased ATP synthesis could be the inhibition of the F_o/F_1-ATP synthase, which has been proposed previously [222] [223]. Considering these findings, GRT16 would show an antagonistic mode of action.

Apart from glioblastoma cells, a correlation between TSPO, mitochondrial respiration and cellular energy metabolism has been established in multiple types of tissue. Since TSPO is predominantly expressed in immune cells and especially upregulated under inflammatory conditions [120], a multitude of investigations focused on TSPO functioning in microglia cells, where an interplay between TSPO and mitochondrial respiration could be established. In XBD173 treated BV-$2_{scramble}$ mouse microglia cells,

a significant increase of basal respiration as well as a decrease of maximal respiration and spare respiratory capacity could be seen, pointing to an impaired respiration. When comparing control BV-$2_{scramble}$ to $TSPO_{knockdown}$ cells, the opposite effect was observed, namely increased maximal and spare respiratory capacity, substantiating the TSPO agonistic properties of XBD173.

Further experiments on oxidative phosphorylation and membrane potential revealed that TSPO led to a diminished energy demand, which corresponded with reduced ATP utilisation [224]. These results are contrary to the results of Milenkovic et al., who found no differences in mitochondrial respiration when comparing human C20 scramble control with shRNA TSPO knockdown cells. However, TSPO knockout cells displayed significantly impaired mitochondrial respiration, as shown by decreases in basal and maximal respiration as well as reduced ATP-related oxygen consumption [129]. Especially, in case of mitochondrial dysfunction, reduced ATP-linked respiration can also reflect the impairment to generate membrane potential [225], which is influenced by the degree of TSPO deficiency [206]. By lentiviral TSPO overexpression, these parameters could be restored to prior levels [129]. A recent study, using primary microglia from TSPO knockout mice, confirmed these earlier findings. TSPO deficiency significantly impaired mitochondrial respiration, as evidenced by a reduced OCR. This was reflected in decreased levels of basal and maximal respiration as well as impaired mitochondrial membrane defects as an expression of respiratory chain defects [206] [226].

In contrast to genetic knockout, the group around Liu GJ investigated a gain-of-function approach, transfecting Jurkat cells with TSPO plasmids, that increased genes affecting respiration and ameliorated ATP production [205]. This is in line with the investigations of Banati et al., who reported a reduced ATP production and accordingly decreased oxygen consumption in $TSPO^{GuwiyangWurra}$-knockout mice in comparison to control microglia [178]. Interestingly, in steroidogenic MA-10 Leydig cells, TSPO KO did not affect mitochondrial respiration and the oxygen consumption rate was not impaired [227]. Since MA-10 cells have high, basal TSPO expression, one would have expected that its deficiency would cause a significant effect. The same result was seen in mouse $TSPO^{-/-}$ and control liver mitochondria that showed no difference in OCR compared to control cells [228], questioning the role of TSPO on mitochondrial respiration.

The Seahorse technology allowed us to simultaneously assess the ECAR to test for compensatory energy pathways. By comparing the reduced ECAR baseline to the

OCR values of the control, the results allude to a favoured use of oxidative phosphorylation rather than glycolysis in BTIC13. However, as OCR and ECAR are not quantitatively related to a metabolic flux, the lower ECAR seen in our study is not necessarily the result of a decreased glycolysis [229]. With impaired mitochondrial respiration, an increase in glycolysis might have been expected to sufficiently supply the cell with energy, as also observed by Fu et al. in mouse GL261 glioma cells [137]. However, based on our results, no conclusion can be drawn about the influence of TSPO on glycolysis. Further, more glycolysis-specific studies should be pursued to be able to make reliable statements about the impact of the protein on glycolytic functioning in BTIC13 wt cells.

6.4 Impact of TSPO ligands on oxidative stress

Many cancers make use of altered redox homeostasis to maintain a pro-tumorigenic environment (as reviewed in [69] [94]). However, ROS are not generally detrimental to the cell and also play a relevant role in various signaling pathways, including inflammation and cell death.

Previous studies indicated a direct link between TSPO and ROS production through T-cell-derived TNFα to create an inflamed environment [230]. Since its discovery decades ago, TNFα has been attributed to playing a central role in cell proliferation and apoptosis [231]. It influences a wide variety of signaling pathways, which, amongst other mechanisms, also induce reactive oxygen species in healthy tissue (as reviewed in [232]) as well as in glioblastoma cells [233]. ROS in turn also influences TNFα downstream signaling pathways, in the form of a feedback loop via NFκB [234] and MAPKs [235].

For our investigations, we therefore chose TNFα and $CoCl_2$ for the induction of ROS. Surprisingly, TNFα did not induce ROS in our experiments, even though their interdependence has been well established, which could point to a resistance mechanism within the cells. With reference to the positive controls, we exclude the possibility that technical problems in the experimental procedure were the reason for this effect. In contrast to TNFα, $CoCl_2$ significantly increased ROS synthesis, which is in line with previous findings in glioblastoma cell lines [131] [236].

As the above-mentioned reduction of the spare respiratory capacity indicated an impaired ability to respond to oxidative stress, we further analysed ROS production to evaluate whether treatment with TSPO ligands could influence ROS generation. However, co-treatment with GRT16 could not modulate ROS release. Similarly, co-treatment with XBD173 showed no clear response to ROS synthesis in $CoCl_2$-challenged cells, even when 25 μM was used. Since the effects seen with GRT16 at increasing concentrations were inconsistent, it is reasonable to assume that these were off-target effects. A similar study previously showed in BV-2 cells that pretreatment with PK11195 did not prevent ROS induction by $CoCl_2$, although an influence of $CoCl_2$ as well as PK11195 on TSPO expression had previously been shown [237]. Of note, the influence of $CoCl_2$ on TSPO levels is concentration-dependent, with higher concentrations increasing and lower concentrations decreasing TSPO expression [131]. However, several studies have proven that TSPO ligands were able to affect ROS production in different cell lines [238] [239] [230] [240] [241] [237]. Recently, the interdependence of TSPO and ROS was also supported in a glioblastoma cell line, as *in vivo* experiments evidenced that XBD173 successfully attenuated ROS production [242].

Aside from the investigation in glioblastoma cells by Jiang et al., the effect of XBD173 on reactive oxygen species has been extensively studied in other cell lines. In human ARPE-19 cells from the eye, XBD173 was found to decrease intracellular levels of ROS [218]. This finding is in line with a study investigating primate choroidal endothelial cells (RF/6A). 25 μM of XBD173 notably reduced intracellular ROS formation and improved antioxidant capacity, as shown by an increase in selected antioxidative genes and also in catalase activity [142]. Noteworthy, both studies treated the cells for 24h with TSPO ligands, as opposed to our two-hour pretreatment. However, in activated C20 human microglia cells, a 2h treatment with TSPO ligands, including XBD173 and Etifoxine, did cause a reduction of intracellular ROS [148]. Yet, in stimulated primary retinal mouse microglia, changes in mitochondrial or cytosolic ROS were not detected upon XBD173 treatment. Nonetheless, a reduction of extracellular ROS was detected, suggesting a more differentiated approach for the investigation of ROS.

The same group evidenced that oxidative stress was related to NOX1 [217]. The NOX family is a key mediator in the production of ROS [243] and it has been proposed that their functioning is TSPO-dependent. In glioblastoma cells, a TSPO dependency of

NOX4 was suggested as TSPO-deficient cells showed a reduced ROS synthesis as a result of attenuated NOX4 [242]. Besides NOX4, other oxidases have been associated with TSPO [244] [245] [133] [217].

In summary, the obtained results do not confirm that pharmacological TSPO modulation regulates the production of ROS in GB progenitor cells, thereby questioning the role of TSPO in the regulation of ROS. However, TNFα, a well-known ROS-inducer, did also not exert the expected effects, pointing into direction of a possible resistance. The selected dosage was based on preliminary studies in glioblastoma cells, albeit the plasticity of the tumour has already been pointed out several times, in which case a re-evaluation would have been advisable. The H2DCFDA assay used in this study is commonly used for the detection of intracellular ROS, although it is known that the assay has several limitations. Notably, reactive species reduce DCFDA to DCF, which can in turn react with O_2 to form superoxides, causing artificial fluorescence increase. One of these oxidizing substrates is cytochrome c, which means that signal intensity is enhanced during apoptosis [246].

To gain deeper insight into redox metabolism and to establish whether GRT16 influences extracellular ROS, additional analysis should be performed. Future approaches should include TSPO-deficient cells to differentiate TSPO-specific effects. The inconsistency of results might also reflect a lack of involvement of TSPO in the pathways involved in oxidative stress or limited capacity of the ligands to protect from oxidative stress. This urges further investigations regarding the regulation of ROS in BTIC13.

6.5 Impact of TSPO ligands on apoptosis

Characteristic for malignant cells is the interference of regulated cell death [66]. For apoptosis, a distinction is made between the extrinsic pathway, which is mediated via death receptors (DR), and the intrinsic pathway. The latter is also known as the mitochondrial pathway, of which the central step is mitochondrial outer membrane permeabilization that occurs due to cellular stress or DNA damage [247]. Since TSPO is also localized in mitochondria, it is not far-fetched to assume that the protein plays a role during apoptosis. Regulation of apoptosis was indicated in numerous studies, induced by various agents in different cell lines.

To elucidate whether GRT16 is able to influence apoptosis in BTIC, we pretreated the cells with TSPO ligands before exposing them to TRAIL, as previous results pointed to a TSPO-dependency of TRAIL-induced apoptosis, as opposed to IFNγ, TNFα or FasL [152]. Our results showed that pretreatment with GRT16, XBD173 and Etifoxine sensitized BTIC13 cells to TRAIL-induced apoptosis, whereas the ligands did not induce apoptosis when applied without TRAIL. Considering recent findings in BTICs, where TSPO was shown to protect cells from TRAIL-induced apoptosis [152], GRT16 would, again, classify as TSPO antagonist.

As already mentioned, the hypothesized mechanism of action of TSPO in the involvement of apoptosis, is the lowering of the mitochondrial membrane potential (ΔΨm). In line with this hypothesis were the results found by Meng et al., who downregulated TSPO expression in cardiomyocytes in an anoxia/reoxygenation model. By doing so, they were able to reduce ROS production with subsequent ΔΨm stabilization, ultimately preventing apoptosis [248]. Same results were obtained in MA-10 cells [249].

Recently, Bader et al. were able to show in BV-2 microglial cells that administration of XBD173 reduced ΔΨm in a concentration-dependent manner. Interestingly, this effect was also seen when TSPO KD cells were incubated with XBD173, suggesting that XBD173 influences the mitochondrial membrane potential TSPO-dependently as well as independently [124]. In contrast, prior experiments using the same cell line showed an increased ΔΨm upon XBD173 treatment, as a result of a higher energetic state of the cell [224].

Since Etifoxine is viewed as a neuroprotective agent, it's prevention of apoptosis is generally hypothesized. As most recently confirmed in a model of traumatic brain injury, the protective effect of Etifoxine is most likely due to the maintenance of the ΔΨm by blockade of oxidative stress [203]. Also, reduced levels of caspase 3 after incubation with Etifoxine were shown in two different models investigating ß-amyloid-induced toxicity [250] and LPS-induced cognitive dysfunction [204]. However, Etifoxine as well as XBD173 have not been studied in cancer cells and therefore our results are the first to show an antineoplastic effect of these TSPO ligands in glioblastoma cells.

Albeit, TSPO as well as TSPO ligands have been shown to act pro-apoptotic in various malignant cell lines. Sutter et al. provided evidence of PK11195, Ro5-4864 and FGIN1-27, inducing apoptosis in a dose-dependent manner in a colorectal cancer cell line [251], which was verified in a follow-up TSPO knockout study [252]. Furthermore,

knockdown of TSPO revealed that FGIN-1-27 requires TSPO to induce apoptosis in C6 cells [151]. Additionally, the pro-apoptotic properties of PK11195 were confirmed in a leukemia [253] and a neuroblastoma cell line [254].

In glioblastoma cell lines, the pro-apoptotic role of the protein could also be substantiated. PK11195 as well as newly designed TSPO agonists (4-Phenylquinazoline-2-carboxamide and 2-phenylindolylglyoxylyldipeptides) both induced $\Delta\Psi m$ dissipation and cell viability inhibition [255] [256]. In comparison to single targets, simultaneous activation of p53 and TSPO caused even higher apoptotic rates in U87MG cells [256].

Still, the debate about the contradictory results regarding TSPO functioning is ongoing. Veenman et al. summarized the effects seen in various glioma and glioblastoma cell lines upon activation with ErCP3. Application of PK11195 and Ro5-4684 inhibited apoptosis by impeding $\Delta\Psi m$ dissipation and downstream signaling, therefore preventing apoptosis [257]. This was further evidenced in TSPO knockdown studies in U-118MG cells, where the application of PK11195 prevented apoptosis similarly to TSPO knockdown [131] [136]. Notably, the effects seen in studies investigating apoptosis by targeting TSPO pharmacologically seem to be dependent on the apoptosis-inducing agents used in the study [258] [131] [257]. In addition, as Zhao et al. noted, even the often used and well-studied ligand PK11195 showed not only different but also TSPO-independent effects [182]. Similarly, even with newer ligands, it is difficult to rule out putative TSPO-independent effects, especially in complexly regulated processes such as apoptosis.

It has already been proven several times that TRAIL resistance is an important part of the complex system by which gliomas evade immune attacks (as reviewed in [259]). The underlying mechanism of how GRT16 and the other ligands sensitized BTICs for TRAIL-mediated apoptosis remains unknown, however, many sensitizing agents act by upregulating DR4/5. In multiple GB cell lines, including stem cells, apoptosis was enhanced by downregulation of c-FLIP [260] [261], leading to subsequent upregulation of death receptors [262] [263]. Hence, overexpression of the anti-apoptotic protein c-FLIP was associated with TRAIL resistance in GB cells [264]. ONC201, which also functions through upregulation of TRAIL and DR4/5 in glioblastoma [265], is currently the only TRAIL-based therapy being investigated in a phase II clinical trial, with promising preliminary results [266] [267].

In consequence of our results, GRT16 can be described as pro-apoptotic molecule, although it only acted synergistically together with apoptosis-inducing substances, like TRAIL. GRT16 therefore represents a putative therapeutic approach to restore the sensitivity of tumor cells to TRAIL-induced apoptosis.

Unfortunately, the ligands in our study were only applied using one concentration (1 μM). In the case of GRT16, this concentration was far below the calculated IC50 value. Concentrations were also low for XBD173 and Etifoxine. When deciding on the initial concentration, previous studies with XBD173 and Etifoxine were used as references [129] [124]. To create comparability between the ligands, all three were assessed using the same concentration. However, without a dose-response curve, the effects cannot be put into relation. Hence, the results seen in our study might not reflect the possible maximal effects that could be achieved at higher concentrations. Accordingly, it would be necessary to repeat the experiment using higher concentrations of the ligand GRT16 to substantiate its effects. Then, it would also be possible to see if GRT16 can induce apoptosis by itself and to delineate toxic effects of the ligand. Furthermore, the underlying mechanism of how GRT16 sensitizes TRAIL-induced apoptosis remains unclear and should be addressed in future studies.

7 Conclusion

In this study, we investigated in which way the novel TSPO ligand GRT16 affects TSPO-associated functions in BTIC13 wildtype cells.

Our preliminary results suggest that GRT16 could indeed be a potential candidate for a treatment approach. We report an increase in TRAIL-induced apoptosis after co-exposure with the ligand. Thereby, GRT16 sensitizes BTIC13 cells to TRAIL, so that it could possibly be used in combinational treatment. Nevertheless, the lack of clarity about the underlying molecular mechanisms responsible for the synergistic effect of GRT16 requires further investigations.

Despite increased cell death rates, there was no increase in cytosolic ROS. Although a slight inhibition could be detected 24h after co-treatment with GRT16 and $CoCl_2$, it cannot be excluded that this is due to off-target effects. However, to fully confirm the effect of GRT16 on reactive oxygen species production, further experiments on other sources of ROS, particularly mitochondria would be required. Especially in the aspect that GRT16 leads to a significant reduction of ATP production, by impairing mitochondrial respiration, the detection of mitochondrial ROS would be of interest.

An increase by GRT16 would be in line with our hypothesis that TSPO promotes a pro-inflammatory phenotype in BTIC13, because ROS also contribute to a pro-inflammatory environment. However, GRT16 didn't exert any effect. Possible effects of GRT16 at elevated TSPO expression levels urge further investigations at later timepoints. Notably, the calculated IC50 value was significantly higher than the previously described plasma concentrations (max. 2.6 μM), at which mild side effects occurred and the concentrations used in following experiments sometimes exceeded these by 10-fold. Nevertheless, GRT16 already showed anti-apoptotic effects when used at 1 μM, so that a physiological and tolerable concentration can be assumed here.

In summary, our results provide a first characterization of the TSPO ligand GRT16 *in vitro*, but some limitations must be considered in future studies. TSPO remains a protein, whose functions in malignant cells are not clearly defined, which is why the interpretation of results with TSPO ligands is difficult. In particular due to the cell-specificity, effects on the entire tumor *in vivo* are unpredictable. In addition, the experiments were only done in BTIC13 wildtype cells and not repeated in knockdown or overexpressing cells. Accordingly, not all effects can be definitively attributed to

TSPO. Also, concentration-dependent influences cannot always be assumed. To gain a more profound understanding of the role of the ligand, more BTIC cell lines should be investigated.

Especially with regard to the heterogeneity of GB cells, a personalized treatment has been aimed for. TSPO ligands could contribute to achieving this goal in subgroups of well-characterized patients with specific sensitivity for this approach. Therefore, translational development of a therapeutic strategy would also mean the definition of biomarkers that indicate tumor cell response to TSPO inhibition.

8 Supplement

8.1 Supplementary figures

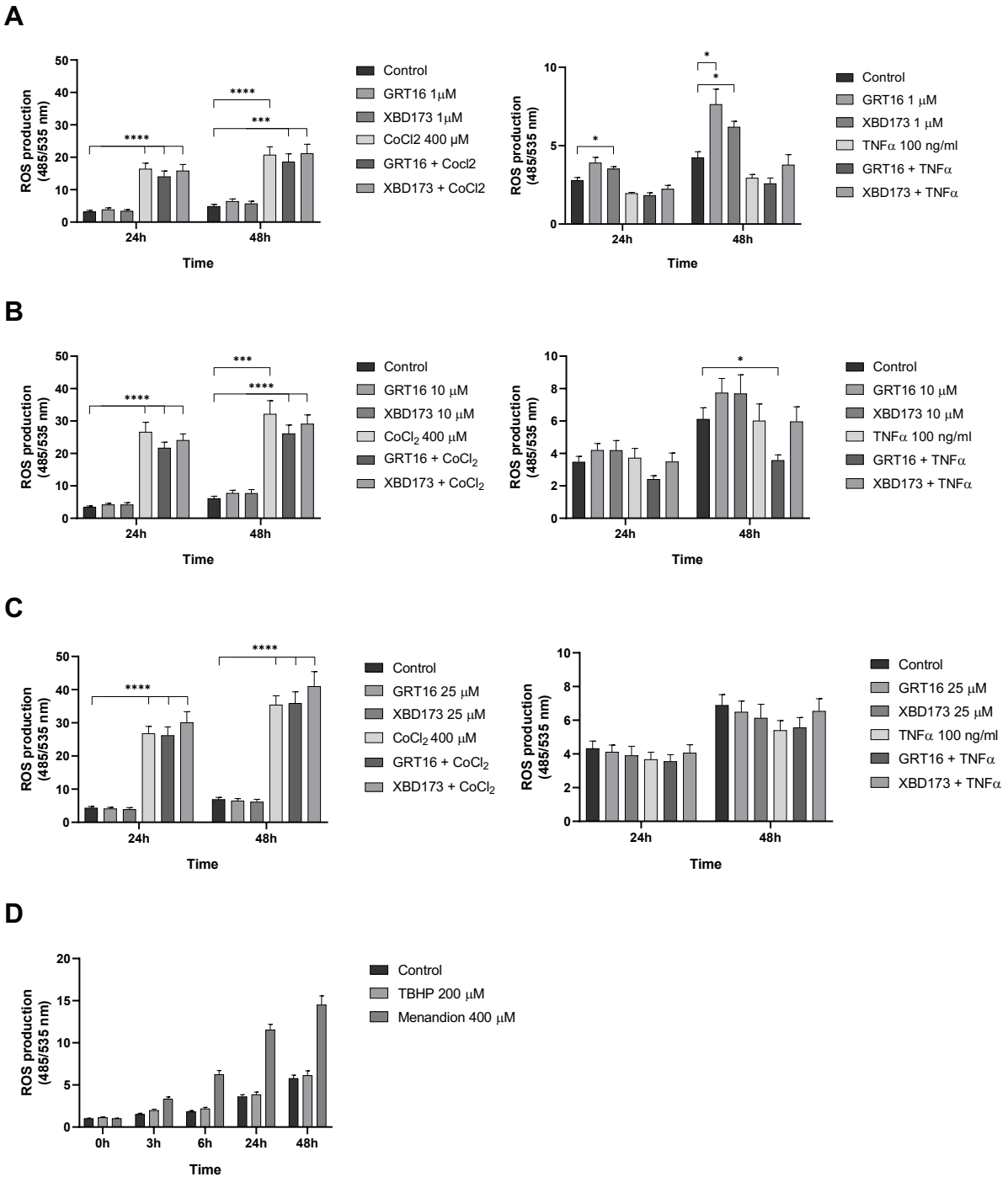

Supplementary figure S6: Impact of TSPO ligands on ROS formation in BTIC13 wt.

BTIC13 cells were pretreated with XBD173 and GRT for 2h, followed by 400 μM of $CoCl_2$ or 100 ng/ml TNFα. **A:** 1 μM of XBD173 and GRT16 (n=4), **B:** 10 μM of XBD173 and GRT16 (n=3), **C:** 25 μM of XBD173 and GRT16 (n=3). **D:** Positive controls (n=10) Data is shown as ± SEM. Two-way ANOVA with Tukey's multiple comparison resulted in significant differences as indicated (p-values: * < 0.05; ** < 0.01; *** < 0.001; ****<0,0001).

A

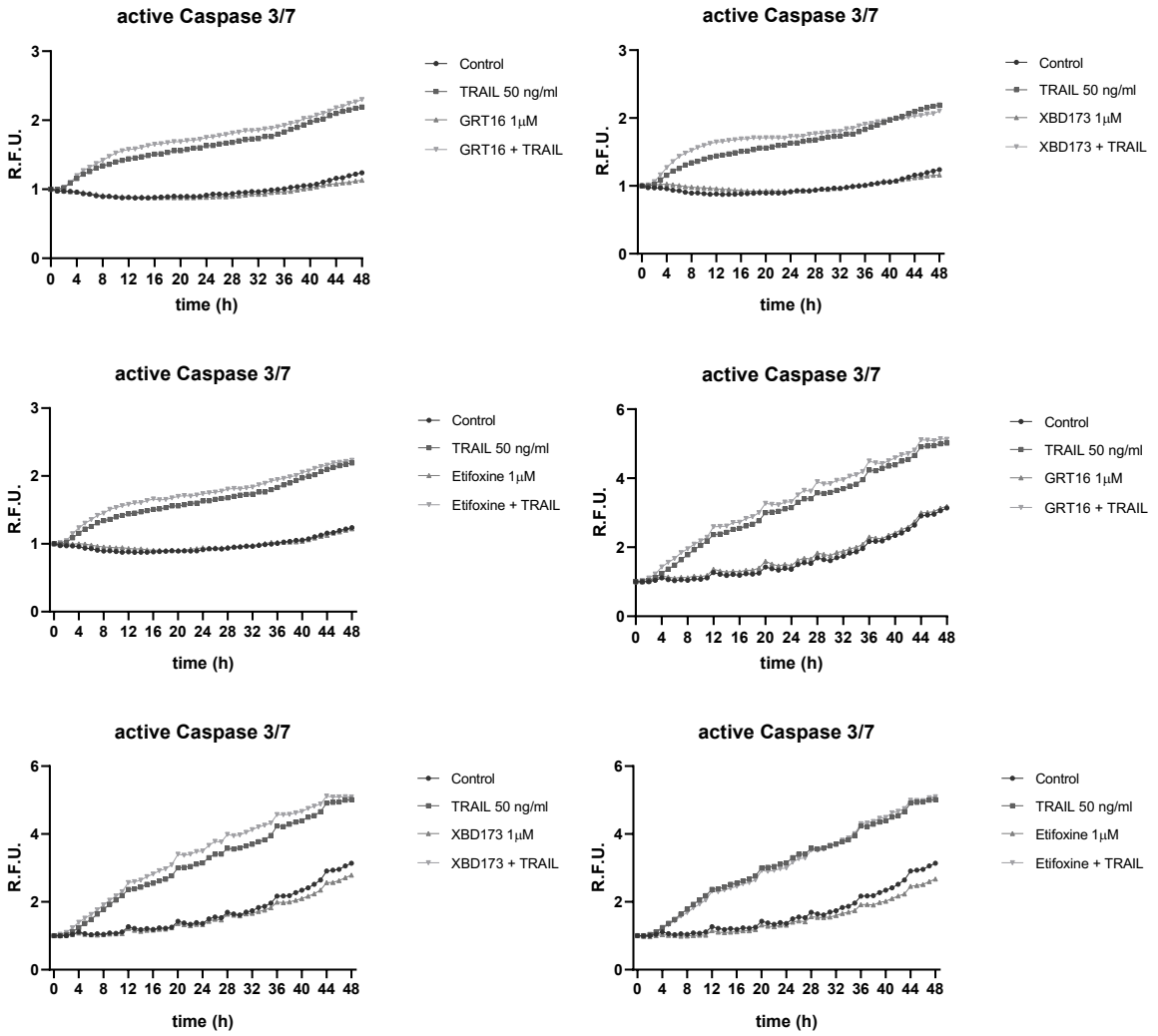

Supplementary figure S7: Impact of TSPO ligands on TRAIL-induced apoptosis in BTIC13 wt.

BTIC13 wt cells were pretreated with 1 μM of XBD173, Etifoxine or GRT for 2h, followed by 50 ng/ml of TRAIL for 3h. DMSO diluted 1:1000 in RHB-A complete medium was used as untreated control. **A:** Real-time cytotoxicity was measured for 48h with IncuCyte® ZOOM systems. Displayed graphs are exemplary for three replicates (n=3). Unpaired two-tailed t-test resulted in no significant differences.

8.2 List of abbreviations

$\Delta\Psi m$	Mitochondrial membrane potential	**fwd**	forward
ANT	Adenine nucleotide transporter	**GAPDH**	Glyceraldehyde 3-phosphate dehydrogenase
ATP	Adenosine triphosphate	**GB**	Glioblastoma
ARPE	Arising retinal pigment epithelia	**G-CIMP**	Glioma CpG- island methylator phenotype
BBB	Blood brain barrier	**GSC**	Glioma stem cell
BCA	Bichinonic Assay	**HIF**	Hypoxia-inducing factor
Bcl-X_L	B-cell lymphoma extra large	**HLA**	Human leukocyte antigen
BTIC	Brain tumor initiating cells	**HRP**	horseradish peroxidase
CAR	Chimeric antigen receptors	**IC**	Inhibitory concentration
cFLIP	cellular FLICE-Like Inhibitory Protein	**IDH**	Isocitrate dehydrogenase
CNS	Central nervous system	**IFN**	Interferon
$CoCl_2$	Cobalt chloride	**IgG**	Immunoglobulin G
Cu	Copper	**IKK**	IκB kinase
DBI	Diazepam Binding Inhibitor	**IL**	Interleukin
DNA	Desoxyribonucleic acid	**JNK**	C-Jun-N-terminal kinase
DMSO	Dimethyl sulfoxide	**KD**	Knockdown
DR	Death receptor	**KO**	Knockout
ECAR	Extracellular acidification rate	**LOH**	Loss of heterozygosity
EGFR	EGF receptor	**LPS**	Lipopolysaccharide
ETC	Electron transport chain	**mA**	Milliampere
FACS	Fluorescence activated cell sorting	**MAPK**	Mitogen-activated protein kinase
FDA	U.S. Food and Drug Administration	**MGMT**	Methylated-DNA-protein-cysteine methyltransferase

Fe	Iron
mPTP	Mitochondrial permeability transition pore
NFκB	nuclear factor NF-kappa-B
NK	Natural killer cell
NOX	NADPH oxidase
NSCLC	Non-small cell lunger cancer
OCR	Oxygen consumption rate
OMM	Outer mitochondrial membrane
PARP	Poly (ADP-ribose)-polymerase
PCR	Polymerase chain reaction
PET	Positron emission tomography
PKC	Protein kinase C
PPIX	Protoporphyrin IX
RELA/p65	nuclear factor NF-kappa-B p65 subunit
rev	Reverse
RNA	Ribonucleic acid
ROMO	Reactive oxygen species modulator
ROS	Reactive oxygen species
rpm	Rounds per minute
SNP	sodium nitroprusside
TMZ	Temozolomide
TNF	Tumor necrosis factor
MnSOD	Manganese superoxide dismutase
TRAIL	TNF-related apoptosis inducing Ligand
Treg	Regulatory T cell
TSPO	Translocator protein
V	Volt
VDAC	Voltage-dependent anion channel
WHO	World Health Organisation
wt	Wild type
XIAP	X-linked inhibitor of apoptosis protein

8.3 List of tables

8.4 List of figures

9 Bibliography

1. Louis DN, Perry A, Wesseling P, Brat DJ, Cree IA, Figarella-Branger D, et al. The 2021 WHO classification of tumors of the central nervous system: A summary. Neuro Oncol. 2021;23(8):1231–51.
2. Ostrom QT, Patil N, Cioffi G, Waite K, Kruchko C, Barnholtz-Sloan JS. CBTRUS statistical report: Primary brain and other central nervous system tumors diagnosed in the United States in 2013-2017. Neuro Oncol. 2020;22(S1):1–96.
3. Stupp R, Mason WP, van den Bent MJ, Weller M, Fisher B, Taphoorn MJB, et al. Radiotherapy plus Concomitant and Adjuvant Temozolomide for Glioblastoma. N Engl J Med. 2005 Mar 10;352(10):987–96.
4. Gilbert MR, Dignam JJ, Armstrong TS, Wefel JS, Blumenthal DT, Vogelbaum MA, et al. A Randomized Trial of Bevacizumab for Newly Diagnosed Glioblastoma. N Engl J Med. 2014;370(8):699–708.
5. Tesileanu CMS, Dirven L, Wijnenga MMJ, Koekkoek JAF, Vincent AJPE, Dubbink HJ, et al. Survival of diffuse astrocytic glioma, IDH1/2 wildtype, with molecular features of glioblastoma, WHO grade IV: A confirmation of the cIMPACT-NOW criteria. Neuro Oncol. 2020;22(4):515–23.
6. Albert NL, Nelwan D V., Fleischmann DF, Quach S, von Rohr K, Kaiser L, et al. Prognostic Value of TSPO PET Before Radiotherapy in Newly Diagnosed IDH–Wild-Type Glioblastoma. J Nucl Med. 2023;64(10):1519–25.
7. Marenco-Hillembrand L, Wijesekera O, Suarez-Meade P, Mampre D, Jackson C, Peterson J, et al. Trends in glioblastoma: outcomes over time and type of intervention: a systematic evidence based analysis. J Neurooncol. 2020;147(2):297–307.
8. Low JT, Ostrom QT, Cioffi G, Neff C, Waite KA, Kruchko C, et al. Primary brain and other central nervous system tumors in the United States (2014-2018): A summary of the CBTRUS statistical report for clinicians. Neuro-Oncology Pract. 2022;9(3):165–82.
9. Louis DN, Perry A, Reifenberger G, von Deimling A, Figarella-Branger D, Cavenee WK, et al. The 2016 World Health Organization Classification of Tumors of the Central Nervous System: a summary. Acta Neuropathol. 2016;131(6):803–20.
10. de Souza CF, Sabedot TS, Malta TM, Stetson L, Morozova O, Sokolov A, et al. A Distinct DNA Methylation Shift in a Subset of Glioma CpG Island Methylator Phenotypes during Tumor Recurrence. Cell Rep. 2018;23(2):637–51.
11. Parsons DW, Jones S, Zhang X, Lin JC, Leary RJ, Angenendt P, et al. An Integrated Genomic Analysis of Human Glioblastoma Multiforme. Science (80-). 2008;321(5897):1807-12.
12. Yan H, Parsons DW, Jin G, McLendon R, Rasheed BA, Yuan W, et al. IDH1 and IDH2 Mutations in Gliomas. N Engl J Med. 2009;360(8):765–73.
13. Lu J, Cowperthwaite MC, Burnett MG, Shpak M. Molecular predictors of long-term survival in glioblastoma multiforme patients. PLoS One. 2016;11(4):1–22.
14. Noushmehr H, Weisenberger DJ, Diefes K, Phillips HS, Pujara K, Berman BP, et al. Identification of a CpG Island Methylator Phenotype that Defines a Distinct Subgroup of Glioma. Cancer Cell. 2010;17(5):510–22.
15. Jiao Y, Killela PJ, Reitman ZJ, Rasheed BA, Heaphy CM, Wilde RF de, et al. Frequent ATRX, CIC, FUBP1 and IDH1 mutations refine the classification of malignant gliomas. Oncotarget. 2012;3(7):709–22.
16. Weidner L, Lorenz J, Quach S, Braun FK, Rothhammer-Hampl T, Ammer LM, et al. Translocator protein (18kDA) (TSPO) marks mesenchymal glioblastoma cell populations characterized by elevated numbers of tumor-associated macrophages. Acta Neuropathol Commun. 2023;11(1):1–21.
17. Wick W, Hartmann C, Engel C, Stoffels M, Felsberg J, Stockhammer F, et al. NOA-04 randomized phase III trial of sequential radiochemotherapy of anaplastic glioma with Procarbazine, Lomustine, and Vincristine

or Temozolomide. J Clin Oncol. 2009;27(35):5874–80.

18. Bent MJ Van Den, Baumert B, Erridge SC, Vogelbaum MA, Anna K, Sanson M, et al. Interim results from the CATNON trial (EORTC). Lancet. 2018;390(10103):1645–53.
19. Vlodavsky E, Soustiel JF. Immunohistochemical expression of peripheral benzodiazepine receptors in human astrocytomas and its correlation with grade of malignancy, proliferation, apoptosis and survival. J Neurooncol. 2007;81(1):1–7.
20. Cai L, Kirchleitner S V., Zhao D, Li M, Tonn JC, Glass R, et al. Glioblastoma exhibits inter-individual heterogeneity of tspo and lat1 expression in neoplastic and parenchymal cells. Int J Mol Sci. 2020;21(2):612.
21. Quach S, Holzgreve A, Kaiser L, Unterrainer M, Dekorsy FJ, Nelwan D V., et al. TSPO PET signal using [18F]GE180 is associated with survival in recurrent gliomas. Eur J Nucl Med Mol Imaging. 2023;50(3):859–69.
22. Ohgaki H, Kleihues P. The Definition of Primary and Secondary Glioblastoma. Clin Cancer Res. 2013;19(4):764–72.
23. Stichel D, Ebrahimi A, Reuss D, Schrimpf D, Ono T, Shirahata M, et al. Distribution of EGFR amplification, combined chromosome 7 gain and chromosome 10 loss, and TERT promoter mutation in brain tumors and their potential for the reclassification of IDHwt astrocytoma to glioblastoma. Vol. 136, Acta Neuropathologica. 2018. 793–803 p.
24. Jaunmuktane Z, Capper D, Jones DTW, Schrimpf D, Sill M, Dutt M, et al. Methylation array profiling of adult brain tumours: diagnostic outcomes in a large, single centre. Acta Neuropathol Commun. 2019;7(1):24.
25. Nonoguchi N, Ohta T, Oh JE, Kim YH, Kleihues P, Ohgaki H. TERT promoter mutations in primary and secondary glioblastomas. Acta Neuropathol. 2013;126(6):931–7.
26. McLendon R, Friedman A, Bigner D, Van Meir EG, Brat DJ, Mastrogianakis GM, et al. Comprehensive genomic characterization defines human glioblastoma genes and core pathways. Nature. 2008;455(7216):1061–8.
27. Verhaak RGW, Hoadley KA, Purdom E, Wang V, Qi Y, Wilkerson MD, et al. Integrated Genomic Analysis Identifies Clinically Relevant Subtypes of Glioblastoma Characterized by Abnormalities in PDGFRA, IDH1, EGFR, and NF1. Cancer Cell. 2010;17(1):98–110.
28. Gill BJ, Pisapia DJ, Malone HR, Goldstein H, Lei L, Sonabend A, et al. MRI-localized biopsies reveal subtype-specific differences in molecular and cellular composition at the margins of glioblastoma. Proc Natl Acad Sci U S A. 2014;111(34):12550–5.
29. Wang Q, Hu B, Hu X, Kim H, Squatrito M, Scarpace L, et al. Tumor Evolution of Glioma-Intrinsic Gene Expression Subtypes Associates with Immunological Changes in the Microenvironment. Cancer Cell. 2017;32(1):42–56.
30. Phillips HS, Kharbanda S, Chen R, Forrest WF, Soriano RH, Wu TD, et al. Molecular subclasses of high-grade glioma predict prognosis, delineate a pattern of disease progression, and resemble stages in neurogenesis. Cancer Cell. 2006;9(3):157–73.
31. Ceccarelli M, Barthel FP, Malta TM, Sabedot TS, Salama SR, Murray BA, et al. Molecular Profiling Reveals Biologically Discrete Subsets and Pathways of Progression in Diffuse Glioma. Cell. 2016;164(3):550–63.
32. Berghoff AS, Kiesel B, Widhalm G, Rajky O, Ricken G, Wohrer A, et al. Programmed death ligand 1 expression and tumor-infiltrating lymphocytes in glioblastoma. Neuro Oncol. 2015;17(8):1064–75.
33. Martinez-Lage M, Lynch TM, Bi Y, Cocito C, Way GP, Pal S, et al. Immune landscapes associated with different glioblastoma molecular subtypes. Acta Neuropathol Commun. 2019;7(1):203.
34. Neftel C, Laffy J, Filbin MG, Hara T, Shore ME, Rahme GJ, et al. An Integrative Model of Cellular States, Plasticity, and Genetics for Glioblastoma. Cell. 2019;178(4):835–49.

35. Patel AP, Tirosh I, Trombetta JJ, Shalek AK, Shawn M, Wakimoto H, et al. Single-cell RNA-seq highlights intratumoral heterogeneity in primary glioblastoma. Science (80-). 2014;344(6190):1396–401.
36. Lathia J, Mack S, Mulkearns-Hubert E, Valentim C, Rich J. Cancer stem cells in glioblastoma. Genes Dev. 2015;29(12):1203–17.
37. Singh SK, Clarke ID, Hide T, Dirks PB. Cancer stem cells in nervous system tumors. Oncogene. 2004;23(6):7267–73.
38. Gimple RC, Bhargava S, Dixit D, Rich JN. Glioblastoma stem cells: lessons from the tumor hierarchy in a lethal cancer. Genes Dev. 2019;33(11–12):591–609.
39. Dirkse A, Golebiewska A, Buder T, Nazarov P V., Muller A, Poovathingal S, et al. Stem cell-associated heterogeneity in Glioblastoma results from intrinsic tumor plasticity shaped by the microenvironment. Nat Commun. 2019;10(1):1–16.
40. Behnan J, Stangeland B, Hosainey SAM, Joel M, Olsen TK, Micci F, et al. Differential propagation of stroma and cancer stem cells dictates tumorigenesis and multipotency. Oncogene. 2017;36(4):570–84.
41. Beier D, Hau P, Proescholdt M, Lohmeier A, Wischhusen J, Oefner PJ, et al. CD133+ and CD133- glioblastoma-derived cancer stem cells show differential growth characteristics and molecular profiles. Cancer Res. 2007;67(9):4010–5.
42. Lan X, Jörg DJ, Cavalli FMG, Richards LM, Nguyen L V., Vanner RJ, et al. Fate mapping of human glioblastoma reveals an invariant stem cell hierarchy. Nature. 2017;549(7671):227–32.
43. Mondal S, Bhattacharya K, Mandal C. Nutritional stress reprograms dedifferention in glioblastoma multiforme driven by PTEN/Wnt/Hedgehog axis: a stochastic model of cancer stem cells. Cell Death Discov. 2018;4(110).
44. Kimura T, Cui D, Kawano H, Yoshitomi-Sakamoto C, Takakura N, Ikeda E. Induced expression of GINS complex is an essential step for reactivation of quiescent stem-like tumor cells within the peri-necrotic niche in human glioblastoma. J Cancer Res Clin Oncol. 2019;145(2):363–71.
45. Hjelmeland AB, Wu Q, Heddleston JM, Choudhary GS, MacSwords J, Lathia JD, et al. Acidic stress promotes a glioma stem cell phenotype. Cell Death Differ. 2011;18(5):829–40.
46. Aulestia FJ, Néant I, Dong J, Haiech J, Kilhoffer MC, Moreau M, et al. Quiescence status of glioblastoma stem-like cells involves remodelling of Ca2+ signalling and mitochondrial shape. Sci Rep. 2018;8(1):1–12.
47. Flavahan WA, Wu Q, Hitomi M, Rahim N, Kim Y, Sloan AE, et al. Brain tumor initiating cells adapt to restricted nutrition through preferential glucose uptake. Nat Neurosci. 2013;16(10):1373–82.
48. Oizel K, Chauvin C, Oliver L, Gratas C, Geraldo F, Jarry U, et al. Efficient mitochondrial glutamine targeting prevails over glioblastoma metabolic plasticity. Clin Cancer Res. 2017;23(20):6292–305.
49. Minata M, Audia A, Shi J, Lu S, Bernstock J, Pavlyukov MS, et al. Phenotypic Plasticity of Invasive Edge Glioma Stem-like Cells in Response to Ionizing Radiation. Cell Rep. 2019;26(7):1893-1905.e7.
50. Hoang-Minh LB, Siebzehnrubl FA, Yang C, Suzuki-Hatano S, Dajac K, Loche T, et al. Infiltrative and drug-resistant slow-cycling cells support metabolic heterogeneity in glioblastoma. EMBO J. 2018;37(23):1–21.
51. Saga I, Shibao S, Okubo J, Osuka S, Kobayashi Y, Yamada S, et al. Integrated analysis identifies different metabolic signatures for tumor-initiating cells in a murine glioblastoma model. Neuro Oncol. 2014;16(8):1048–56.
52. Tardito S, Oudin A, Ahmed SU, Fack F, Keunen O, Zheng L, et al. Glutamine synthetase activity fuels nucleotide biosynthesis and supports growth of glutamine-restricted glioblastoma. Nat Cell Biol. 2015;17(12):1556–68.
53. Mao P, Joshi K, Li J, Kim SH, Li P, Santana-Santos L, et al. Mesenchymal glioma stem cells are maintained by activated glycolytic metabolism involving aldehyde dehydrogenase 1A3. Proc Natl Acad Sci U S A. 2013;110(21):8644–9.

54. Lottaz C, Beier D, Meyer K, Kumar P, Hermann A, Schwarz J, et al. Transcriptional profiles of CD133+ and CD133- glioblastoma-derived cancer stem cell lines suggest different cells of origin. Cancer Res. 2010;70(5):2030–40.
55. Bhat KPL, Balasubramaniyan V, Vaillant B, Ezhilarasan R, Hummelink K, Hollingsworth F, et al. Mesenchymal Differentiation Mediated by NF-κB Promotes Radiation Resistance in Glioblastoma. Cancer Cell. 2013;24(3):331–46.
56. Jin X, Kim LJY, Wu Q, Wallace LC, Prager BC, Sanvoranart T, et al. Targeting glioma stem cells through combined BMI1 and EZH2 inhibition. Nat Med. 2017;23(11):1352–61.
57. Cusulin C, Chesnelong C, Bose P, Bilenky M, Kopciuk K, Chan JA, et al. Precursor States of Brain Tumor Initiating Cell Lines Are Predictive of Survival in Xenografts and Associated with Glioblastoma Subtypes. Stem Cell Reports. 2015;5(1):1–9.
58. Hossain A, Gumin J, Gao F, Figueroa J, Shinojima N, Takezaki T, et al. Mesenchymal Stem Cells Isolated from Human Gliomas Increase Proliferation and Maintain Stemness of Glioma Stem Cells Through the IL-6/gp130/STAT3 Pathway. Stem Cells. 2015;33(8):2400–15.
59. Wang H, Lathia JD, Wu Q, Wang J, Li Z, John M, et al. Targeting Interleukin 6 Signaling Suppresses Glioma Stem Cell Survival and Tumor Growth. Stem Cells. 2009;27(10):2393–404.
60. Marziali G, Signore M, Buccarelli M, Grande S, Palma A, Biffoni M, et al. Metabolic/Proteomic Signature Defines Two Glioblastoma Subtypes with Different Clinical Outcome. Sci Rep. 2016;6:1–13.
61. Segerman A, Niklasson M, Haglund C, Bergström T, Jarvius M, Xie Y, et al. Clonal Variation in Drug and Radiation Response among Glioma-Initiating Cells Is Linked to Proneural-Mesenchymal Transition. Cell Rep. 2016;17(11):2994–3009.
62. Hara T, Chanoch-Myers R, Mathewson ND, Myskiw C, Atta L, Bussema L, et al. Interactions between cancer cells and immune cells drive transitions to mesenchymal-like states in glioblastoma. Cancer Cell. 2021;39(6):779–92.
63. Teng J, Da Hora CC, Kantar RS, Nakano I, Wakimoto H, Batchelor TT, et al. Dissecting inherent intratumor heterogeneity in patient-derived glioblastoma culture models. Neuro Oncol. 2017;19(6):820–32.
64. Aderetti DA, Hira VVV, Molenaar RJ, van Noorden CJF. The hypoxic peri-arteriolar glioma stem cell niche, an integrated concept of five types of niches in human glioblastoma. Biochim Biophys Acta - Rev Cancer. 2018;1869(2):346–54.
65. Karpel-Massler G, Fresia Pareja, Aime´ P, Shu C, Chau L, Westhoff M-A, et al. PARP Inhibition Restores Extrinsic Apoptotic Sensitivity in Glioblastoma. PLoS One. 2014;9(12):e114583.
66. Hanahan D, Weinberg RA. Hallmarks of cancer: The next generation. Cell. 2011;144(5):646–74.
67. Shi T, Zhu J, Zhang X, Mao X. The Role of Hypoxia and Cancer Stem Cells in Development of Glioblastoma. Cancers (Basel). 2023;15(9).
68. Sun RC, Denko NC. Hypoxic regulation of glutamine metabolism through HIF1 and SIAH2 supports lipid synthesis that is necessary for tumor growth. Cell Metab. 2014;19(2):285–92.
69. Sabharwal SS, Schumacker PT. Mitochondrial ROS in cancer: Initiators, amplifiers or an Achilles' heel? Nat Rev Cancer. 2014;14(11):709–21.
70. Raimondi V, Ciccarese F, Ciminale V. Oncogenic pathways and the electron transport chain: a dangeROS liaison. Br J Cancer. 2020;122(2):168–81.
71. Wang X, Liu J, Jiang L, Wei X, Niu C, Wang R, et al. Bach1 Induces Endothelial Cell Apoptosis and Cell-Cycle Arrest through ROS Generation. 2016;2016.
72. Wei J, Wu A, LY K, Y W, G F, I F, et al. Hypoxia potentiates glioma-mediated immunosuppression. PLoS One. 2011;6(1):e16195.
73. Guo X, Xue H, Shao Q, Wang J, Guo X, Chen X, et al. Hypoxia promotes glioma-associated macrophage

infiltration via periostin and subsequent M2 polarization by upregulating TGF-beta and M-CSFR. Oncotarget. 2016;7(49):80521–42.

74. Miska J, Lee-Chang C, Rashidi A, Muroski ME, Chang AL, Lopez-Rosas A, et al. HIF-1α Is a Metabolic Switch between Glycolytic-Driven Migration and Oxidative Phosphorylation-Driven Immunosuppression of Tregs in Glioblastoma. Cell Rep. 2019;27(1):226–37.
75. Zhou W, Ke SQ, Huang Z, Flavahan W, Fang X, Paul J, et al. Periostin secreted by glioblastoma stem cells recruits M2 tumour-associated macrophages and promotes malignant growth. Nat Cell Biol. 2015;17(2):170–82.
76. Hambardzumyan D, Gutmann DH, Kettenmann H. The role of microglia and macrophages in glioma maintenance and progression. Nat Neurosci. 2016;19(1):20–7.
77. Chen Z, Feng X, Herting CJ, Garcia VA, Nie K, Pong WW, et al. Cellular and molecular identity of tumor-associated macrophages in glioblastoma. Cancer Res. 2017;77(9):2266–78.
78. Zinnhardt B, Pigeon H, Thézé B, Viel T, Wachsmuth L, Fricke IB, et al. Combined PET imaging of the inflammatory tumor microenvironment identifies margins of unique radiotracer uptake. Cancer Res. 2017;77(8):1831–41.
79. Vitale I, Manic G, Coussens LM, Kroemer G, Galluzzi L. Macrophages and Metabolism in the Tumor Microenvironment. Cell Metab. 2019;30(1):36–50.
80. Schmitz ML, Weber A, Roxlau T, Gaestel M, Kracht M. Signal integration, crosstalk mechanisms and networks in the function of inflammatory cytokines. Biochim Biophys Acta - Mol Cell Res. 2011;1813(12):2165–75.
81. Fecci PE, Sweeney AE, Grossi PM, Nair SK, Learn CA, Mitchell DA, et al. Systemic anti-CD25 monoclonal antibody administration safely enhances immunity in murine glioma without eliminating regulatory T cells. Clin Cancer Res. 2006;12(14):4294–305.
82. Hussain SF, Yang D, Suki D, Aldape K, Grimm E, Heimberger AB. The role of human glioma-infiltrating microglia/macrophages in mediating antitumor immune responses. Neuro Oncol. 2006;8(3):261–79.
83. Heimberger AB, Abou-Ghazal M, Reina-Ortiz C, Yang DS, Sun W, Qiao W, et al. Incidence and prognostic impact of FoxP3+ regulatory T cells in human gliomas. Clin Cancer Res. 2008;14(16):5166–72.
84. Dumas AA, Pomella N, Rosser G, Guglielmi L, Vinel C, Millner TO, et al. Microglia promote glioblastoma via mTOR-mediated immunosuppression of the tumour microenvironment. EMBO J. 2020;39(15):1–21.
85. Li Z, Liu X, Guo R, Wang P. CD4+Foxp3− type 1 regulatory T cells in glioblastoma multiforme suppress T cell responses through multiple pathways and are regulated by tumor-associated macrophages. Int J Biochem Cell Biol. 2016;81(Pt A):1–9.
86. Mohme M, Schliffke S, Maire CL, Runger A, Glau L, Mende KC, et al. Immunophenotyping of Newly Diagnosed and Recurrent Glioblastoma Defines Distinct Immune Exhaustion Profiles in Peripheral and Tumor-infiltrating Lymphocytes. Clin Cancer Res. 2018;24(17):4187–200.
87. Woroniecka K, Chongsathidkiet P, Rhodin K, Kemeny H, Dechant C, Harrison Farber S, et al. T-cell exhaustion signatures vary with tumor type and are severe in glioblastoma. Clin Cancer Res. 2018;24(17):4175–86.
88. Stupp R, Taillibert S, Kanner A, Read W, Steinberg D, Lhermitte B, et al. Effect of Tumor-Treating Fields Plus Maintenance Temozolomide vs Maintenance Temozolomide Alone on Survival in Patients With Glioblastoma: A Randomized Clinical Trial. JAMA. 2017;318(23):2306–16.
89. Fabian D, Eibl M del PGP, Alnahhas I, Sebastian N, Giglio P, Puduvalli V, et al. Treatment of glioblastoma (GBM) with the addition of tumor-treating fields (TTF): A review. Cancers (Basel). 2019;11(2):1–12.
90. Gilbert MR, Wang M, Aldape KD, Stupp R, Hegi ME, Jaeckle KA, et al. Dose-dense temozolomide for newly diagnosed glioblastoma: A randomized phase III clinical trial. J Clin Oncol. 2013;31(32):4085–91.

91. Aldape K, Brindle KM, Chesler L, Chopra R, Gajjar A, Gilbert MR, et al. Challenges to curing primary brain tumours. Nat Rev Clin Oncol. 2019;16(8):509–20.
92. Wang L, Shang Z, Zhou Y, Hu X, Chen Y, Fan Y, et al. Autophagy mediates glucose starvation-induced glioblastoma cell quiescence and chemoresistance through coordinating cell metabolism, cell cycle, and survival. Cell Death Dis. 2018;9(2).
93. Gersey ZC, Rodriguez GA, Barbarite E, Sanchez A, Walters WM, Ohaeto KC, et al. Curcumin decreases malignant characteristics of glioblastoma stem cells via induction of reactive oxygen species. BMC Cancer. 2017;17(1):1–11.
94. Reczek CR, Chandel NS. The two faces of reactive oxygen species in cancer. Annu Rev Cancer Biol. 2017;1:79–98.
95. Huang H, Zhang S, Li Y, Liu Z, Mi L, Cai Y, et al. Suppression of mitochondrial ROS by prohibitin drives glioblastoma progression and therapeutic resistance. Nat Commun. 2021;12(1):1–16.
96. Lau J, Ilkhanizadeh S, Wang S, Miroshnikova YA, Salvatierra NA, Wong RA, et al. STAT3 Blockade Inhibits Radiation-Induced Malignant Progression in Glioma. Cancer Res. 2015;75(20):4302–11.
97. Halliday J, Helmy K, Pattwell SS, Pitter KL, LaPlant Q, Ozawa T, et al. In vivo radiation response of proneural glioma characterized by protective p53 transcriptional program and proneural-mesenchymal shift. Proc Natl Acad Sci U S A. 2014;111(14):5248–53.
98. Brown CE, Badie B, Barish ME, Weng L, Ostberg JR, Chang WC, et al. Bioactivity and safety of IL13Rα2-redirected chimeric antigen receptor CD8+ T cells in patients with recurrent glioblastoma. Clin Cancer Res. 2015;21(18):4062–72.
99. Brown CE, Alizadeh D, Starr R, Weng L, Wagner JR, Naranjo A, et al. Regression of Glioblastoma after Chimeric Antigen Receptor T-Cell Therapy. N Engl J Med. 2016;375(26):2561–9.
100. O'Rourke DM, Nasrallah MP, Desai A, Melenhorst JJ, Mansfield K, Morrissette JJD, et al. A single dose of peripherally infused EGFRvIII-directed CAR T cells mediates antigen loss and induces adaptive resistance in patients with recurrent glioblastoma. Sci Transl Med. 2017;9(399).
101. Cozzi S, Najafi M, Gomar M, Ciammella P, Iotti C, Iaccarino C, et al. Delayed Effect of Dendritic Cells Vaccination on Survival in Glioblastoma: A Systematic Review and Meta-Analysis. Curr Oncol. 2022;29(2):881–91.
102. Lohr J, Ratliff T, Huppertz A, Ge Y, Dictus C, Ahmadi R, et al. Effector T-cell infiltration positively impacts survival of glioblastoma patients and is impaired by tumor-derived TGF-β. Clin Cancer Res. 2011;17(13):4296–308.
103. Rapp C, Warta R, Stamova S, Nowrouzi A, Geisenberger C, Gal Z, et al. Identification of T cell target antigens in glioblastoma stem-like cells using an integrated proteomics-based approach in patient specimens. Acta Neuropathol. 2017;134(2):297–316.
104. Beckhove P, Hau P. The role of TSPO in T cell immune control of glioblastoma -DFG, FOR2858, Project A3. unpublished manuscript. 2019.
105. Braestrup C, Squires RF. Specific benzodiazepine receptors in rat brain characterized by high-affinity (3H)diazepam binding. Proc Natl Acad Sci. 1977;74(9):3805–9.
106. Anholt RRH, Pedersen PL, De Souza EB, Snyder SH. The peripheral-type benzodiazepine receptor. Localization to the mitochondrial outer membrane. J Biol Chem. 1986;261(2):576–83.
107. Jaremko M, Jaremko Ł, Jaipuria G, Becker S, Zweckstetter M. Structure of the mammalian TSPO/PBR protein. Biochem Soc Trans. 2015;43:566–71.
108. Li H, Papadopoulos V. Peripheral-type benzodiazepine receptor function in cholesterol transport. Identification of a putative cholesterol recognition/interaction amino acid sequence and consensus pattern. Endocrinology. 1998;139(12):4991–7.

109. Li H, Yao ZX, Degenhardt B, Teper G, Papadopoulos V. Cholesterol binding at the cholesterol recognition/interaction amino acid consensus (CRAC) of the peripheral-type benzodiazepine receptor and inhibition of steroidogenesis by an HIV TAT-CRAC peptide. Proc Natl Acad Sci U S A. 2001;98(3):1267–72.
110. Iatmanen-Harbi S, Senicourt L, Papadopoulos V, Lequin O, Lacapere JJ. Characterization of the high-affinity drug ligand binding site of mouse recombinant TSPO. Int J Mol Sci. 2019;20(6).
111. Lacapere J-J, Duma L, Finet S, Kassiou M, Papadopoulos V. Insight into the Structural Features of TSPO: Implications for Drug Development. Trends Pharmacol Sci. 2020 Feb 1;41(2):110–22.
112. Lacapère JJ, Papadopoulos V. Peripheral-type benzodiazepine receptor: Structure and function of a cholesterol-binding protein in steroid and bile acid biosynthesis. Steroids. 2003;68(7–8):569–85.
113. Papadopoulos V, Baraldi M, Guilarte TR, Knudsen TB, Lacapère JJ, Lindemann P, et al. Translocator protein (18 kDa): new nomenclature for the peripheral-type benzodiazepine receptor based on its structure and molecular function. Trends Pharmacol Sci. 2006;27(8):402–9.
114. Jaremko Ł, Jaremko M, Giller K, Becker S, Zweckstetter M. Conformational Flexibility in the Transmembrane Protein TSPO. Chem - A Eur J. 2015;21(46):16555–63.
115. Selvaraj V, Stocco DM, Tu LN. Minireview: Translocator protein (TSPO) and steroidogenesis: A reappraisal. Mol Endocrinol. 2015;29(4):490–501.
116. Gavish M, Bachman I, Shoukrun R, Katz Y, Veenman L, Weisinger G, et al. Enigma of the peripheral benzodiazepine receptor. Pharmacol Rev. 1999;51(4):629–50.
117. Chen M-K, Guilarte TR. Translocator Protein 18kDA (TSPO): Molecular Sensor of Brain Injury & Repair. Pharmacol Ther. 2008;118(1):1–17.
118. Cosenza-Nashat M, Zhao ML, Suh HS, Morgan J, Natividad R, Morgello S, et al. Expression of the translocator protein of 18 kDa by microglia, macrophages and astrocytes based on immunohistochemical localization in abnormal human brain. Neuropathol Appl Neurobiol. 2009;35(3):306–28.
119. Bhoola NH, Mbita Z, Hull R, Dlamini Z. Translocator protein (TSPO) as a potential biomarker in human cancers. Int J Mol Sci. 2018;19(8).
120. Pannell M, Economopoulos V, Wilson TC, Kersemans V, Isenegger PG, Larkin JR, et al. Imaging of translocator protein upregulation is selective for pro-inflammatory polarized astrocytes and microglia. Glia. 2020;68(2):280–97.
121. Veenman L, Levin E, Weisinger G, Leschiner S, Spanier I, Snyder SH, et al. Peripheral-type benzodiazepine receptor density and in vitro tumorigenicity of glioma cell lines. Biochem Pharmacol. 2004;68(4):689–98.
122. Zheng J, Boisgard R, Siquier-Pernet K, Decaudin D, Dollé F, Tavitian B. Differential expression of the 18 kDa translocator protein (TSPO) by neoplastic and inflammatory cells in mouse tumors of breast cancer. Mol Pharm. 2011;8(3):823–32.
123. Rupprecht R, Ranimes G, Eser D, Baghai TC, Schule C, Nothdurfter C, et al. Translocator protein (18 kD) as target for anxiolytics without benzodiazepine-like side effects. Science (80-). 2009;325(5939):490–3.
124. Bader S, Wolf L, Milenkovic VM, Gruber M, Nothdurfter C, Rupprecht R, et al. Differential effects of TSPO ligands on mitochondrial function in mouse microglia cells. Psychoneuroendocrinology. 2019;106(March):65–76.
125. Lin YC, Cheung G, Porter E, Papadopoulos V. The neurosteroid pregnenolone is synthesized by a mitochondrial P450 enzyme other than CYP11A1 in human glial cells. J Biol Chem. 2022;298(7):102110.
126. Miettinen H, Kononen J, Haapasalo H, Helén P, Sallinen P, Harjuntausta T, et al. Expression of Peripheral-Type Benzodiazepine Receptor and Diazepam Binding Inhibitor in Human Astrocytomas: Relationship to Cell Proliferation. Cancer Res. 1995;55(12):2691–5.

127. Gatliff J, East D, Crosby J, Abeti R, Harvey R, Craigen W, et al. TSPO interacts with VDAC1 and triggers a ROS-mediated inhibition of mitochondrial quality control. Autophagy. 2014;10(12):2279–96.
128. Lejri I, Grimm A, Hallé F, Abarghaz M, Klein C, Maitre M, et al. TSPO Ligands Boost Mitochondrial Function and Pregnenolone Synthesis. J Alzheimer's Dis. 2019;72(4):1045–58.
129. Milenkovic VM, Slim D, Bader S, Koch V, Heinl ES, Alvarez-Carbonell D, et al. CRISPR-cas9 mediated TSPO gene knockout alters respiration and cellular metabolism in human primary microglia cells. Int J Mol Sci. 2019;20(13).
130. Kroemer G, Galluzzi L, Brenner C. Mitochondrial membrane permeabilization in cell death. Physiol Rev. 2007;87(1):99–163.
131. Zeno S, Zaaroor M, Leschiner S, Veenman L, Gavish M. CoCl2 induces apoptosis via the 18 kDa translocator protein in U118MG human glioblastoma cells. Biochemistry. 2009 Jun 2;48(21):4652–61.
132. Batarseh A, Li J, Papadopoulos V. Protein kinase Cε regulation of translocator protein (18 kDa) Tspo gene expression is mediated through a MAPK pathway targeting STAT3 and c-Jun transcription factors. Biochemistry. 2010;49(23):4766–78.
133. Loth MK, Guariglia SR, Re DB, Perez J, de Paiva VN, Dziedzic JL, et al. A Novel Interaction of Translocator Protein 18 kDa (TSPO) with NADPH Oxidase in Microglia. Mol Neurobiol. 2020;57(11):4467–87.
134. Shargorodsky L, Veenman L, Caballero B, Pe'er Y, Leschiner S, Bode J, et al. The nitric oxide donor sodium nitroprusside requires the 18 kDa Translocator Protein to induce cell death. Apoptosis. 2012;17(7):647–65.
135. Rechichi M, Salvetti A, Chelli B, Costa B, Da Pozzo E, Spinetti F, et al. TSPO over-expression increases motility, transmigration and proliferation properties of C6 rat glioma cells. Biochim Biophys Acta - Mol Basis Dis. 2008;1782(2):118–25.
136. Bode J, Veenman L, Caballero B, Lakomek M, Kugler W, Gavish M. The 18 kDa translocator protein influences angiogenesis, as well as aggressiveness, adhesion, migration, and proliferation of glioblastoma cells. Pharmacogenet Genomics. 2012;22(7):538–50.
137. Fu Y, Wang D, Wang H, Cai M, Li C, Zhang X, et al. TSPO deficiency induces mitochondrial dysfunction, leading to hypoxia, angiogenesis, and a growth-promoting metabolic shift toward glycolysis in glioblastoma. Neuro Oncol. 2020;22(2):240–52.
138. Bode J, Veenman L, Vainshtein A, Kugler W, Rosenberg N, Gavish M. Modulation of Gene Expression Associated with the Cell Cycle and Tumorigenicity of Glioblastoma Cells by the 18 kDa Translocator Protein (TSPO). Austin J Pharmacol Ther. 2014;2(10):1053.
139. Butow RA, Avadhani NG. Mitochondrial signaling: The retrograde response. Mol Cell. 2004;14(1):1–15.
140. Eisenberg-Bord M, Schuldiner M. Ground control to major TOM: mitochondria–nucleus communication. FEBS J. 2017;284(2):196–210.
141. Vizioli MG, Liu T, Miller KN, Robertson NA, Gilroy K, Lagnado AB, et al. Mitochondria-to-nucleus retrograde signaling drives formation of cytoplasmic chromatin and inflammation in senescence. Genes Dev. 2020;34(5):428–45.
142. Biswas L, Farhan F, Reilly J, Bartholomew C, Shu X. TSPO ligands promote cholesterol efflux and suppress oxidative stress and inflammation in choroidal endothelial cells. Int J Mol Sci. 2018;19(12).
143. Franco R, Fernández-Suárez D. Alternatively activated microglia and macrophages in the central nervous system. Prog Neurobiol. 2015;131:65–86.
144. Wu SY WK. The roles of microglia/macrophages in tumor progression of brain cancer and metastatic disease. Front Biosci (Landmark Ed). 2017;22:1805–29.
145. Ivashkiv LB. IFNγ: signalling, epigenetics and roles in immunity, metabolism, disease and cancer immunotherapy. Nat Rev Immunol. 2018;18(9):545–58.
146. Narayan N, Mandhair H, Smyth E, Dakin SG, Kiriakidis S, Wells L, et al. The macrophage marker

translocator protein (TSPO) is down-regulated on pro-inflammatory ‘M1’ human macrophages. PLoS One. 2017;12(10):1–19.

147. Beckers L, Ory D, Geric I, Declercq L, Koole M, Kassiou M, et al. Increased Expression of Translocator Protein (TSPO) Marks Pro-inflammatory Microglia but Does Not Predict Neurodegeneration. Mol Imaging Biol. 2018;20(1):94–102.
148. Da Pozzo E, Tremolanti C, Costa B, Giacomelli C, Milenkovic VM, Bader S, et al. Microglial pro-inflammatory and anti-inflammatory phenotypes are modulated by translocator protein activation. Int J Mol Sci. 2019;20(18):1–21.
149. Zhou D, Ji L, Chen Y. TSPO Modulates IL-4-Induced Microglia/Macrophage M2 Polarization via PPAR-γ Pathway. J Mol Neurosci. 2020;70(4):542–9.
150. Yasin N, Veenman L, Singh S, Azrad M, Bode J, Vainshtein A, et al. Classical and novel TSPO ligands for the mitochondrial TSPO can modulate nuclear gene expression: Implications for mitochondrial retrograde signaling. Int J Mol Sci. 2017;18(4):1–35.
151. Veenman L, Gavish M. he role of 18 kDa mitochondrial translocator protein (TSPO) in programmed cell death, and effects of steroids on TSPO expression. Curr Mol Med. 2012;12(4):398–412.
152. Menevse AN, Ammer LM, Vollmann-Zwerenz A, Kupczyk M, Lorenz J, Weidner L, et al. TSPO acts as an immune resistance gene involved in the T cell mediated immune control of glioblastoma. Acta Neuropathol Commun. 2023;11(1):1–23.
153. Le Fur G, Vaucher N, Perrier ML, Flamier A, Benavides J, Renault C, et al. Differentiation between two ligands for peripheral benzodiazepine binding sites, [3H]R05-4864 and [3H]PK 11195, by thermodynamic studies. Life Sci. 1983;33(5):449–57.
154. Zhang L, Hu K, Shao T, Hou L, Zhang S, Ye W, et al. Recent developments on PET radiotracers for TSPO and their applications in neuroimaging. Acta Pharm Sin B. 2021;11(2):373–93.
155. Kühnert S, Bahrenberg G, Kless A, Schröder W, inventors; Grünenthal GmbH A. Substituted 2-oxo-and 2-thioxo-dihydroquinoline-3-carboxamides as KCNQ2/3 modulators. Patent family based on WO 2012/025239. Publication date 1 Mar 2012. International Application No. PCT/EP2011/004280. International Filing Date 26 Aug 2011. 2012.
156. Bloms-Funke P, Schumacher M, Liu S, Su D, Li J, Liere P, et al. A novel dual mode-of-action anti-hyperalgesic compound in rats which is neuroprotective and promotes neuroregeneration. Eur J Pharmacol. 2022;15(923):174935.
157. Rupprecht R, Papadopoulos V, Rammes G, Baghai TC, Fan J, Akula N, et al. Translocator protein (18 kDa) (TSPO) as a therapeutic target for neurological and psychiatric disorders. Nat Rev Drug Discov. 2010;9(12):971–88.
158. Knoll S, Bludau O, Koch S, Schumacher M, Rupprecht R, Grosche A. Müller cell specific TSPO function as a beneficial element for preserva- tion of retinal neurons after transient retinal ischemia. In: Retinal Degenration: Environment Matters [Internet]. Potsdam, Germany; 2022. p. 51–2. Available from: https://www.pro-retina-stiftung.de/wp-content/uploads/2022/04/Conference-Report-2022-1.pdf
159. Ravikumar B, Crawford D, Dellovade T, Savinainen A, Graham D, Liere P, et al. Differential efficacy of the TSPO ligands etifoxine and XBD-173 in two rodent models of Multiple Sclerosis. Neuropharmacology. 2016;108:229–37.
160. Karlstetter M, Nothdurfter C, Aslanidis A, Moeller K, Horn F, Scholz R, et al. Translocator protein (18 kDa) (TSPO) is expressed in reactive retinal microglia and modulates microglial inflammation and phagocytosis. J Neuroinflammation. 2014;11(3).
161. Scholz R, Caramoy A, Bhuckory MB, Rashid K, Chen M, Xu H, et al. Targeting translocator protein (18 kDa) (TSPO) dampens pro-inflammatory microglia reactivity in the retina and protects from degeneration.

J Neuroinflammation. 2015;12(1):1–12.

162. Kita A, Kohayakawa H, Kinoshita T, Ochi Y, Nakamichi K, Kurumiya S, et al. Antianxiety and antidepressant-like effects of AC-5216, a novel mitochondrial benzodiazepine receptor ligand. Br J Pharmacol. 2004;142(7):1059–72.
163. Nothdurfter C, Rammes G, Baghai TC, Schüle C, Schumacher M, Papadopoulos V, et al. Translocator protein (18kDa) as a target for novel anxiolytics with a favourable side-effect profile. J Neuroendocrinol. 2012;24(1):82–92.
164. Kita A, Kinoshita T, Kohayakawa H, Furukawa K, Akaike A. Lack of tolerance to anxiolysis and withdrawal symptoms in mice repeatedly treated with AC-5216, a selective TSPO ligand. Prog Neuro-Psychopharmacology Biol Psychiatry. 2009;33(6):1040–5.
165. Owen DR, Guo Q, Kalk NJ, Colasanti A, Kalogiannopoulou D, Dimber R, et al. Determination of [11C]PBR28 binding potential in vivo: A first human TSPO blocking study. J Cereb Blood Flow Metab. 2014;34(6):989–94.
166. Nguyen N, Fakra E, Pradel V, Jouve E, Alquier C, Le Guern ME, et al. Erratum: Efficacy of etifoxine compared to lorazepam monotherapy in the treatment of patients with adjustment disorders with anxiety: A double-blind controlled study in general practice. Hum Psychopharmacol. 2006;21(8):562.
167. Aleksandrovsky YA, Krasnov VN, Neznanov NG, Romasenko LV. Efficacy of etifoxine in comparison with phenazepam in the treatment of patients with adjustment disorders (an open randomized controlled study). Russ J Psychiatry. 2010;(1):74–78.
168. Stein DJ. Etifoxine Versus Alprazolam for the Treatment of Adjustment Disorder with Anxiety: a Randomized Controlled Trial. Adv Ther. 2015;32(1):57–68.
169. Vicente B, Saldivia S, Hormazabal N, Bustos C, Rubí P. Etifoxine is non-inferior than clonazepam for reduction of anxiety symptoms in the treatment of anxiety disorders: a randomized, double blind, non-inferiority trial. Psychopharmacology (Berl). 2020;237(11):3357–67.
170. Deplanque D, Machuron F, Waucquier N, Jozefowicz E, Duhem S, Somers S, et al. Etifoxine impairs neither alertness nor cognitive functions of the elderly: A randomized, double-blind, placebo-controlled crossover study. Eur Neuropsychopharmacol. 2018;28(8):925–32.
171. Poisbeau P, Gazzo G, Calvel L. Anxiolytics targeting GABAA receptors: Insights on etifoxine. World J Biol Psychiatry. 2018;19(sup1):S36–45.
172. Juif PE, Melchior M, Poisbeau P. Characterization of the fast GABAergic inhibitory action of etifoxine during spinal nociceptive processing in male rats. Neuropharmacology. 2015;91:117–22.
173. Luc Do Rego J, Vaudry D, Vaudry H. The non-benzodiazepine anxiolytic drug etifoxine causes a rapid, receptor-independent stimulation of neurosteroid biosynthesis. PLoS One. 2015;10(3):1–20.
174. Verma A, Nye JS, Snyder SH. Porphyrins are endogenous ligands for the mitochondrial (peripheral-type) benzodiazepine receptor. Proc Natl Acad Sci U S A. 1987;84(8):2256–60.
175. Bovolin P, Schlichting J, Miyata M, Ferrarese C, Guidotti A, Alho H. Distribution and characterization of diazepam binding inhibitor (DBI) in peripheral tissues of rat. Regul Pept. 1990;29(2–3):267–81.
176. Lacapère JJ, Delavoie F, Li H, Péranzi G, Maccario J, Papadopoulos V, et al. Structural and functional study of reconstituted peripheral benzodiazepine receptor. Biochem Biophys Res Commun. 2001;284(2):536–41.
177. Krueger KE, Papadopoulos V. Peripheral-type benzodiazepine receptors mediate translocation of cholesterol from outer to inner mitochondrial membranes in adrenocortical cells. J Biol Chem. 1990;265(25):15015–22.
178. Banati RB, Middleton RJ, Chan R, Hatty CR, Wai-Ying Kam W, Quin C, et al. Positron emission tomography and functional characterization of a complete PBR/TSPO knockout. Nat Commun. 2014;5:1–12.

179. Tu LN, Morohaku K, Manna PR, Pelton SH, Butler WR, Stocco DM, et al. Peripheral benzodiazepine receptor/translocator protein global knock-out mice are viable with no effects on steroid hormone biosynthesis. J Biol Chem. 2014;289(40):27444–54.
180. Fan J, Campioli E, Midzak A, Culty M, Papadopoulos V. Conditional steroidogenic cell-targeted deletion of TSPO unveils a crucial role in viability and hormone-dependent steroid formation. Proc Natl Acad Sci U S A. 2015;112(23):7261–6.
181. Barron AM, Ji B, Kito S, Suhara T, Higuchi M. Steroidogenic abnormalities in translocator protein knockout mice and significance in the aging male. Biochem J. 2018;475(1):75–85.
182. Zhao AH, Tu LN, Mukai C, Sirivelu MP, Pillai V V., Morohaku K, et al. Mitochondrial translocator protein (TSPO) function is not essential for heme biosynthesis. J Biol Chem. 2016;291(4):1591–603.
183. Guo Y, Kalathur RC, Liu Q, Kloss B, Bruni R, Ginter C, et al. Structure and activity of tryptophan-rich TSPO proteins. Science (80-). 2015;347(6221):551–5.
184. Islinger M, Costello JL, Kors S, Soupene E, Levine TP, Kuypers FA, et al. The diversity of ACBD proteins – From lipid binding to protein modulators and organelle tethers. Biochim Biophys Acta - Mol Cell Res. 2020;1867(5):118675.
185. Wang M, Wang X, Zhao L, Ma W, Rodriguez IR, Fariss RN, et al. Macroglia-microglia interactions via TSPO signaling regulates microglial activation in the mouse retina. J Neurosci. 2014;34(10):3793–806.
186. Ostrom QT, Cioffi G, Gittleman H, Patil N, Waite K, Kruchko C, et al. CBTRUS Statistical Report: Primary Brain and Other Central Nervous System Tumors Diagnosed in the United States in 2012-2016. Neuro Oncol. 2019;21:1–100.
187. Chen J, Li Y, Yu TS, McKay RM, Burns DK, Kernie SG, et al. A restricted cell population propagates glioblastoma growth after chemotherapy. Nature. 2012;488(7412):522–6.
188. Ammer L-M, Vollmann-Zwerenz A, Ruf V, Wetzel CH, Riemenschneider MJ, Albert NL, et al. The Role of Translocator Protein TSPO in Hallmarks of Glioblastoma. Cancers (Basel). 2020;12(10):2973.
189. Khamis ZI, Al-Akkary N, Hua T, Draughon SA, Li Y, Sang Q-XA. Clinical investigations of immunotherapy for human primary brain tumors. Neuroimmunol Neuroinflammation. 2020;
190. Leidgens V, Proske J, Rauer L, Moeckel S, Renner K, Bogdahn U, et al. Stattic and metformin inhibit brain tumor initiating cells by reducing STAT3-phosphorylation. Oncotarget. 2017;8(5):8250–63.
191. Siegel RL, Miller KD, Fuchs HE, Jemal A. Cancer statistics, 2022. CA Cancer J Clin. 2022;72(1):7–33.
192. Tsodikov A, Gulati R, Heijnsdijk EA, Pinsky PF, Moss SM, Qiu S, et al. School of Health Sciences, PL 100 33014 University of Tampere, Finland Ann Intern Med. 2017;167(7):449–55.
193. Levin TR, Corley DA, Jensen CD, Schottinger JE, Quinn VP, Zauber AG, et al. Effects of Organized Colorectal Cancer Screening on Cancer Incidence and Mortality in a Large Community-Based Population. Gastroenterology. 2018;155(5):1383–91.
194. Katalinic A, Eisemann N, Kraywinkel K, Noftz MR, Hübner J. Breast cancer incidence and mortality before and after implementation of the German mammography screening program. Int J Cancer. 2020;147(3):709–18.
195. Herrlinger U, Tzaridis T, Mack F, Steinbach JP, Schlegel U, Sabel M, et al. Lomustine-temozolomide combination therapy versus standard temozolomide therapy in patients with newly diagnosed glioblastoma with methylated MGMT promoter (CeTeG/NOA–09): a randomised, open-label, phase 3 trial. Lancet. 2019;393(10172):678–88.
196. Wolf L, Bauer A, Melchner D, Hallof-Buestrich H, Stoertebecker P, Häen E, et al. Enhancing Neurosteroid Synthesis- Relationship to the pharmacology of Translocator Protein (18kDa)(TSPO) Ligands and Benzodiazepines. Pharmacopsychiatry. 2015;48(2):72–7.
197. Owen DRJ, Lewis AJM, Reynolds R, Rupprecht R, Eser D, Wilkins MR, et al. Variation in binding affinity of

the novel anxiolytic XBD173 for the 18 kDa translocator protein in human brain. Synapse. 2011;65(3):257–9.

198. Costa B, Da Pozzo E, Cavallini C, Taliani S, Da Settimo F, Martini C. Long Residence Time at the Neurosteroidogenic 18 kDa Translocator Protein Characterizes the Anxiolytic Ligand XBD173. ACS Chem Neurosci. 2016;7(8):1041–6.
199. Costa B, Cavallini C, Da Pozzo E, Taliani S, Da Settimo F, Martini C. The Anxiolytic Etifoxine Binds to TSPO Ro5-4864 Binding Site with Long Residence Time Showing a High Neurosteroidogenic Activity. ACS Chem Neurosci. 2017;8(7):1448–54.
200. Verleye M, Akwa Y, Liere P, Ladurelle N, Pianos A, Eychenne B, et al. The anxiolytic etifoxine activates the peripheral benzodiazepine receptor and increases the neurosteroid levels in rat brain. Pharmacol Biochem Behav. 2005;82(4):712–20.
201. Owen DR, Phillips A, O'Connor D, Grey G, Aimola L, Nicholas R, et al. Human pharmacokinetics of XBD173 and etifoxine distinguish their potential for pharmacodynamic effects mediated by translocator protein. Br J Clin Pharmacol. 2022;88(9):4230–6.
202. Bloms-funke P, Bankstahl M, Bankstahl J, Kneip C, Wolfgang L, Schr W. Neuropharmacology The novel dual-mechanism Kv7 potassium channel / TSPO receptor activator GRT-X is more effective than the Kv7 channel opener retigabine in the 6-Hz refractory seizure mouse model. Neuropharmacology. 2022;203:108884.
203. Shehadeh M, Palzur E, Apel L, Soustiel JF. Reduction of traumatic brain damage by Tspo ligand etifoxine. Int J Mol Sci. 2019;20(11).
204. Zhang H, Ma L, Guo W zhi, Jiao L bo, Zhao H yu, Ma Y qun, et al. TSPO ligand etifoxine attenuates LPS-induced cognitive dysfunction in mice. Brain Res Bull. 2020;165(June):178–84.
205. Liu GJ, Middleton RJ, Kam WWY, Chin DY, Hatty CR, Chan RHY, et al. Functional gains in energy and cell metabolism after TSPO gene insertion. Cell Cycle. 2017;16(5):436–47.
206. Yao R, Pan R, Shang C, Li X, Cheng J, Xu J, et al. Translocator Protein 18 kDa (TSPO) Deficiency Inhibits Microglial Activation and Impairs Mitochondrial Function. Front Pharmacol. 2020;11(June):1–10.
207. Mi Y, Guo N, Luan J, Cheng J, Hu Z, Jiang P, et al. The Emerging Role of Myeloid-Derived Suppressor Cells in the Glioma Immune Suppressive Microenvironment. Front Immunol. 2020;11(April):1–11.
208. Dapash M, Hou D, Castro B, Lee-Chang C, Lesniak MS. The interplay between glioblastoma and its microenvironment. Cells. 2021;10(9):1–14.
209. Piperi C, Samaras V, Levidou G, Kavantzas N, Boviatsis E, Petraki K, et al. Prognostic significance of IL-8-STAT-3 pathway in astrocytomas: Correlation with IL-6, VEGF and microvessel morphometry. Cytokine. 2011;55(3):387–95.
210. Sharma I, Singh A, Siraj F, Saxena S. IL-8/CXCR1/2 signalling promotes tumor cell proliferation, invasion and vascular mimicry in glioblastoma. J Biomed Sci. 2018;25(1):1–13.
211. Feng Y, Wang J, Tan D, Cheng P, Wu A. Relationship between circulating inflammatory factors and glioma risk and prognosis: A meta-analysis. Cancer Med. 2019;8(17):7454–68.
212. Kai K, Komohara Y, Esumi S, Fujiwara Y, Yamamoto T, Uekawa K, et al. Macrophage/microglia-derived IL-1β induces glioblastoma growth via the STAT3/NF-κB pathway. Hum Cell. 2022;35(1):226–37.
213. Weiss T, Puca E, Silginer M, Hemmerle T, Pazahr S, Bink A, et al. Immunocytokines are a promising immunotherapeutic approach against glioblastoma. Sci Transl Med. 2020;12(564).
214. Bender DE, Schaettler MO, Sheehan KCF, Johanns TM, Dunn GP. Cytokine Profiling in Plasma from Patients with Brain Tumors Versus Healthy Individuals using 2 Different Multiplex Immunoassay Platforms. Biomark Insights. 2021;16:11772719211006666.
215. Owen DR, Narayan N, Wells L, Healy L, Smyth E, Rabiner EA, et al. Pro-inflammatory activation of primary

microglia and macrophages increases 18 kDa translocator protein expression in rodents but not humans. J Cereb Blood Flow Metab. 2017;37(8):2679–90.

216. Hotfilder M, Knupfer H, Mohlenkamp G, Pennekamp P, Knupfers M, Van Gool S, et al. Interferon-gamma increases IL-6 production in human glioblastoma cell lines. Anticancer Res. 2000;20(6 B):4445–50.
217. Wolf A, Herb M, Schramm M, Langmann T. The TSPO-NOX1 axis controls phagocyte-triggered pathological angiogenesis in the eye. Nat Commun. 2020;11(1):1–17.
218. Rashid K, Verhoyen M, Taiwo M, Langmann T. Translocator protein (18 kDa) (TSPO) ligands activate Nrf2 signaling and attenuate inflammatory responses and oxidative stress in human retinal pigment epithelial cells. Biochem Biophys Res Commun. 2020;528(2):261–8.
219. Li HD, Li M, Shi E, Jin WN, Wood K, Gonzales R, et al. A translocator protein 18 kDa agonist protects against cerebral ischemia/reperfusion injury. J Neuroinflammation. 2017;14(1):1–9.
220. Simon-O'Brien E, Gauthier D, Riban V, Verleye M. Etifoxine improves sensorimotor deficits and reduces glial activation, neuronal degeneration, and neuroinflammation in a rat model of traumatic brain injury. J Neuroinflammation. 2016;13(1):1–15.
221. Daugherty DJ, Selvaraj V, Chechneva O V., Liu XB, Pleasure DE, Deng W. A TSPO ligand is protective in a mouse model of multiple sclerosis. EMBO Mol Med. 2013;5(6):891–903.
222. Krestinina O V., Grachev DE, Odinokova I V., Reiser G, Evtodienko Y V., Azarashvili TS. Effect of peripheral benzodiazepine receptor (PBR/TSPO) ligands on opening of Ca2+-induced pore and phosphorylation of 3.5-kDa polypeptide in rat brain mitochondria. Biochem. 2009;74(4):421–9.
223. Veenman L, Alten J, Linnemannstöns K, Shandalov Y, Zeno S, Lakomek M, et al. Potential involvement of F0F1-ATP(synth)ase and reactive oxygen species in apoptosis induction by the antineoplastic agent erucylphosphohomocholine in glioblastoma cell lines. Apoptosis. 2010;15(7):753–68.
224. Scheck L. Characterization of Tspo 18 Kda in Neurosteroid Synthesis and Mitochondrial Metabolism. Diss Uni Regensbg. 2017;
225. Divakaruni AS, Paradyse A, Ferrick DA, Murphy AN, Jastroch M. Analysis and interpretation of microplate-based oxygen consumption and pH data. 1st ed. Vol. 547, Methods in Enzymology. Elsevier Inc.; 2014. 309–354 p.
226. Fairley ALH, Lai KO, Wong JH, Salvatore AV, Barron AM, Kong L. Mitochondrial control of microglial phagocytosis by the translocator protein and hexokinase 2 in Alzheimer's disease. Proc Natl Proc Natl Acad Sci United States Am. 2023;120(8).
227. Tu LN, Zhao AH, Hussein M, Stocco DM, Selvaraj V. Translocator protein (TSPO) affects mitochondrial fatty acid oxidation in steroidogenic cells. Endocrinology. 2016;157(3):1110–21.
228. Šileikyte J, Blachly-Dyson E, Sewell R, Carpi A, Menabò R, Di Lisa F, et al. Regulation of the mitochondrial permeability transition pore by the outer membrane does not involve the peripheral benzodiazepine receptor (translocator protein of 18 kDa (TSPO)). J Biol Chem. 2014;289(20):13769–81.
229. Schmidt CA, Fisher-Wellman KH, Darrell Neufer P. From OCR and ECAR to energy: Perspectives on the design and interpretation of bioenergetics studies. J Biol Chem. 2021;297(4):101140.
230. Issop L, Ostuni MA, Lee S, Laforge M, Péranzi G, Rustin P, et al. Translocator Protein-mediated stabilization of mitochondrial architecture during inflammation stress in colonic cells. PLoS One. 2016;11(4):1–23.
231. Brenner D, Blaser H, Mak TW. Regulation of tumour necrosis factor signalling: Live or let die. Nat Rev Immunol. 2015;15(6):362–74.
232. Blaser H, Dostert C, Mak TW, Brenner D. TNF and ROS Crosstalk in Inflammation. Trends Cell Biol. 2016;26(4):249–61.
233. Shen SC, Wu MS, Lin HY, Yang LY, Chen YH, Chen YC. Reactive oxygen species-dependent nitric oxide

production in reciprocal interactions of glioma and microglial cells. J Cell Physiol. 2014;229(12):2015–26.

234. Morgan MJ, Liu ZG. Crosstalk of reactive oxygen species and NF-κB signaling. Cell Res. 2011;21(1):103–15.
235. Son Y, Cheong Y-K, Kim N-H, Chung H-T, Kang DG, Pae H-O. Mitogen-Activated Protein Kinases and Reactive Oxygen Species: How Can ROS Activate MAPK Pathways? J Signal Transduct. 2011;2011:1–6.
236. Deveci HA, Akyuva Y, Nur G, Nazıroğlu M. Alpha lipoic acid attenuates hypoxia-induced apoptosis, inflammation and mitochondrial oxidative stress via inhibition of TRPA1 channel in human glioblastoma cell line. Biomed Pharmacother. 2019;111:292–304.
237. Amara R, Zeineh N, Monga S, Weizman A, Gavish M. The Effect of the Classical TSPO Ligand PK 11195 on In Vitro Cobalt Chloride Model of Hypoxia-like Condition in Lung and Brain Cell Lines. Biomolecules. 2022;12(10).
238. de Tassigny A d. A, Assaly R, Schaller S, Pruss RM, Berdeaux A, Morin D. Mitochondrial translocator protein (TSPO) ligands prevent doxorubicin-induced mechanical dysfunction and cell death in isolated cardiomyocytes. Mitochondrion. 2013;13(6):688–97.
239. Joo HK, Lee YR, Kang G, Choi S, Kim CS, Ryoo S, et al. The 18-kDa translocator protein inhibits vascular cell adhesion molecule-1 expression via inhibition of mitochondrial reactive oxygen species. Mol Cells. 2015;38(12):1064–70.
240. Baez E, Guio-Vega GP, Echeverria V, Sandoval-Rueda DA, Barreto GE. 4′-Chlorodiazepam Protects Mitochondria in T98G Astrocyte Cell Line from Glucose Deprivation. Neurotox Res. 2017;32(2):163–71.
241. Sun X, Guo S, Wang W, Cao Z, Dan J, Cheng J, et al. Potential involvement of the 18 kDa translocator protein and reactive oxygen species in apoptosis of THP-1 macrophages induced by sonodynamic therapy. PLoS One. 2018;13(5):1–16.
242. Jiang H, Li F, Cai L, Chen Q. Role of the TSPO–NOX4 axis in angiogenesis in glioblastoma. Front Pharmacol. 2022;13(October):1–10.
243. Lambeth JD, Neish AS. Nox enzymes and new thinking on reactive oxygen: A double-edged sword revisited. Annu Rev Pathol Mech Dis. 2014;9:119–45.
244. Guilarte TR, Loth MK, Guariglia SR. TSPO Finds NOX2 in Microglia for Redox Homeostasis. Trends Pharmacol Sci. 2016;37(5):334–343.
245. Gatliff J, East DA, Singh A, Alvarez MS, Frison M, Matic I, et al. A role for TSPO in mitochondrial Ca2+ homeostasis and redox stress signaling. Cell Death Dis. 2017;8(6):1–15.
246. Kalyanaraman B, Darley-Usmar V, Davies KJA, Dennery PA, Forman HJ, Grisham MB, et al. Measuring reactive oxygen and nitrogen species with fluorescent probes: Challenges and limitations. Free Radic Biol Med. 2012;52(1):1–6.
247. Bock FJ, Tait SWG. Mitochondria as multifaceted regulators of cell death. Nat Rev Mol Cell Biol. 2020;21(2):85–100.
248. Meng Y, Tian M, Yin S, Lai S, Zhou Y, Chen J, et al. Downregulation of TSPO expression inhibits oxidative stress and maintains mitochondrial homeostasis in cardiomyocytes subjected to anoxia/reoxygenation injury. Biomed Pharmacother. 2020;121(August 2019):109588.
249. Fan J, Wang K, Zirkin B, Papadopoulos V. CRISPR/Cas9–Mediated tspo gene mutations lead to reduced mitochondrial membrane potential and steroid formation in MA-10 mouse tumor leydig cells. Endocrinology. 2018;159(2):1130–46.
250. Riban V, Meunier J, Buttigieg D, Villard V, Verleye M. In Vitro and In Vivo Neuroprotective Effects of Etifoxine in β-Amyloidinduced Toxicity Models. CNS Neurol Disord - Drug Targets. 2020;19(3):227–40.
251. Sutter AP, Maaser K, Höpfner M, Barthel B, Grabowski P, Faiss S, et al. Specific ligands of the peripheral benzodiazepine receptor induce apoptosis and cell cycle arrest in human esophageal cancer cells. Int J

Cancer. 2002;102(4):318–27.

252. Shoukrun R, Veenman L, Shandalov Y, Leschiner S, Spanier I, Karry R, et al. The 18-kDa translocator protein, formerly known as the peripheral-type benzodiazepine receptor, confers proapoptotic and antineoplastic effects in a human colorectal cancer cell line. Pharmacogenet Genomics. 2008;18(11):977–88.
253. Santidrián AF, Cosialls AM, Coll-Mulet L, Iglesias-Serret D, De Frias M, González-Gironès DM, et al. The potential anticancer agent PK11195 induces apoptosis irrespective of p53 and ATM status in chronic lymphocytic leukemia cells. Haematologica. 2007;92(12):1631–8.
254. Mendonça-Torres MC, Roberts SS. The translocator protein (TSPO) ligand PK11195 induces apoptosis and cell cycle arrest and sensitizes to chemotherapy treatment in pre- and post-relapse neuroblastoma cell lines. Cancer Biol Ther. 2013;14(4):319–26.
255. Castellano S, Taliani S, Viviano M, Milite C, Da Pozzo E, Costa B, et al. Structure-activity relationship refinement and further assessment of 4-phenylquinazoline-2-carboxamide translocator protein ligands as antiproliferative agents in human glioblastoma tumors. J Med Chem. 2014 Mar 27;57(6):2413–28.
256. Daniele S, Taliani S, Da Pozzo E, Giacomelli C, Costa B, Trincavelli ML, et al. Apoptosis therapy in cancer: The first single-molecule co-activating p53 and the translocator protein in Glioblastoma. Sci Rep. 2014 Apr 23;4(4749).
257. Veenman L, Gavish M, Kugler W. Apoptosis Induction by Erucylphosphohomocholine via the 18 kDa Mitochondrial Translocator Protein: Implications for Cancer Treatment. Anticancer Agents Med Chem. 2014;14(4):559–77.
258. Kugler W, Veenman L, Shandalov Y, Leschiner S, Spanier I, Lakomek M, et al. Ligands of the mitochondrial 18 kDa translocator protein attenuate apoptosis of human glioblastoma cells exposed to erucylphosphohomocholine. Cell Oncol. 2008;30(5):435–50.
259. Deng L, Zhai X, Liang P, Cui H. Overcoming trail resistance for glioblastoma treatment. Biomolecules. 2021;11(4):1–17.
260. Bangert A, Cristofanon S, Eckhardt I, Abhari BA, Kolodziej S, Häcker S, et al. Histone deacetylase inhibitors sensitize glioblastoma cells to TRAIL-induced apoptosis by c-myc-mediated downregulation of cFLIP. Oncogene. 2012;31(44):4677–88.
261. Liu J, Gao Q, Xie T, Liu Y, Luo L, Xu C, et al. Synergistic effect of TRAIL and irradiation in elimination of glioblastoma stem-like cells. Clin Exp Med. 2018;18(3):399–411.
262. Son Y gyu, Kim EH, Kim JY, Kim SU, Kwon TK, Yoon AR, et al. Silibinin sensitizes human glioma cells to TRAIL-mediated apoptosis via DR5 up-regulation and down-regulation of c-FLIP and survivin. Cancer Res. 2007;67(17):8274–84.
263. Zhu ZC, Liu JW, Yang C, Li MJ, Wu RJ, Xiong ZQ. Targeting KPNB1 overcomes TRAIL resistance by regulating DR5, Mcl-1 and FLIP in glioblastoma cells. Cell Death Dis. 2019;10(2):118.
264. Panner A, James CD, Berger MS, Pieper RO. mTOR Controls FLIP S Translation and TRAIL Sensitivity in Glioblastoma Multiforme Cells . Mol Cell Biol. 2005;25(20):8809–23.
265. Jeon HM, Oh YT, Shin YJ, Chang N, Kim D, Woo D, et al. Dopamine receptor D2 regulates glioblastoma survival and death through MET and death receptor 4/5. Neoplasia (United States). 2023;39(February):09.
266. Chi AS, Tarapore RS, Hall MD, Shonka N, Gardner S, Umemura Y, et al. Pediatric and adult H3 K27M-mutant diffuse midline glioma treated with the selective DRD2 antagonist ONC201. J Neurooncol. 2019;145(1):97–105.
267. Tanrıkulu B, Yaşar AH, Canpolat C, Çorapçıoğlu F, Tezcanli E, Abacioglu U, et al. Preliminary findings of German-sourced ONC201 treatment in H3K27 altered pediatric pontine diffuse midline gliomas. J Neurooncol. 2023;163(3):565–75.

10 Erklärung

Ich erkläre hiermit, dass ich die vorliegende Arbeit ohne unzulässige Hilfe Dritter und ohne Benutzung anderer als der angegebenen Hilfsmittel angefertigt habe. Die aus anderen Quellen direkt oder indirekt übernommenen Daten und Konzepte sind unter Angabe der Quelle gekennzeichnet. Insbesondere habe ich nicht die entgeltliche Hilfe von Vermittlungs- bzw. Beratungsdiensten (Promotionsberater oder andere Personen) in Anspruch genommen. Niemand hat von mir unmittelbar oder mittelbar geldwerte Leistungen für Arbeit erhalten, die im Zusammenhang mit dem Inhalt der vorgelegten Dissertation stehen. Die Arbeit wurde bisher weder im In- noch im Ausland in gleicher oder ähnlicher Form einer anderen Prüfungsbehörde vorgelegt.

Celine Rohrmus

11 Danksagung

Zunächst möchte ich einen großen Dank an meinen Doktorvater Herrn Prof. Dr. med. Peter Hau für die hervorragende persönliche Betreuung und fachliche Unterstützung bei der Umsetzung der Arbeit aussprechen. Ich bin sehr dankbar für die Möglichkeit, meine Doktorarbeit am Lehrstuhl der Neurologie durchgeführt haben zu können. Ebenso bedanke ich mich herzlichst bei meiner Betreuerin, Arabel, für die anregenden Diskussionen, ihre Vorschläge und das konstruktive Feedback. Ohne ihre Geduld und Mühen, wäre diese Arbeit nicht möglich gewesen. Mein besonderer Dank geht an Birgit und Laura, ohne deren unermüdliche fachliche, aber auch persönliche Unterstützung und Ermunterung die Arbeit mir nicht so viel Freude bereitet hätte.

An dieser Stelle möchte ich auch meinen Eltern großen Dank aussprechen, die mich auf meinem Weg immer mit Rat und Tat unterstützen. Ihr liebevolles und bekräftigendes Umfeld hat mir die Umsetzung dieser Arbeit erst ermöglicht.